CHALMERS
UNIVERSITY OF TECHNOLOGY

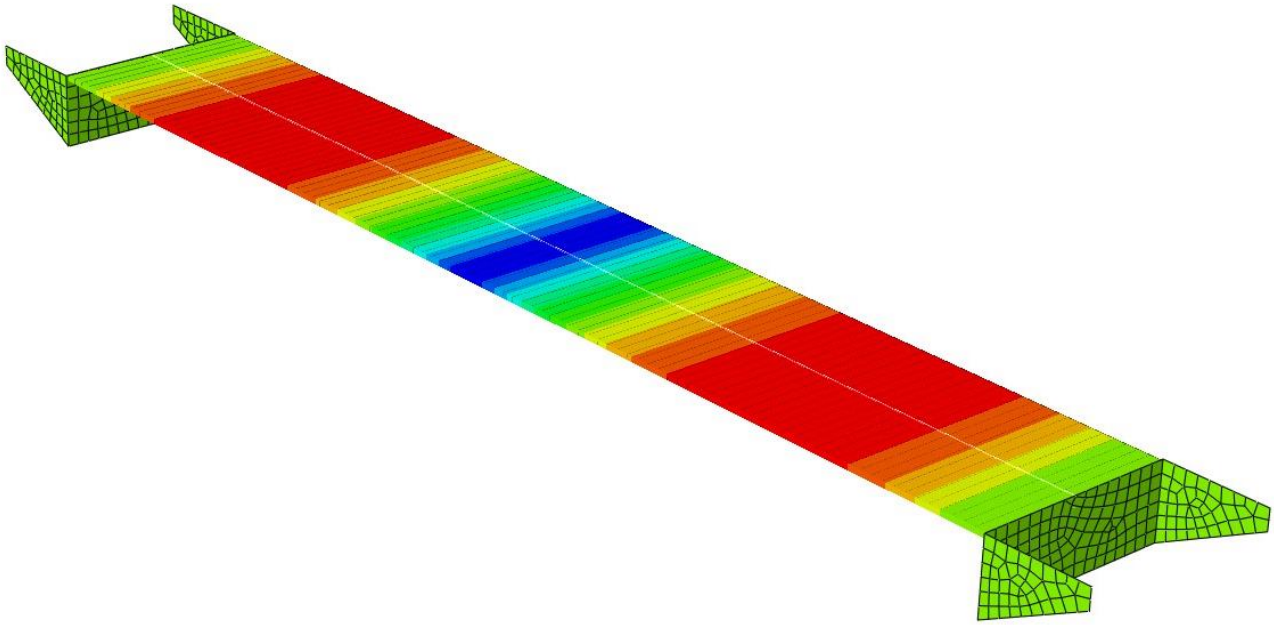

Early estimations of dimensions for prestressed concrete bridges

Optimization by Set-based Parametric Design of Cross-Section and Prestressing Force in a Preliminary Stage

Master's thesis in Master Programme Structural Engineering & Building technology

DANIEL ASPEGREN
ERIK MÖÖRK

Department of Architecture and Civil Engineering
Division of Structural Engineering
Concrete Structures

CHALMERS UNIVERSITY OF TECHNOLOGY
Gothenburg, Sweden 2021
www.chalmers.se

MASTER'S THESIS ACEX30

Early Estimations of Dimensions for Prestressed Concrete Bridges

Optimization by Set-Based Parametric Design of Cross-Section and Prestressing Force in a Preliminary Stage

Master's Thesis in the Master's Programme Structural Engineering and Building Technology

DANIEL ASPEGREN
ERIK MÖÖRK

CHALMERS
UNIVERSITY OF TECHNOLOGY

Department of Architecture and Civil Engineering
Division of Structural Engineering
Concrete structures
CHALMERS UNIVERSITY OF TECHNOLOGY
Gothenburg, Sweden 2021

Early Estimations of Dimensions for Prestressed Concrete Bridges
Optimization by Set-Based Parametric Design of Cross-Section and Prestressing Force in a Preliminary Stage

Master's Thesis in the Master's Programme Structural Engineering and Building Technology

DANIEL ASPEGREN

ERIK MÖÖRK

Examensarbete ACEX30
Institutionen för Arkitektur och Samhällsbyggnadsteknik
Chalmers tekniska högskola, 2021

Department of Architecture and Civil Engineering
Division of Structural Engineering
Concrete Structures
Chalmers University of Technology
SE-412 96 Göteborg
Sweden
Telephone: + 46 (0)31-772 1000

Cover: Picture of FE model in BRIGADE/Plus of studied two-span continuous prestressed concrete bridge, showing the sectional moment distribution.

Department of Architecture and Civil Engineering
Gothenburg, Sweden, 2021

Early Estimations of Dimensions for Prestressed Concrete Bridges
Optimization by Set-Based Parametric Design of Cross-Section and Prestressing Force in a Preliminary Stage
Master's Thesis in the Master's Programme Structural Engineering and Building Technology

DANIEL ASPEGREN
ERIK MÖÖRK
Department of Architecture and Civil Engineering
Division of Structural Engineering
Concrete Structures
Chalmers University of Technology

ABSTRACT

When designing concrete bridges, estimations of the dimensions and reinforcement content are made to estimate the cost of the bridge in an early phase. When the final bridge is designed, the estimated dimensions based on experience and simplification is often used and checked against the national regulations. If the dimensions comply with the regulations, the estimated design is used as the final design and there is not often time to reduce and optimize the dimensions to make the bridge more material efficient.

This master thesis presents an optimization method for the early estimations of the design for continuous prestressed concrete bridges. This method is based on set-based parametric design and the optimization is performed with a python script where this method is implemented. The optimization is focusing on the relationship between beam height, number of prestressed tendons and the parabolic tendon layout with the aim to minimize the global warming potential (GWP) and cost for the superstructure. The script with the optimization method has been created to enable an effective approach to reach an optimized solution in the preliminary design phase, which will result in a more material efficient final bridge design.

To reach the lowest GWP and cost, a slender cross-section with a large number of prestressed tendons is desirable. Depending on the case-specific conditions, the tendon layout is preferable designed in different ways. For shorter bridges, a tendon layout that is minimizing the secondary moment is preferable to obtain a slender cross-section, while for longer bridges the self-weight is increased and therefore a tendon layout that results in a larger secondary moment is the most favourable.

The method was used to create designs which was compared with two existing bridges designed by Inhouse Tech Göteborg AB. The designs showed an improvement, for both cost and GWP compared to the existing bridges. Above all, there are opportunities for a more optimized and material-efficient design if the tendon layout is adapted to the case specific conditions.

Key words: Prestressed concrete bridge, Preliminary design, Set-based parametric design, BRIGADE/Plus, Tendon layout, Optimization

Uppskattning av dimensioner för förspända broar i tidiga skeden
Optimering av tvärsnitt och förspänningskraft genom Set-Based Parametric Design i preliminärdimensioneringsfasen

Examensarbete inom masterprogrammet Structural Engineering and Building Technology

DANIEL ASPEGREN
ERIK MÖÖRK

Institutionen för arkitektur och samhällsbyggnadsteknik
Avdelningen för konstruktionsteknik
Betongbyggnad
Chalmers tekniska högskola

SAMMANFATTNING

Vid utformning av förspända betongbroar görs en tidig uppskattning av dimensionerna och armeringsinnehållet för att uppskatta kostnaden för bron. Vid utformningen av den slutliga bron används ofta de dimensioner som uppskattats i tidigt skede, baserat på erfarenhet och antaganden mot de nationella bestämmelserna. Om brodesignen uppfyller reglerna används denna utformning för den slutgiltiga bron och det finns ofta inte tid att minska och optimera materialanvändningen i bron.

Detta examensarbete presenterar en optimeringsmetod för de tidiga uppskattningarna av utformningen hos kontinuerliga förspända betongbroar. Denna metod baseras på *set-based parametric design* och optimeringen utförs med hjälp av en python-kod där denna optimeringsmetod är implementerad. Optimeringen fokuserar på förhållandet mellan balkhöjd, antal förspända kablar samt den paraboliska kabelföringen i syfte att minimera den globala uppvärmningspotentialen (GWP) och kostnad för överbyggnaden. Python-koden har skapats för att möjliggöra ett effektivt och användarvänligt tillvägagångssätt för att nå en optimerad lösning i preliminärdimensioneringen och resulterar därför i en mer materialeffektiv slutlig brodesign.

För lägsta miljöpåverkan och kostnad, är ett lågt tvärsnitt med ett stort antal förspända kablar önskvärt. Beroende på de specifika förhållandena för varje bro är det fördelaktigt att utforma kabelföringen på olika sätt. För kortare broar är en kabelföring som minimerar tvångsmomentet mest optimalt för att få ett minimerat tvärsnitt, men för längre broar ökar egenvikten och därför är en kabelföring som resulterar i ett större tvångsmoment det mest gynnsamma.

Metoden användes för att ta fram utformningar som jämfördes med två befintliga broar konstruerade av Inhouse Tech Göteborg AB. Utformningarna visar en förbättring avseende både kostnad och GWP jämfört med de befintliga broarna. Framför allt finns det möjligheter till en mer optimerad och materialeffektiv lösning om kabelföringen anpassas till de projektspecifika förutsättningarna.

Nyckelord: Förspända betongbro, Preliminärdimensionering, Kabelföring, Optimering

Contents

Preface

This Master's Thesis has been carried out at the division of Structural Engineering at Chalmers University of Technology as the final work in the master's program Structural Engineering and Building Technology. The thesis has been performed in collaboration with Inhouse Tech Göteborg AB.

We would like to thank our supervisors Oscar Yman and Max Fredriksson from Inhouse Tech Göteborg AB for their support and input during the work of this thesis, and for their enthusiasm and quick response despite the special conditions of the covid pandemic. Thanks also to Isak Svensson at Inhouse Tech Göteborg AB for your python guidance and to Göran Hannrup at PEAB for your quick and effective expertise in labour and material cost of concrete bridges.

We would also like to thank our examinator and supervisor, Mario Plos at Chalmers University of Technology for his input on FE modelling and feedback on the project.

Göteborg, June 2021

Daniel Aspegren
Erik Möörk

List of Figures

List of Tables

Abbreviations

3D	Three dimensional
ALS	Accidental limit state
CO_2-eq	Carbon dioxide equivalents
DOF	Degrees of freedom
EC	Eurocode
EPD	Environmental product declaration
GWP	Global warming potential
LM	Load model
SEK	Swedish crowns
SLS	Service limit state
STR	Internal failure or large deformations in the structure or structural parts where the material strength is decisive.
ULS	Ultimate limit state

Notations

Roman upper-case letters

A_{ct}	Concrete area in the tensile zone
A_c	Concrete area
A_p	Cross-section area of the prestressing steel
$A_{s.min}$	Minimum cross-section area of reinforcement
B_{es}	Width of the end-shield
E_c	Modulus of elasticity for the concrete
E_p	Modulus of elasticity for prestressing steel
F_{cs}	Shrinkage force
F_p	Force in the prestressing steel
$G_{k.j}$	Characteristic permanent load
H_1	Height of end-shield
I	Moment of inertia
K_0	Coefficient for earth pressure at rest
K_p	Coefficient for passive earth pressure
L	Total length of bridge

L_0	Distance from the support to where the tendon is at the same level as the centre of gravity of the cross-section
L_{CG}	Distance from the bottom of the beam to the centre of gravity
L_{ww}	Length of wingwalls
M_{Ed}	Design moment
M_p	Primary moment
M_{Rd}	Moment capacity
M_s	Secondary moment
P	Prestressing force
$T_{shrinkage}$	Temperature change to represent the shrinkage
Q_k	Characteristic point load
$Q_{k.1}$	Main characteristic variable load
$Q_{k.i}$	Characteristic variable load
R	Reaction force

Roman lower-case letters

b_w	Width of beam web
cc_{duct}	Centre to centre distance between tendon ducts
d_p	Distance from top of the beam to the centre of the prestressing steel
e	Eccentricity of the tendon from the centre of gravity
e_{span}	Maximum eccentricity of the tendon in the span
f_{cd}	Design compressive strength of concrete
f_{ck}	Characteristic compressive strength of concrete
f_{ctm}	Mean tensile strength of concrete
$f_{ct.eff}$	Tensile strength of concrete when cracking occurs. Set to f_{ctm} or lower ($f_{ctm}(t)$) if cracking occurs before 28 days after cast.
$f_{p.0,1k}$	Characteristic 0,1% strain limit for prestressing steel
f_{pd}	Design tensile capacity of prestressing steel
f_{pk}	Characteristic tensile capacity of prestressing steel
k	Coefficient that compensates the impact of uneven residual stresses in the cross-section before cracking and change of internal level arm
k_c	Coefficient that considers stress distribution in the cross-section before cracking
l	Theoretical span length

n_1	Number of load fields
n_{tendon}	Number of tendons
$n_{tendon.max}$	Maximum number of tendons
$q_{earth.increased}$	Increased earth pressure due to movement against earth
$q_{earth.rest}$	Earth pressure at rest depending on depth (z)
q_k	Characteristic distributed load
$q_{self\text{-}weight}$	Distributed load only including the self-weight
$q_{surcharge}$	Surcharge load
t_f	Thickness of flange
w	Total carriageway width
x	Coordinate along the bridge
z	Depth from zero-pressure level

Greek letters

α_{Qi}	Adaption factor for concentrated loads
α_{qi}	Adaption factor for distributed loads
α_{span}	Factor to decrease the eccentricity of the tendon in the span (e_{span})
α_c	Thermal expansion coefficient for concrete
γ_s	Safety partial factor for steel
$\gamma_{G.j}$	Safety partial factor for permanent loads
γ_Q	Safety partial factor for variable loads
γ_p	Safety partial factor for prestressing force
γ	Density of the earth
δ	Horizontal movement of the bridge
δ_{max}	Maximum horizontal movement
$\Delta\varepsilon_p$	Strain in the tendons due to load effect
ε_{cs}	Shrinkage strain of concrete
ε_{p0i}	Initial strain of the prestressing steel
ε_p	Total strain in tendon
ε_{p0}	Strain in the tendons due to prestressing
ε_{cu}	Strain in concrete
ξ_j	Reduction factor
ρ_{min}	Factor to decide minimum normal reinforcement
$\varphi(\infty, t_0)$	Final creep coefficient [-]

σ_s	Absolut value of the stress in the reinforcement after cracking. Not larger than the yield stress, f_{yk}
$\sigma_{p.max}$	Maximum stress in the prestressing steel
$\sigma_{p.m0}$	Stress directly after the release of the tensioning the maximum
σ_{cc}	Concrete compressive stress
σ_{cp}	Concrete stress at the level of prestressing steel
σ_{ct}	Concrete tensile stress
χ_∞	Relaxation factor after long time
Ψ_0	Load combination factor
Ψ_1	Load combination factor
Ψ_2	Load combination factor

1 Introduction

1.1 Background

In bridge design, early estimations of the dimensions and reinforcement amount are made to estimate the cost of the bridge. The estimation is generally based upon experience and simplified calculations. While most of the specific design regarding the bridge is made during the detailed design phase, the dimensions are usually not changed. Instead, the detailed design is using the dimensions from the early estimations. This means that the amount of material for the bridge is largely decided based upon estimations and experience instead of calculations. It is therefore a risk that a lot of unnecessary material is used.

From a sustainable as well as an economic perspective, it is important to optimize the structures to maximize material efficiency. In 2017, the construction industry accounted for 19% of the Swedish greenhouse gas emissions (Boverket, 2021). Global warming is a major concern around the world, and the Swedish construction industry has developed a joint goal to achieve net-zero emissions in 2045 (Naturvårdsverket, 2020). To contribute to this goal, structures should be designed with a method based on optimization rather than experience and estimations.

1.2 Aim and Objectives

This master's thesis aims to make the early estimations of the dimensions more accurate than if they are based on experience and estimations only. This will result in a reduced amount of material needed for the bridge, which is desirable from both an environmental and an economical perspective.

The goal is to create a tool in the shape of a python script that can be used together with the design software BRIGADE/Plus version 6.2-20 (Scanscot Technology, 2021) to make early estimations that are more accurate for two-span prestressed concrete bridges. The tool will be able to handle different input data, such as bridge width and span lengths, and present a design solution that will be optimized from an economical or environmental point of view. This will make the design more effective without being more time-consuming than the design based on experience.

The main objectives for this thesis are:

- Identify parameters in the design with a large influence on the result.
- Develop an optimization method for the studied bridge type using set-based parametric design.
- Design the cross-section and prestressing steel of the bridge with respect to bending in the longitudinal direction.
- Create an optimized combination between beam height and amount of prestressing steel concerning cost and global warming potential (GWP).
- Perform comparisons with existing bridges to evaluate the potential of the optimization method.

1.3 Limitations

- The normal reinforcement steel is not optimized or designed.
- Optimization of material will not be included; standard concrete and prestressing steel are used.
- The design will be based on the European Standard, Eurocode (EC), and the Swedish regulations.

1.4 Methodology

The first phase of the project was a literature study regarding both parametric design and the theory of prestressed bridges. From this, the most important parameters for the design were identified and the standardized method when designing this type of bridge was studied. To get a better understanding of python scripting, an introductory course was studied.

The next step was to create a Python script that builds a finite element (FE) model. Python is a programming language that is used in this thesis to control the design software BRIGADE/Plus, to do post-processing of the results from the FE analysis and to summarize the results. BRIGADE/Plus is an FE program developed by Scanscot (2021) for bridge design that uses ABAQUS as FE-solver. The script builds the FE model in the design software based on parametric design to enable optimization of the bridge and to enable the possibility to change span length, width, and other dimensions of the bridge. The entire geometry of the bridge including wingwalls, end-shields, and the prestressing steel is included in the model.

To verify that the model works as intended and that the assumptions and simplifications are accurate, a comparison has been made with simplified hand calculations of a specific load case. A convergence study of the mesh size has also been performed.

The tendon layout was designed based on the results from the literature study and an investigation of how different parameters for the layout are affecting the structural behaviour. The layout of the tendons is determined by a few parameters and the combination of these parameters gives different layouts for the tendon.

The parametric optimization is focusing on finding the most efficient combination between beam height and number of prestressing cables. Different tendon layouts are used for each height to find an optimized solution. The method implemented in the optimization to find this solution is based on set-based parametric design. The script does an FE analysis and performs the required design checks according to EC for all load combinations. The approved solutions have been evaluated and compared with respect to their cost and GWP to achieve the most optimal solution.

The method was used to create designs for different bridges which were evaluated through a comparison to existing bridges. This is to analyse the potential of this optimization method and to study if the current design method can be improved such that more material efficient bridge designs can be found.

2 Design of prestressed concrete bridges

In the following chapter, the theory and design process for continuous prestressed beam bridges is described. The behaviour, which loads that are acting on the bridge, and the preliminary design process in current engineering practice are the focus.

2.1 Continuous post-tensioned bridge

The bridge studied in this thesis is a prestressed continuous bridge with two spans. This is also the type of bridge that is treated in this chapter. Figure 2.1 illustrates the principal bridge, with connected structural parts. A detailed explanation of the modelled bridge is given in Chapter 4.

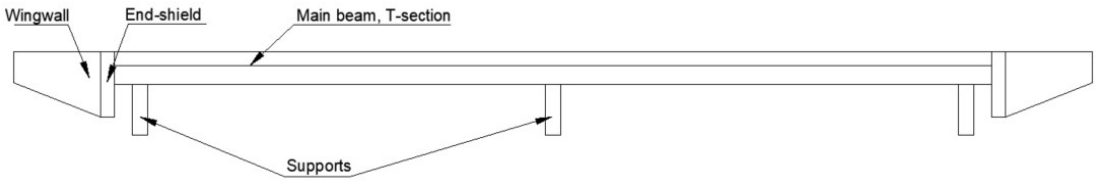

Figure 2.1 - Principal design of the studied bridge.

2.1.1 The aim of prestressing

When a concrete beam is subjected to bending, cracks appear at the tension side when the stress exceeds the tension capacity of the concrete. By applying the prestressing, the structure is exposed to a compressive normal force which leads to a delay of the cracking in the concrete. As long as the cross-section remains uncracked, the flexural rigidity is larger than for a cracked section, and the deflection is therefore decreased compared to a normal reinforced concrete structure.

When estimating the size of the beam for a certain span length, *l*, recommendations on the span to beam depth, *h*, ratios are often used. This ratio can be almost twice as large when using prestressed concrete beams compared to normally reinforced beams according to (Engström, 2011b). The span to depth ratio for simply supported beams are about $(l/h)_{max} \approx 20$ for normal reinforced concrete beams and almost $(l/h)_{max} \approx 40$ for prestressed concrete beams.

2.1.2 Post-tensioning

There are two different methods for prestressing of concrete, pre-tensioning, and post-tensioning where the prestressing steel is tensioned before and after casting of the concrete, respectively. In this thesis, cast in-situ concrete bridges are studied. For such bridges, post-tensioning systems are used and therefore only this method is treated here.

When using post-tensioning in bridge constructions, ducts for the prestressing steel are placed in the formwork. When the concrete has been cast and reached an adequate strength, the steel is tensioned to achieve the prestressing effect (Engström, 2011b). In practice, the tensioning is done by attaching an anchorage of the prestressing steel on one end and a hydraulic jack on the opposite end of the concrete beam. The hydraulic jack then tensions the steel to the desired tendon force.

When the steel at the hydraulic jack is released and anchored a phenomenon called anchorage slip often occurs. The anchorage slip results in a drop in the tendon force, but due to frictional forces along the tendon in the opposite direction of the tendon force, the decrease in tendon force only occurs over a length x_{as} closest to the edge (Engström, 2011b). This action is illustrated in Figure 2.2.

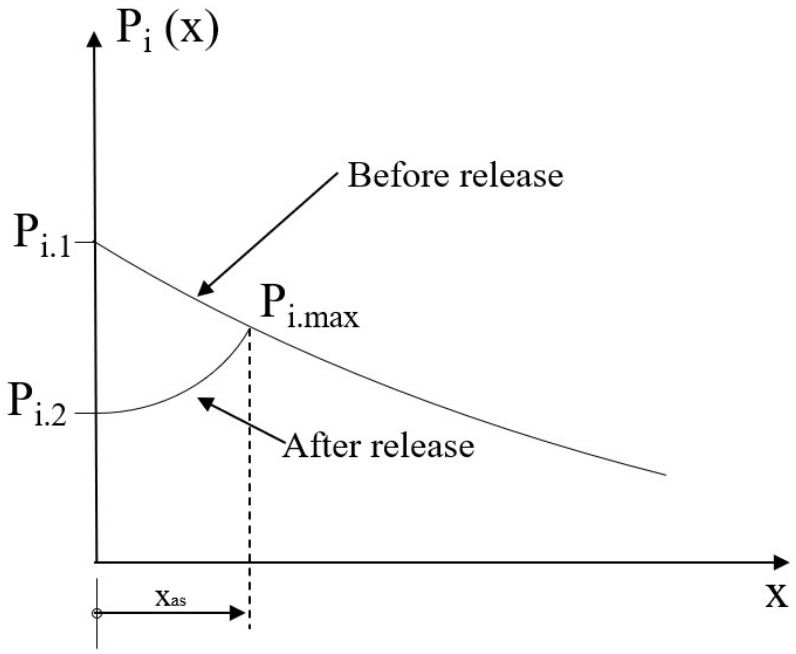

Figure 2.2 - Effect of anchorage slip on the prestressing force. Based on Engström (2011b).

2.1.3 Tendon layout

The most used tendon profile for continuous beams has a parabolic shape and is placed to counteract the bending moment due to vertical loads. The profile of the prestressing tendon is described with its eccentricity *e(x)* to the centreline of the beam, where *x* is the coordinate along the beam. The common tendon profile for the type of continuous beam investigated in this thesis together with its eccentricity *e(x)* is illustrated in Figure 2.3. The shape of the tendon profile is designed so that it follows the moment diagram along the beam (Engström, 2011a). The resulting moment from the prestressing force, $P(x)$, multiplied with $e(x)$ is called the primary moment, M_p.

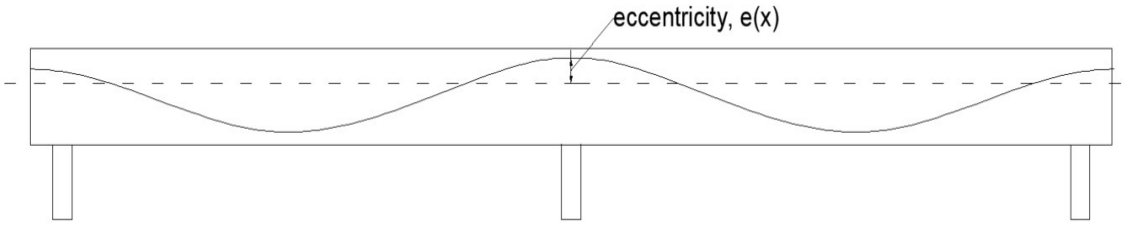

Figure 2.3 - Common tendon profile with eccentricity e(x).

If the response of the tendon force with the corresponding profile in Figure 2.3 is studied, the prestressing force wants to bend the beam upwards, giving it a negative curvature. To prevent the beam from lifting at the mid support, a downward reaction force, *R*, is generated here. Consequently, to obtain vertical equilibrium in this stage, upward forces have to act on the two end supports (Dolan & Hamilton, 2019). These three reaction forces will create a linear moment distribution, and this moment is called secondary moments, M_s, illustrated in Figure 2.4.

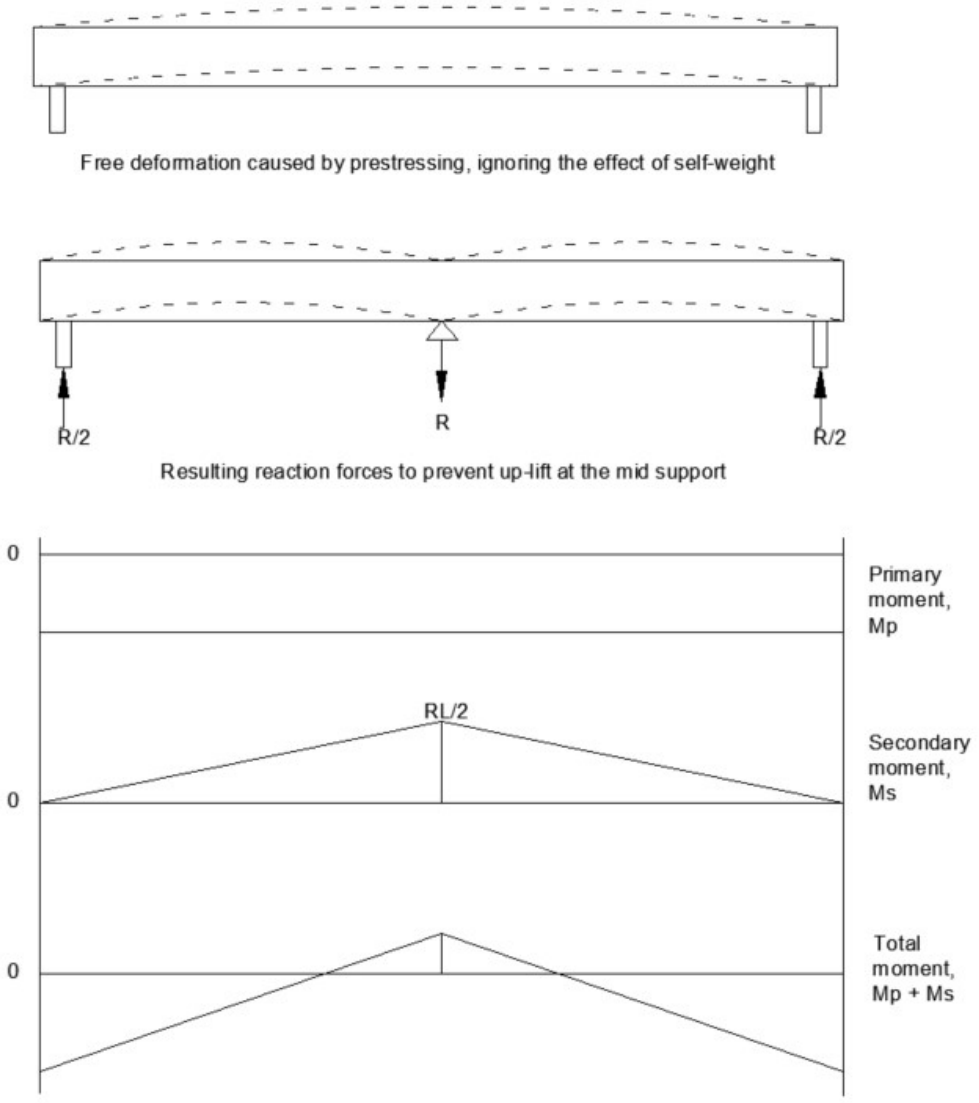

Figure 2.4 - Principle for how the secondary moment's Ms is generated. Based on Dolan and Hamilton (2019)

The effect of the secondary moment creates a complex design situation, since $P(x) * e(x)$ often is designed to counteract the sectional moment from the external load effect, $M_{Ed.q}(x)$. The complexity comes from that the final sectional moment, $M_{Ed}(x)$, is including $M_{Ed.q}(x)$ but also an addition from the secondary moment M_s which is unknown until both the tendon force *P* and the eccentricity *e* is decided.

2.1.4 Long term effects

When analysing the response of the structure it is needed to analyse both the short- and the long-term response. The short-term response can for example be the analysis of the structure when the prestress is applied.

An analysis of the long-term response includes the time-dependent effects on the structure that develops over long time, such as creep, shrinkage, and relaxation. The creep of concrete can be taken into account by using an effective modulus of elasticity, $E_{c.ef}$, which is a fictitious parameter that is used in the calculations (Engström, 2011b). The relaxation of prestressing steel can be handled in the same way with the effective modulus of elasticity for the steel, E_p. These parameters are calculated with equation (2.1) and (2.2).

$$E_{c.ef} = \frac{E_c}{1+\varphi(\infty,t_0)} \tag{2.1}$$

$\varphi(\infty, t_0)$ final creep coefficient [-]
E_c modulus of elasticity for the concrete [Pa]

$$E_{p.ef} = E_p * (1 - \chi_\infty) \tag{2.2}$$

E_p Modulus of elasticity for prestressing steel
χ_∞ Relaxation factor after long time

The shrinkage of concrete needs to be handled separately. The shrinkage causes an internal restraint similarly to the prestressing, but the effect has the opposite sign. Since the shrinkage causes a shortening of the structure, the strain of the prestressing steel is reduced which leads to a reduction of the prestressing force. To handle this in the calculations, a shrinkage force, $F_{cs,}$ is subtracted from the effective prestressing force, P_{0i} (Engström, 2011b). This gives the new internal restraint force:

$$P_{0i} - F_{cs} = E_p * \left(\varepsilon_{p0i} - \varepsilon_{cs}\right) * A_p \tag{2.3}$$

ε_{p0i} Initial strain of the prestressing steel
ε_{cs} Shrinkage strain of the concrete
A_p Cross-section area of the prestressing steel

2.2 Loads

A road bridge constructed in Sweden is required to be designed according to the European Standard, Eurocode (EC) and the regulations from the Swedish Transport Administration (Trafikverket, 2019b). Since only the superstructure will be handled here, only the loads that influence the superstructure will be presented.

Permanent loads:

- Self-weight - The weight of the main beam, edge beams, railing, bridge deck with 100 mm pavement, end-shield, and wingwalls.
- Earth pressure - There is an earth pressure acting in the horizontal direction on the end-shields which are connected to the main beam. The effect on the main beam is that the earth pressure causes a normal force and a moment.
- Support settlement – A displacement of the supports due to settlement needs to be considered. The displacement can be on one or more supports, whichever gives the least favourable effect.
- Shrinkage – Due to the shrinkage of concrete, the prestressing force is reduced.

Variable loads:

- Traffic load – Vertical load representing the vehicles driving on the bridge. Further explained in chapter 2.2.1.
- Acceleration/Breaking load – Horizontal load occur when the vehicles on the bridge are breaking or accelerating. The load is placed on the pavement surface (SIS, 2003a).
- Surcharge load – When vehicles are placed on the ground next to the surface, the earth pressure increases on the end-frames which increases the moment and normal force as described above.
- Temperature effects – When the temperature increases or decreases it creates restraint forces in the structure which need to be included. The elongation of the structure due to increased temperature creates an increased earth pressure on the end-shields.
- Wind load – Horizontal load acting perpendicular to the bridge. The wind load is acing both on the structure itself and the vehicles on the bridge.

2.2.1 Traffic loads

The Swedish Transport Agency together with the Swedish Transport Administration (Trafikverket) set the regulations for bridge structures in Sweden. There are four load models (LM) in Eurocode 1 (SIS, 2003a) and one National Vehicle model (Trafikverket, 2019a). The LMs have different purposes, LM1 and LM2 are the two most standardized models that should be used, while the client decides if LM3 should be applied, while LM4 shall not be applied (Trafikverket, 2019b). In this thesis, LM1 and the National Vehicle model will be integrated into the design, LM2 can only be decisive for span lengths between 3 and 7 meters (Trafikverket, 2019b) and will not be included here. LM3 will not be included.

In Eurocode 1 (SIS, 2003a) different traffic load models are described. The models are designed to represent all real traffic load situations that could act on the bridge. When implementing the different load models the bridge is divided into load fields with a

width of w_1. Depending on the total carriageway width, w, one should design the bridge with a different number of load fields, Table 2.1 and Figure 2.5 describes this Eurocode method.

Table 2.1 - Number of load fields and their widths depending on total width w (SIS, 2003a).

Total carriageway width	Number of load fields	Width w_1 of each load field	Width of the remaining area
w < 5.4 m	$n_1 = 1$	3 m	$w - 3\ m$
5.4 m < w < 6 m	$n_1 = 2$	$\frac{w}{2}$	0
6 m < w	$n_1 = int(\frac{w}{3})$	3 m	$w - 3\ m \times n_1$

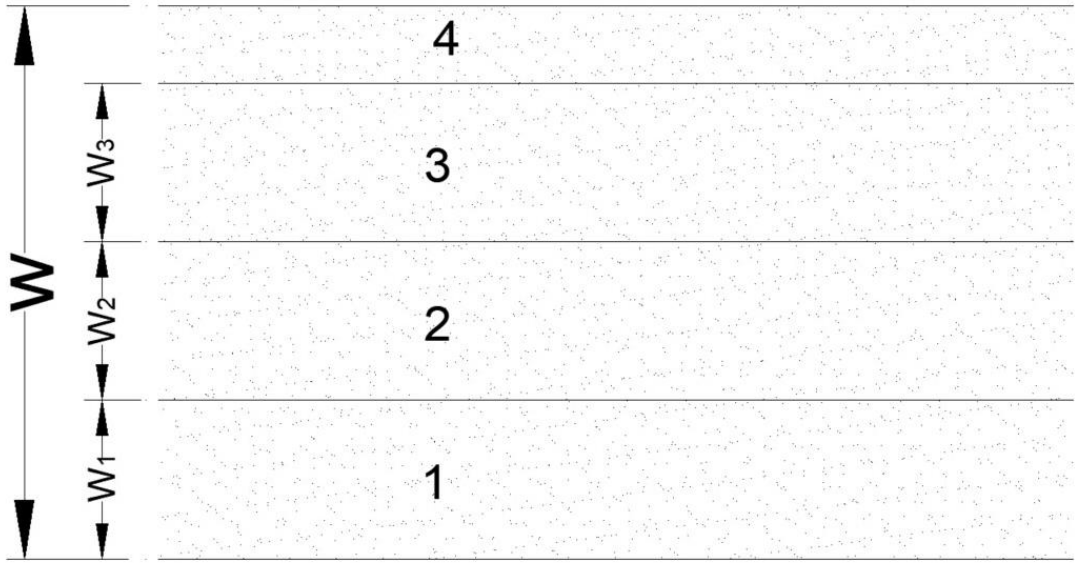

Figure 2.5 - Placement of load fields. Based on SIS, 2003a.

The load fields must be placed and numbered such that it results in the most conservative load effect for each check or calculation.

2.2.1.1 Load model 1

Load Model 1 has two different sub-systems; one group of axle loads and a uniformly distributed load. Only one group of axle load needs to be applied in each load field and the uniform load should be placed such that the most unfavourable effect is obtained (SIS, 2003a). The detailed load placement in LM1 is shown in Figure 2.6

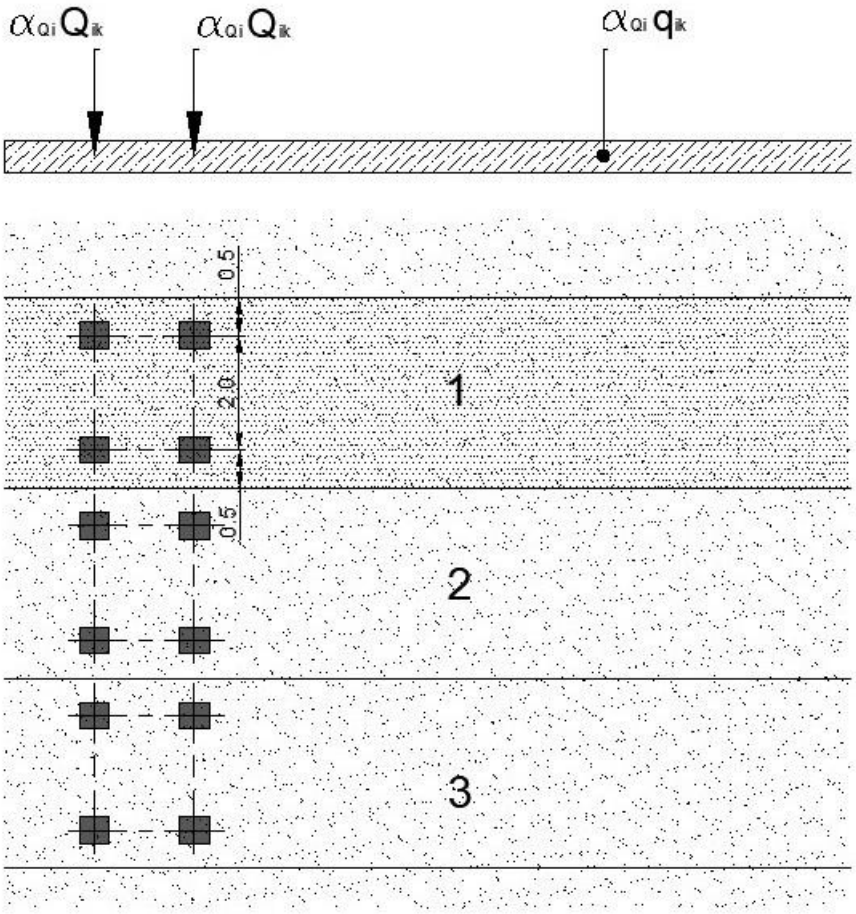

Figure 2.6 - Load placement in LM1 according to Eurocode 1. Based on SIS, 2003a.

2.2.1.2 National Vehicle model

In the National Vehicle model several different load cases A-O, stated by the Swedish Transport Administration (Trafikverket, 2019a), should be tested separately and be placed with the most unfavourable placement. The Vehicle can be placed in a maximum of two load fields, with a loading factor of 1.0 and 0.8, respectively. If more than two load fields are present on the bridge the other fields are subjected to a uniform load of 0 or 5 kN/m.

2.2.2 Load combinations

In Eurocode (SIS, 2002a) the load combinations for both Service Limit State (SLS) and Ultimate Limit State (ULS) is described. For ULS four different stages require verification, in this thesis only one of these four stages is relevant:

- **STR**: Internal failure or large deformations in the structure or structural parts where the material strength is decisive.

The load combination for STR is presented in Equation (2.4) and (2.5) and the most unfavourable load effect of the two should be used in the design. In Equation (2.4) the

permanent loads are considered most unfavourable while in Equation (2.5) the variable loads are considered more unfavourable.

$$\sum_{j\geq 1} \gamma_{G.j}\, G_{k.j}"+"\gamma_p P"+"\gamma_{Q.1}\Psi_{0.1}Q_{k.1}"+"\sum_{i>1}\gamma_{Q.i}\,\Psi_{0.i}Q_{k.i} \quad (2.4)$$

$$\sum_{j\geq 1} \xi_j\,\gamma_{G.j}\, G_{k.j}"+"\gamma_p P"+"\gamma_{Q.1}Q_{k.1}"+"\sum_{i>1}\gamma_{Q.i}\,\Psi_{0.i}Q_{k.i} \quad (2.5)$$

For the SLS calculations, three different load combinations are used, all stated in Equation 2.6 to 2.8.

Characteristic load combination normally, used for irreversible limit states.

$$\sum_{j\geq 1} G_{k.j}"+"P_k"+"Q_{k.1}"+"\sum_{i>1}\Psi_{0.i}Q_{k.i} \quad (2.6)$$

Frequent load combination, normally used for reversible limit states.

$$\sum_{j\geq 1} G_{k.j}"+"P"+"\Psi_{1.1}Q_{k.1}"+"\sum_{i>1}\Psi_{2.i}Q_{k.i} \quad (2.7)$$

Quasi-permanent load combination, normally used for long term effect and effects regarding the appearance of the load-carrying structure.

$$\sum_{j\geq 1} G_{k.j}"+"P"+"\sum_{i>1}\Psi_{2.i}Q_{k.i} \quad (2.8)$$

"+"	Means “To be combined with”
Σ	Means “The combined effect of”
$G_{k.j}$	Characteristic permanent load
$\gamma_{G.j}$	Safety partial factor for permanent loads
γ_Q	Safety partial factor for variable loads
γ_p	Safety partial factor for prestressing force
Ψ_0	Load combination factor
Ψ_1	Load combination factor
Ψ_2	Load combination factor
$Q_{k.1}$	Main characteristic variable load.
$Q_{k.i}$	Characteristic variable load.
P	Prestressing force
ξ_j	Reduction factor

2.3 Preliminary design

In the preliminary design phase, the goal is to define a cross-section, a layout for the prestressing tendon and a prestressing force. These three parameters are chosen such that the bridge design fulfils the criteria in ULS and SLS (SIS, 2005a). The checks that need to be performed are presented in Section 2.3.2 and 2.3.3.

2.3.1 Prestressing and reinforcement steel

In Eurocode 2 (SIS, 2005a) the minimum reinforcement is prescribed, see Equation (2.9). The Swedish regulations (Trafikverket, 2019b) have additional requirements for the minimum reinforcement, described in Equation (2.10). For the cross-section of the beam studied in this thesis (T-beam), the minimum reinforcement is only used to increase the positive moment capacity at the sections over and next to the mid support, which often are critical sections for the design.

$$A_{s,min.EC}\sigma_s = k_c k f_{ct.eff} A_{ct} \tag{2.9}$$

$A_{s,min.EC}$ Minimum cross-section area of reinforcement according to Eurocode.

σ_s Absolut value of the stress in the reinforcement after cracking. Not larger than the yield stress, f_{yk}

k_c Coefficient that considers stress distribution in the cross-section before cracking.

k Coefficient that compensates the impact of uneven residual stresses in the cross-section before cracking and change of internal level arm.

$f_{ct.eff}$ f_{ctm} or lower ($f_{ctm}(t)$) if cracking occurs before 28 days after cast.

f_{ctm} Mean tensile strength of concrete.

A_{ct} Concrete area in the tensile zone.

The Swedish addition to EC is that the amount of cross-sectional area of the reinforcement should be at least:

$$A_{s,min} = min(4.0\frac{cm^2}{m}, 4.0 * \frac{f_{ctm}}{3}\frac{cm^2}{m}, \rho_{min} * A_c, A_{s,min.EC}) \tag{2.10}$$

$A_{s,min}$ Minimum cross-section area of reinforcement

A_c Concrete cross-sectional area.

ρ_{min} 0.08 if b_w / h > 5, otherwise 0.05

Eurocode 2 (SIS, 2005a) limits the maximum tendon force by introducing the maximum allowable stress at the active side during tensioning according to Equation 2.11.

$$\sigma_{p.max} = \min \begin{matrix} 0.8\, f_{pk} \\ 0.9\, f_{p0,1k} \end{matrix} \quad (2.11)$$

f_{pk} Characteristic tensile capacity
$f_{p0,1k}$ Characteristic 0,1% strain limit

Directly after the release of the tensioning the maximum allowable stress is reduced and stated in Equation 2.12.

$$\sigma_{p.m0} = \min \begin{matrix} 0.75\, f_{pk} \\ 0.85\, f_{p0,1k} \end{matrix} \quad (2.12)$$

2.3.2 Ultimate limit state

Calculations of the capacity in ULS is rather similar to a normal reinforced concrete section. The behaviour of the prestressing steel can be treated with two different stress-strain relationships according to Eurocode 2 (SIS, 2005a). One where there is no limit for the strain, but the maximum stress is set according to Equation 2.13.

$$f_{pd} = \frac{f_{p0,1k}}{\gamma_s} \quad (2.13)$$

For the other stress-strain diagram there is a limit for the strain, ε_{pud}, but the stress is allowed to increase over f_{pd} according to Figure 2.7.

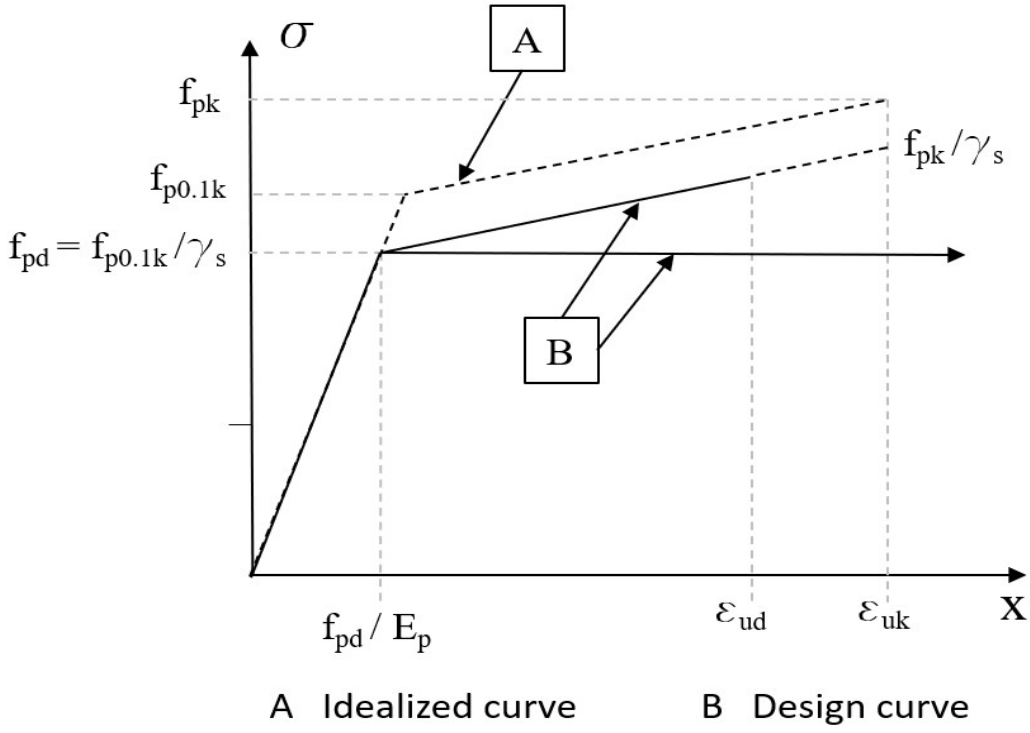

Figure 2.7 - Stress-strain diagrams for ULS design adapted from Eurocode 2 (SIS, 2005a).

Another difference from normal reinforced concrete is that there is an initial strain in the steel from the prestressing, ε_{p0}. Together with the strain from the load effect, $\Delta\varepsilon_p$, the total strain of the prestressing steel, ε_p, can be calculated.

$$\varepsilon_p = \varepsilon_{p0} + \Delta\varepsilon_p \tag{2.14}$$

The moment capacity for the section is calculated according to Equation 15 with the strain relationship presented in Figure 2.8

$$M_{Rd} = F_P * z \tag{2.15}$$

M_{Rd}	Moment capacity
F_P	Prestressing force
z	Internal level arm

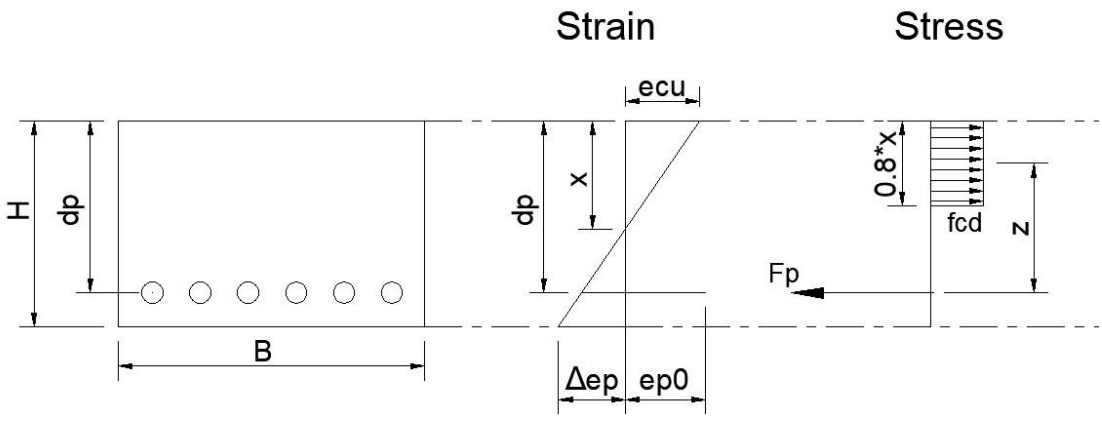

Figure 2.8 – Strain relationship for prestressed concrete section.

ε_{p0}	Strain in the tendons due to prestressing
$\Delta\varepsilon_p$	Strain in the tendons due to load effect
ε_p	Total strain in tendon
ε_{cu}	Strain in concrete

2.3.3 Service limit state

According to Eurocode 2 (SIS, 2005a), the following stress limitations need to be fulfilled.

For structures in exposure class XD, XF, or XS the maximum concrete compression stress under characteristic loading is limited due to micro-cracks, which can appear for concrete under high stress. The limit is set to:

$$|\sigma_{cc}| \leq 0.6 * f_{ck}$$

To assume linear creep, the concrete compression stress under quasi-permanent load needs to be limited to:

$$|\sigma_{cc}| \leq 0.45 * f_{ck}$$

To avoid cracking, which can be critical in prestressed concrete structures, a check that the concrete is in compression within $\pm\ 100mm$ from the tendon duct is performed. This limit holds for structures in exposure class XD1 and XD3, which the different parts of the superstructure can be assumed to be in. The concrete stress is calculated under frequent load combination.

$$\sigma_{cp} \leq 0$$

It is also needed to perform a crack width control. The maximum crack width is depending on the exposure class and can be found in Table 7.1N in Eurocode 2 (SIS, 2005a). If the whole concrete structure is in compression under quasi-permanent loading, no crack width control needs to be performed.

There is also a requirement from the Swedish Transport Administration (Trafikverket) on the total deformation. Maximum deflection in both longitudinal and transverse direction is set to *l*/400 under frequent load combination, where *l* is the theoretical span length (Trafikverket, 2019b).

2.3.4 Accidental limit state – Rupture of prestressing steel

In the Accidental limit state (ALS) the load-bearing capacity should be checked with a reduced amount of prestressing steel. According to Krav Brobyggande (Trafikverket, 2019b), the amount should be set to one prestressing cable that is missing. The reduced amount of prestressing steel should then fulfil the following requirements (SIS, 2005b):

SLS – Frequent: $\sigma_{ct} \leq f_{ctm}$

ULS $M_{Ed} \leq M_{Rd}$
with the material coefficients $\gamma_{steel} = 1.0\ and\ \gamma_{concrete} = 1.2$

The ALS check is not included in this preliminary design phase but needs to be included in the final design of the bridge.

2.4 FE modelling of concrete structures

Prestressed concrete bridges have a non-linear behaviour after cracking of the concrete (Rombach, 2004). When designing this bridge type, the FE-analysis is conducted for the structural analysis, with the focus on determining the sectional forces and stresses in the structure. In the standardized structural design, the structural analysis is conducted through a linear analysis which is a simplification that needs verification (Rombach, 2004). A non-linear FE-analysis, reflecting the real non-linear material response, is too time-consuming in engineering practice. Therefore, the simplification in the linear analysis is assumed to be accurate enough and is approved in Eurocode 2

to be used for both ULS and SLS calculations (SIS, 2005a). In linear analysis, it is possible to superimpose the load effects from the loads (Pacoste et al., 2012).

A beam with a T-shaped cross-section could be modelled in different ways. Either it could be modelled with shell elements representing the bridge deck and the girder web, respectively. This would give a high degree of accuracy, but also requires more computational power. (Rombach, 2004). The use of shell elements is also depending on that the web and flange are slender enough, otherwise they need to be modelled as solid elements according to Rombach. The cross-sectional shape typically used for the type of bridge studied here is not considered slender and therefore, shell elements are not used.

Another way of modelling is to use shell elements for the bridge deck, and beam elements for the main bridge girder, with the beam elements connected to the shell elements at the mid-surface of the bridge deck. In this case, the dimensions have to be modified such that the total bending stiffness of the model is the same as for the real structure (Rombach, 2004). The simplest way of modelling is to only use a beam element with a T-section for the analysis, which gives the sectional forces for the beam directly. This could preferably be used in an early phase in the design process where short computational time is important, and the accuracy of using beam elements only is high enough.

When modelling the supports, the translations and rotations are often set to be fixed or to be free. This is a commonly used simplification from the reality where there is a stiffness in the connection between the supporting structure and the superstructure. To model the connections in a more realistic way, the use of translational and rotational springs can be used (Pacoste et al., 2012).

2.5 Cost and global warming potential for the materials

In this study, the optimization criteria are either the investment cost of the concrete and prestressed steel or the global warming potential of the two materials. The cost is evaluated in Swedish crowns (SEK) as a comparison for the change in investment cost. The total cost of the bridge is not calculated, the cost criteria are only used for comparison of the different bridge designs. The GWP is evaluated in CO_2 – equivalents, which is a measurement of how large the impact is on global warming. It's a way of making the greenhouse gases comparable to each other by multiplying them with a factor that represents how large the impact is on global warming (Naturvårdsverket, n.d.). All greenhouse gases that are emitted in the production of the material is then summed into a value of CO_2 – equivalents per cubic meter material.

The material cost and GWP of the materials may differ depending on the production and the material class. The values chosen for this comparison is from commonly used material for a road bridge in Sweden. The CO_2 – equivalents for concrete are from an Environmental Product Declaration (EPD) made for a recipe that is supposed to represent a standard concrete for bridges in Sweden (Svensk Betong, 2017). This value is also used in the Swedish Transport Administration's tool Klimatkalkyl (Trafikverket, 2020), which is used to calculate the GWP of bridges. The value for prestressing steel is also taken from the tool Klimatkalkyl (Trafikverket, 2020) and is multiplied with the

density for steel, 7800 kg/m^3. Values for both concrete and prestressing steel can be found in Table 2.3.

For the economic comparison, the cost of concrete and prestressing steel will be calculated separately and summarized for each bridge design. The cost of concrete will only include the material used in the superstructure. This is due to the change in dimensions of the cross-section will only have a small influence on the cost of the work needed for the casting and formwork. The cost of concrete in class C35/45 which is normally used for this type of bridge is set to 1800 SEK/m^3 (Yavari et al., 2016).

For the prestressing steel, the cost of work will be included since it directly corresponds to the number of tendons that are used in the bridge. The calculation of the cost will include both a fixed and a variable cost. The fixed part is for each tendon which represents the cost of each anchor and the work that is needed for one anchor. The variable part is the material cost and the amount of work needed per meter cable. The time of work needed is then multiplied with a representable cost for one construction worker. All the values in Table 2.2 are representable for standard bridge construction in Sweden and are given by Göran Hannrup (personal communication, 19 April 2021), Work Manager at PEAB in Gothenburg.

Table 2.2 - Cost of material and work for prestressing steel

	Material cost	**Work time**	**Work cost (500 SEK/h)**
Anchor	5000 SEK	3h	1500 SEK
Cable / Duct	450 SEK/m	0.15 h/m	75 SEK/m

The final values which are used for the evaluation in this thesis of the designs are presented in Table 2.3.

Table 2.3 - Cost and C02 - equivalents for the optimized materials.

	GWP [CO_2-eq/m^3]	**Cost [SEK/m^3]**
Concrete C35/45	388	1800
Prestressing steel	8580	*

**Calculated according to Table 2.2*

3 Parametric design

Parametric design is a type of design process that utilizes a few parameters to determine the structural form, its members and their geometry, and to iterate changes of the parameters to obtain alternative structures.

3.1 Parametric modelling

Parametric modelling is a new technique in civil engineering practice, originally used by architects for computer models of complex three-dimensional (3D) structures (Fu, 2018). By using parametric modelling, it is not necessary to remodel since it is sufficient to change some parameters and obtain a new 3D design. The implementation of parametric modelling on software is often made through programming code in the shape of a script, where different dimensions and variables are dependent on the parameters.

Structural engineers have over the years developed and adopted this method and taken advantage of it. When a parameter (e.g., beam height) is modified, the model will automatically change (Fu, 2018), including tendon layout, cross-section, etc.

3.2 Parametric optimization

Parametric optimization is performed to obtain the most optimal value of specific parameters such that the solution is either maximized or minimized concerning chosen evaluation criteria. Optimization of complex structures, defined through parametric modelling, as the prestressed bridge in this thesis, becomes complicated since the design problem does not have a closed-form solution (Gosavi, 2015).

In Figure 3.1 the complexity of the design process for a prestressed bridge is illustrated by a flow chart and compared with the design process of a normal reinforced concrete bridge. This design process results in a more complex optimization where the section forces are dependent on the geometry of the structure and the tendon layout.

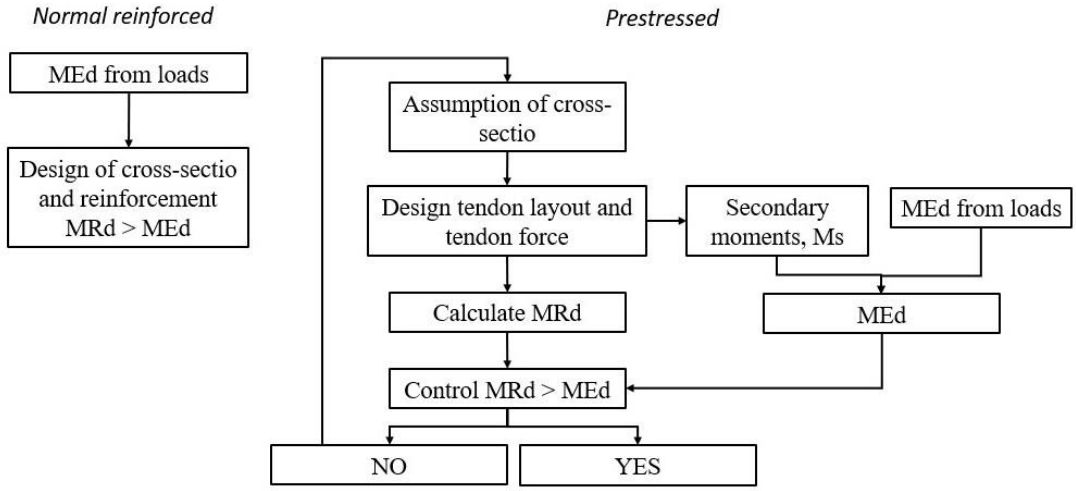

Figure 3.1 - Simplified flow chart of the design process for a normal reinforced concrete bridge and a prestressed concrete bridge.

Without the closed-form solution, an iterative process is needed to reach the most optimal design. However, an iteration process leads to an increase in computational time and power.

The optimization method implemented in this thesis is using set-based parametric design (SBPD) (Rempling et al., 2019). In today's design process, the normal design method is called Point-based design (PBD). With this method, one design is chosen in the early stage of the preliminary design, often based on experience and previous designs. This design is modified throughout the design process until the design meets the requirements (Ström et al., 2016). With this PBD method, it is not ensured that an optimal design concerning material efficiency has been reached although it fulfils the requirements.

Because of the lack of efficiency for the PBD method, engineers have developed the method Set-based design (SBD). The difference between PBD and SBD is that in SBD several alternative solutions, a set of solutions, are involved in the process from the beginning to include a wider range of solutions. These wide differences in solutions are under the process narrowed down after evaluation and discussion between the different stakeholders and design instances (Rempling et al., 2019). The SBD was first developed in the car industry, and the sets have a wide range of robust designs choices, i.e., if it would be related to bridge construction it can be used in an early design stage where the type of bridge, material choice, etc. would be design choices to be determined during the SBD process.

The SBD has been developed to Set-based parametric design (SBPD) when the SBD was included in software engineering. SBPD is a merge of both parametric modelling and the SBD method. A normal area of use for the SBPD is three-dimensional design (3D-Design) (Rempling et al., 2019). The SBPD compared to SBD can be implemented in a deeper level of detailing since, for example, specific geometry parameters can be chosen as parameters to investigate while the SBD main focus has been to establish an efficient production and design process between different stakeholders.

Neither the SBD nor the SBPD has been implemented to a large extent in the structural engineering industry. Although Rempling et al. (2019) investigate the possibility to implement the SBPD in the early design phase of a bridge, where both bridge type and specific geometry properties are investigated and compared to achieve an optimal bridge design.

This thesis is implementing SPBD in the preliminary design process by optimizing a selection of parameters for a specific bridge type. The method requires sets for each parameter, both the parameters and their sets are explained more in Chapter 5, where the implementation of SBPD is explained in more detail for this thesis.

4 Parametric modelling for prestressed bridge

In this chapter, the FE model which is used for the optimization in Chapter 5, is described. The focus is on how it is modelled to represent the behaviour of the bridge, what geometrical assumptions have been used, and the loads that are included with a description of how they are applied in the FE model.

4.1 Tendon Layout

For the tendon layout, the built-in spline tool in BRIGADE/Plus (Scanscot Technology, 2021) is used. The spline tool creates a parabolic shape from coordinates chosen by the user (Scanscot Technology, 2015). The coordinates to be determined are chosen to the 6 points illustrated in Figure 4.1. The tendon layout is determined through testing of different values for these points, from the literature study and discussion with experienced structural engineers. Two important parameters have been used for the placement of the tendon. These two parameters, which are the distance between point two and point five, L_0, and the eccentricity $e(x)$ at the lowest point in the span, e_{span}, are both illustrated in Figure 4.1.

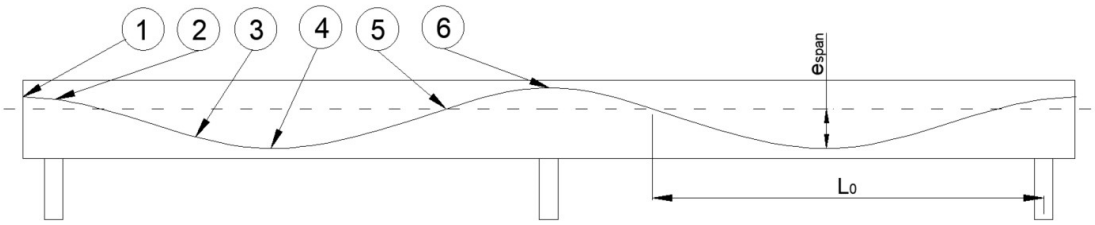

Figure 4.1 - Coordinates for input to generate tendon layout in the FE model.

Point 1
The first points eccentricity is determined to the minimum of 550mm from the top of the beam or 25% of the distance between the centre of gravity and the top of the beam. This is to avoid large tensile stresses in the bottom of the beam. 550mm is a normal minimum distance to have enough spacing for anchorage and hydraulic jacks at both ends.

Point 2
Outside the end support, it is desirable to minimize the inclination of the tendon. Therefore, a second point is added over the support where the eccentricity is set to the minimum of 600mm from the top of the beam and 20% of the distance between the centre of gravity and the top of the beam.

Point 3
The purpose of point three is to lower the cable a bit before the maximum eccentricity in the span. The placement in the longitudinal direction is chosen to 35% of L_0 from the support and set with the eccentricity 85% of the maximum eccentricity e_{span}.

Point 4

The lowest point of the cable is located at 60% of L_0 from the end support. The maximum eccentricity in the span region, $e_{span,}$ is found at this point. It has an impact on the secondary moment, where an increased e_{span} creates a larger secondary moment. With evaluation from different design configuration tested, e_{span} has different effects for different geometries and designs. To adapt the optimization for every bridge design, the parameter e_{span} is chosen as a new parameter to include in the SBPD. The set for this parameter is chosen to contain a minimum of 3 values, to keep the computational time as low as possible but at the same time be adaptable for the different span lengths.

The minimum concrete cover for prestressed steel is 80 mm with an additional 10mm added in the design to compensate for deviations (SIS, 2005a). To ensure enough space for additional normal reinforcement in the final design phase, the concrete cover for this thesis is set to 150 mm. With the standard dimension of the duct of around 100 mm, the lowest point of the midline for the duct is 200mm from the bottom of the cross-section. The parameter e_{span} is varied with a factor, α_{span}, which is a percentage of the distance between the centre of gravity and the bottom of the cross-section, L_{CG}. The eccentricity of the cable is calculated according to Equation 4.1. The set for e_{span} is decided to vary in the range depending on the factor α_{span} set to a value between 0% and 20%. Figure 4.2 demonstrates the effect e_{span} has on the secondary moment where the size and shape for the secondary moment for the different e_{span}.

$$e_{span} = L_{CG} - (200\,mm + \alpha_{span} * L_{CG}) \tag{4.1}$$

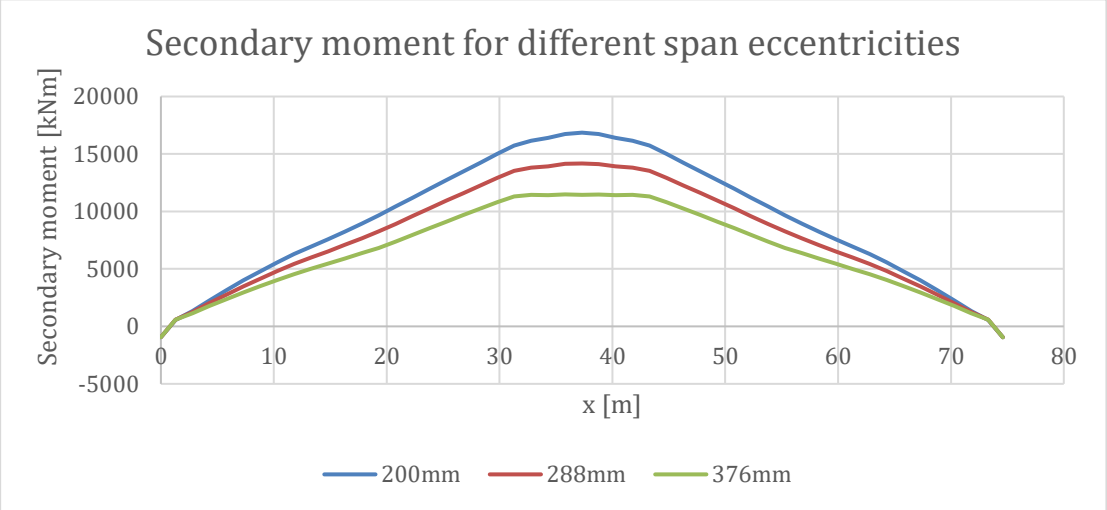

Figure 4.2 - Secondary moment for an 8m wide bridge with 36m spans with different eccentricities in the span. Distance presented for the different eccentricities is the distance from the bottom of the beam to the centre of the tendon.

Point 5

Where the cable crosses the centre of gravity, point 5, is set by the earlier mentioned variable L_0.

As a starting point, the tendon layout is designed such that it follows the shape of the moment diagram for the bridge. In the investigation which can be seen in Figure 4.3, different factors multiplied with the span length were chosen as value for L_0 for a bridge

with 32m span lengths, which is representative for this type of bridge. From the figure, the value of L_0 should be fixed to 85% of the span length for the curve of the capacity to follow the curve of the load effect in the best way.

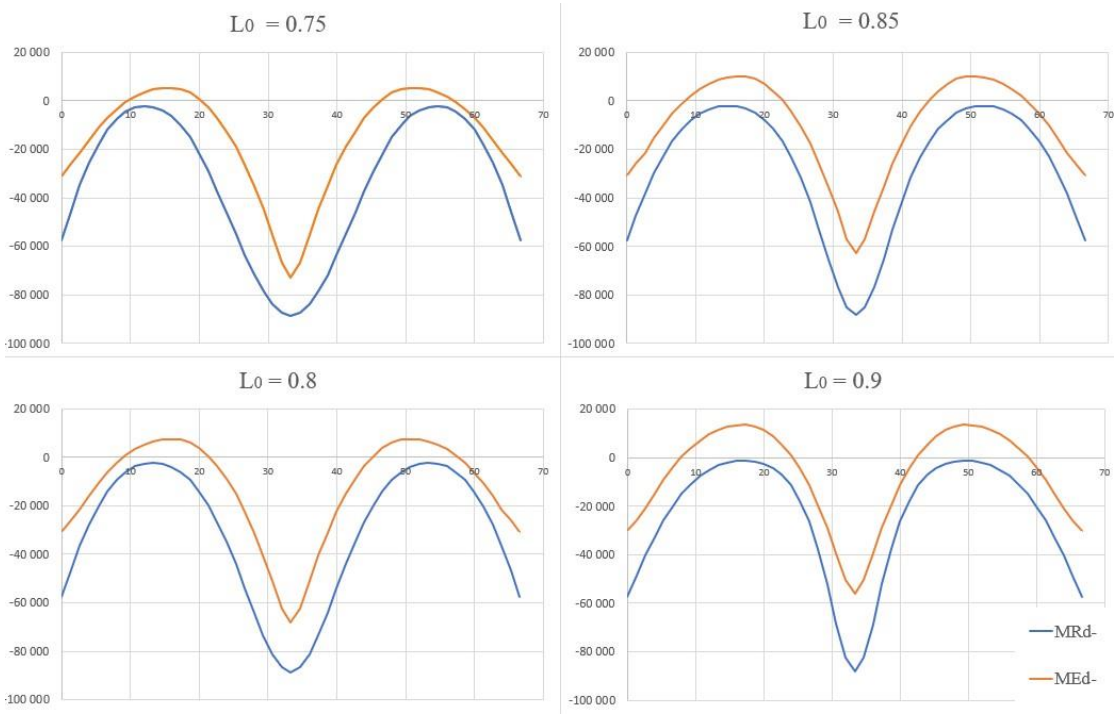

Figure 4.3 - Case study of how the moment capacity follows the sectional moment for different values of L0.

This point also influences the secondary moment similarly to the factor e_{span}, a larger value on L_0 creates a larger secondary moment. Since it is favourable to decrease the secondary moment for some bridges, the value of L_0 is chosen to be included as an optimization parameter. In the set of L_0 values between 75% and 85% can preferably be included in the optimization to find the best solution.

Point 6

The final point will be located at the maximum allowable eccentricity over the mid support, i.e., 200mm from the top edge of the cross-section. This parameter is not changed since the mid support often is a critical section where maximum capacity is needed and a high tendon over the mid support is decreasing the secondary moment, which is desirable.

4.2 FINITE ELEMENT MODEL

This section describes the resulting FE model with geometry simplifications, assumptions, and other important steps in the modelling process. The shape of the structural parts and the geometrical relations are set in consultation with an experienced engineer to represent a common bridge of this type. The structural model consists of one main beam and two cross beams at the end supports. The remaining parts are modelled to simulate the load effect on the structural model, in terms of load positions and inclusion of self-weight, which is described in more detail for each part under Section 4.2.1.

4.2.1 Geometry and element types

The base model has a fixed geometry shape which can be seen in Figure 4.4 and 4.5. Depending on the case-specific input, the dimensions, lengths, and other properties can vary but the main shape of the bridge will remain the same.

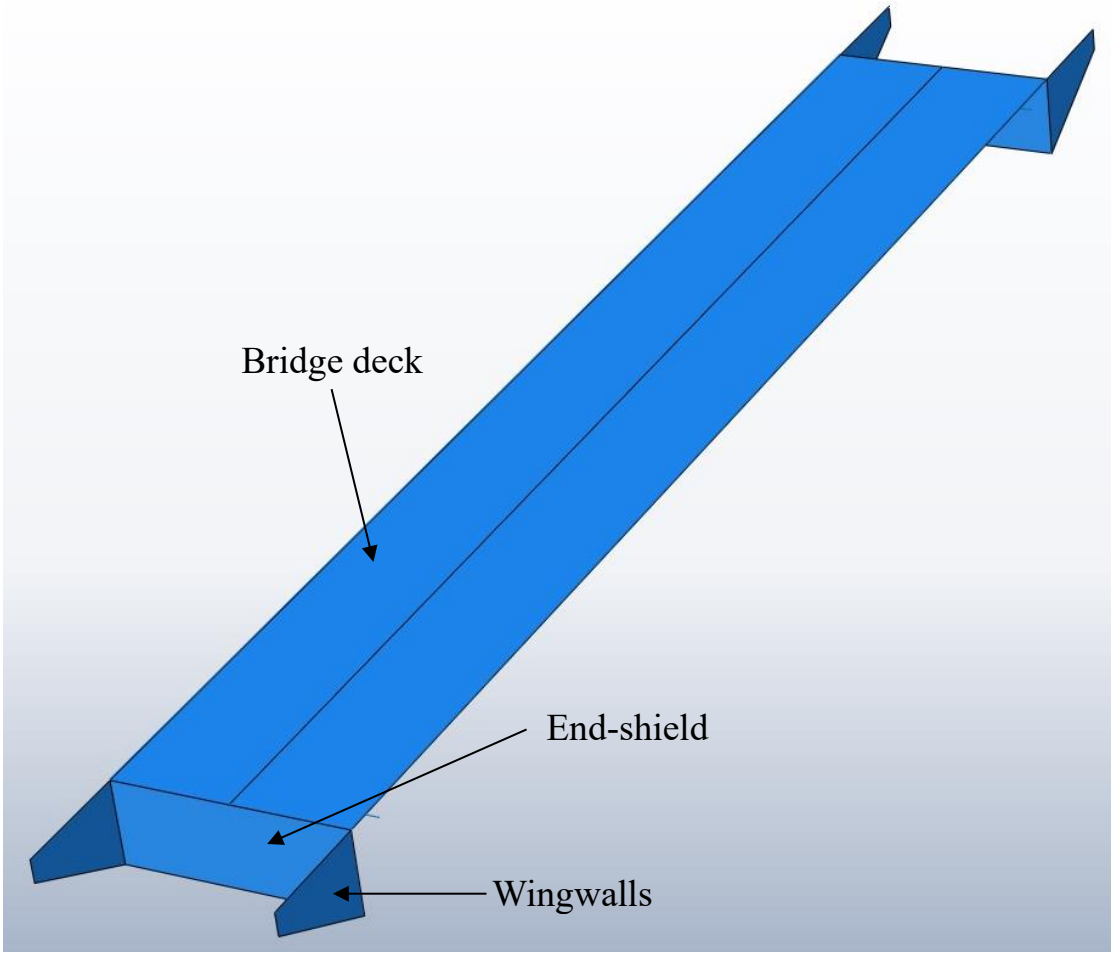

Figure 4.4 - Shape of the bridge from the FE model, including the bridge deck.

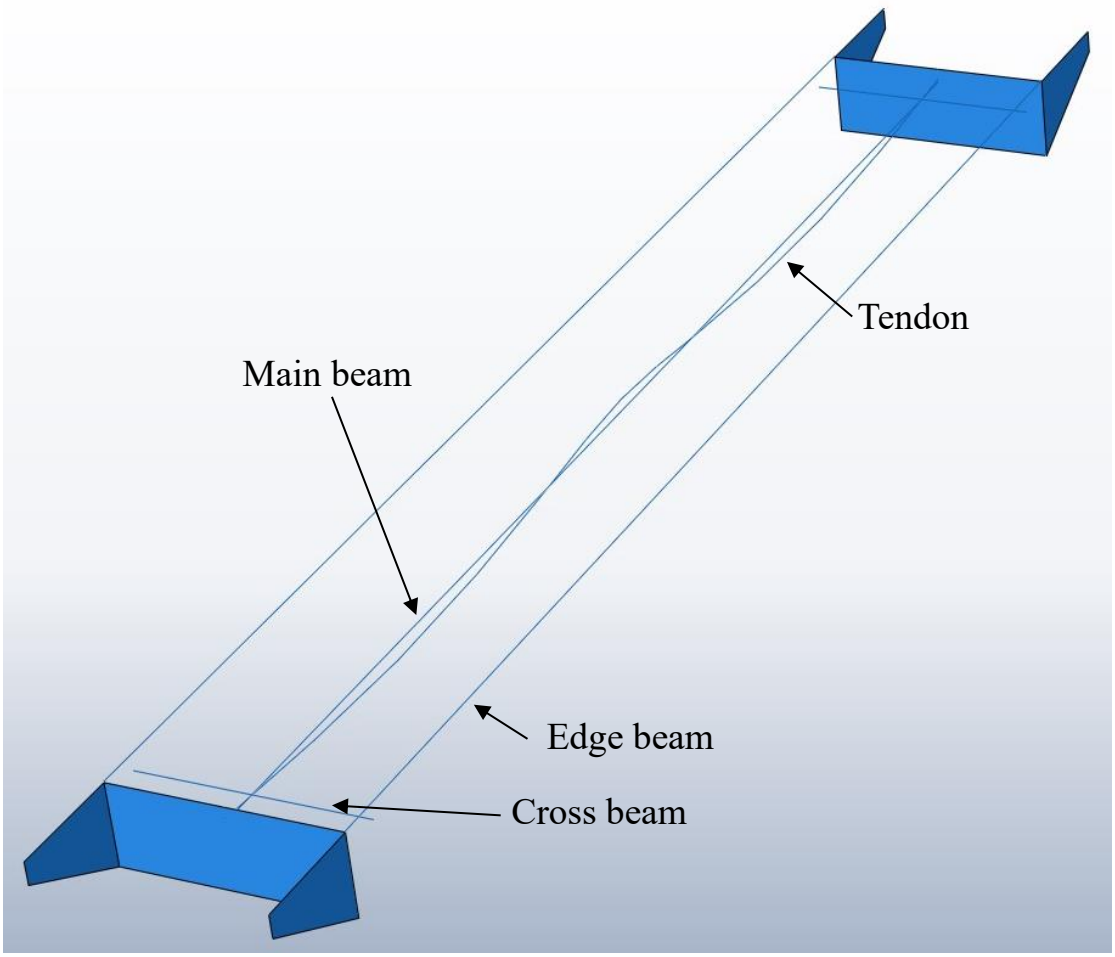

Figure 4.5 - Shape of the bridge from the FE model, excluding the bridge deck to show the different beams and the tendon.

4.2.1.1 Main beam

The main beam is the load-carrying part where the sectional forces and stresses will be checked in the post-processing. The beam is modelled with beam elements to obtain good results regarding bending as described in Section 2.4 and still maintain an efficient FE model. The cross-section treated in this thesis is a T-section with constant dimensions along the beam. BRIGADE/Plus and the construction industry has different sign conventions for the sectional moment. To counteract this and achieve post-processing results for the structural engineering industry, the cross-section is modelled as a flipped I-section without a top flange and the bottom flange representing the top flange in a T-section. The cross-section is orientated as the correct T-section and the sectional moments will follow the structural engineering sign convention.

The width of the top flange is modelled 100 mm shorter on each side compared with the bridge deck, according to Krav Brobyggande (Trafikverket, 2019b). Both the thickness of the top flange and the web width is specified in the input data to the python script controlling the model, although in this thesis the top flange thickness is set to be 0.3 m and the web width is set to half of the bridge deck as a standard value. However,

these values can be modified to adapt to the specific bridge studied. The material for the main beam is set to a standard concrete class, with the corresponding properties.

4.2.1.2 Bridge deck

The bridge deck's main purpose is to act as a loading area for the traffic loads with the correct eccentricity from the middle of the bridge. Shell elements are used for the bridge deck to obtain the loading area. Since it is the main beam that is to be designed, the other structural parts must not affect the load effect on the beam. Therefore, a fictitious material for the bridge deck is defined.

The material is defined with almost zero stiffness in the longitudinal direction while it is very stiff in the transverse direction. The traffic loads are therefore carried straight into the middle of the deck where a tie connection, which is described in Section 4.2.2, transfers the load to the beam. Since the bridge deck is included as the top flange in the cross section of the beam, the density for the shell element is set to 0.

4.2.1.3 Edge beam

The edge beams are modelled with beam elements and a rectangular cross-section, only to include their self-weight in the FE analysis. The material is a fictitious material with almost zero stiffness in every direction to minimize the contribution to the stiffness of the structure, but it has the same density as concrete.

4.2.1.4 Cross beam

At each end support, a cross beam is modelled with the same length as the bridge width. The cross beam enables more accurate support conditions for the main beam and increases the possibilities to include an analysis of the substructure in the future. The same concrete is used for the cross beam as for the main beam.

4.2.1.5 Tendon

The prestressing tendon is modelled with a wire element which has the layout as presented in Section 4.1. The cross-sectional area for the element is set to the combined area of all cables in the bridge for the studied case. The material for the prestressing steel is set to a standard prestressing steel with the density of 7800 kg/m^3 and tensile strength f_{puk} of 1860 MPa, the material properties can be changed if other steel qualities are used.

4.2.1.6 Wingwalls and end-shields

The wingwalls are lined up in the longitudinal direction of the bridge, where the length of the wingwall, L_{ww}, and height of the end of the wingwall, H_2, needs to be set. The height of the wingwall closest to the bridge, H_1, can be obtained by assuming a 1:2 slope of the inclined side. The height of the end-shields is set to have the same height as the wingwall, H_1. The geometry can be seen in Figure 4.6. In this thesis L_{ww} is set to 5.8 m and H_2 is set to 1.1 m.

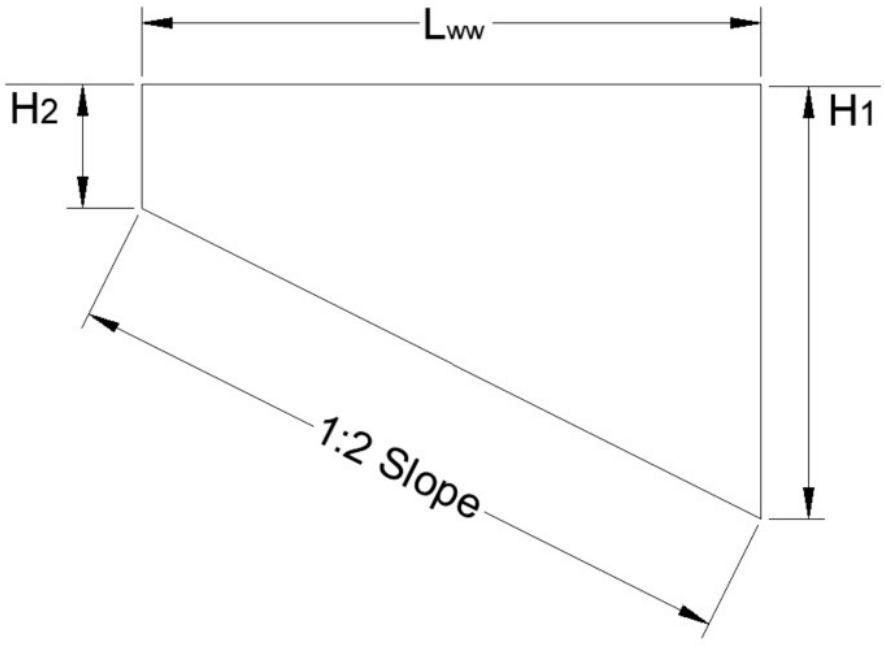

Figure 4.6 - Illustration of the wingwall design

Both the end shield and the wingwall are shell elements to enable a loading surface for the earth pressure. The material is set to a standard concrete class.

4.2.2 Tie connections

Since the bridge deck is created as a shell element to carry the loads into the beam, a tie between these two parts is created. This is done by attaching the midline of the bridge deck to the main beam, by using the same element sizes on both parts the connection will interact vertically as shown in Figure 4.7. The tie is acting as a stiff connection which enables the moment and the sectional forces to be transferred from the bridge deck to the beam, which is the load-carrying structural element.

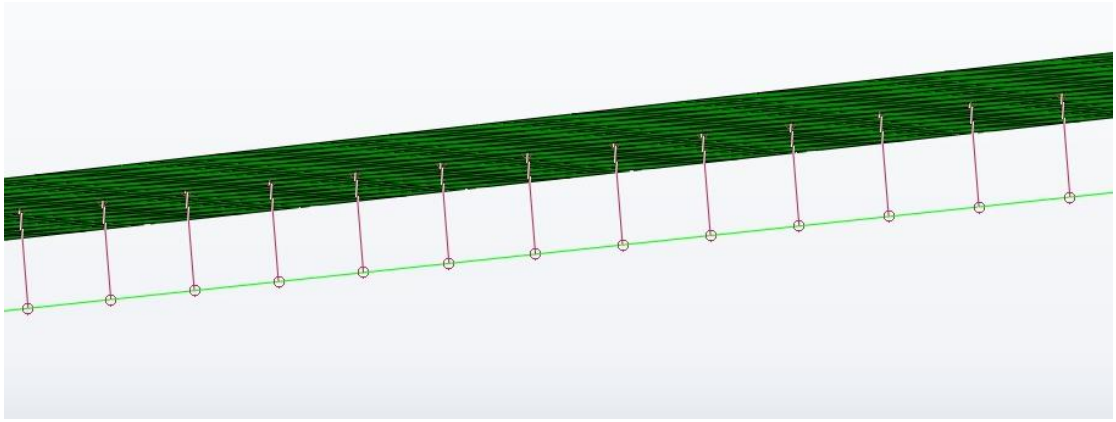

Figure 4.7 - Tie connection between bridge deck and beam. Picture from BRIGADE/Plus.

In the same way, the edge beams have been tied to the respective edged of the bridge deck to transfer the self-weight with its eccentricity, Figure 4.8 shows this connection in the FE-model.

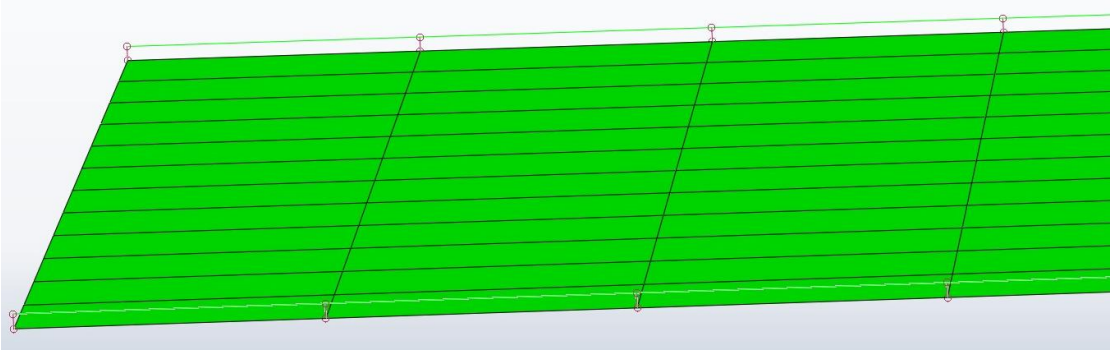

Figure 4.8 - Tie connection between edge beam and bridge deck. Picture from BRIGADE/Plus.

4.2.3 Boundary conditions

Figure 4.9 demonstrates the positions for the boundary conditions, located at the edges of the cross beams and the mid support. The mid support is constructed as a fixed bearing for the displacement degrees of freedom (DOF) and free for the rotation DOF. To strengthen the opportunities for future development and use of this optimization tool the DOFs in the transverse and longitudinal direction of the mid support is modelled as spring support to enable the modelling of a substructure in the future. For this model, the spring supports have been assigned a high spring stiffness since the substructure's behaviour is unknown.

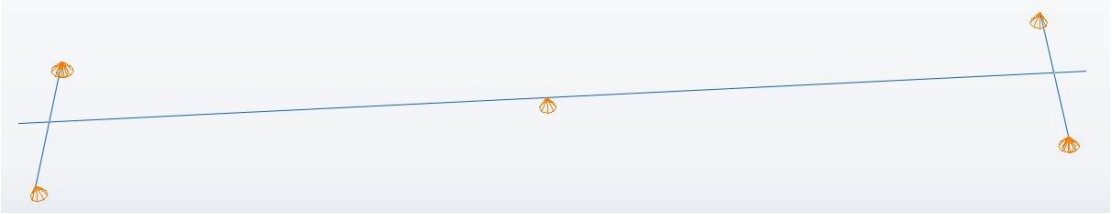

Figure 4.9 - Placement of boundary conditions. Image from BRIGADE/Plus.

The end supports are movable bearings to avoid internal forces and restraints. To prevent a rigid body movement, two of the four edge supports are locked in the transverse direction, as illustrated in Figure 4.10.

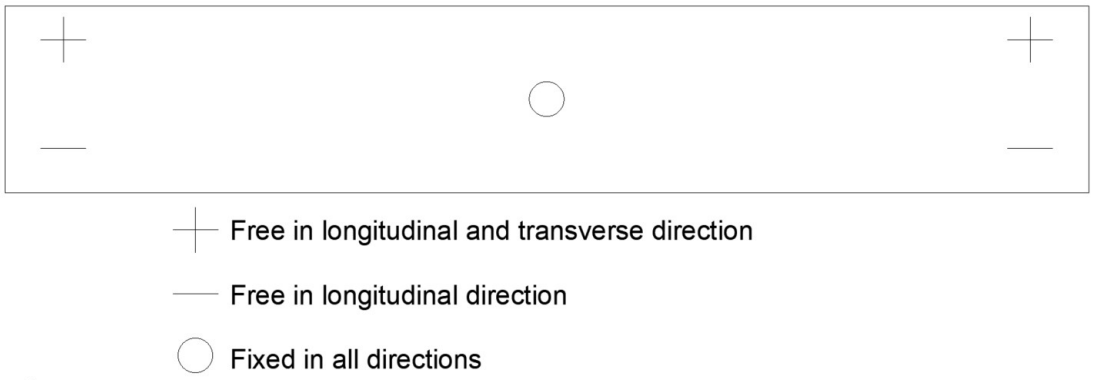

Figure 4.10 - Illustration of the support behaviours. Translational degrees of freedom. Bridge seen from above

4.2.4 Mesh size – Convergence study

To ensure a mesh size that has sufficient accuracy and minimal computational time a convergence study has been done. The study is based on the base model with two 32m spans and 1.3 m between the end supports and the end-shields. Since the length of the bridge is dependent on the case specific conditions, the mesh sizes are constructed as a function of the total bridge length, which is 66.6m for the current model. The mesh sizes used are:

$$\frac{L}{10}, \frac{L}{20}, \frac{L}{50}, \frac{L}{100}, \frac{L}{200} \; and \; \frac{L}{400}$$

The evaluated result is the bending moment with only the self-weight active. From Figure 4.11 the point of evaluation has been chosen to $x = 33.3\,m$, i.e., directly over the mid support.

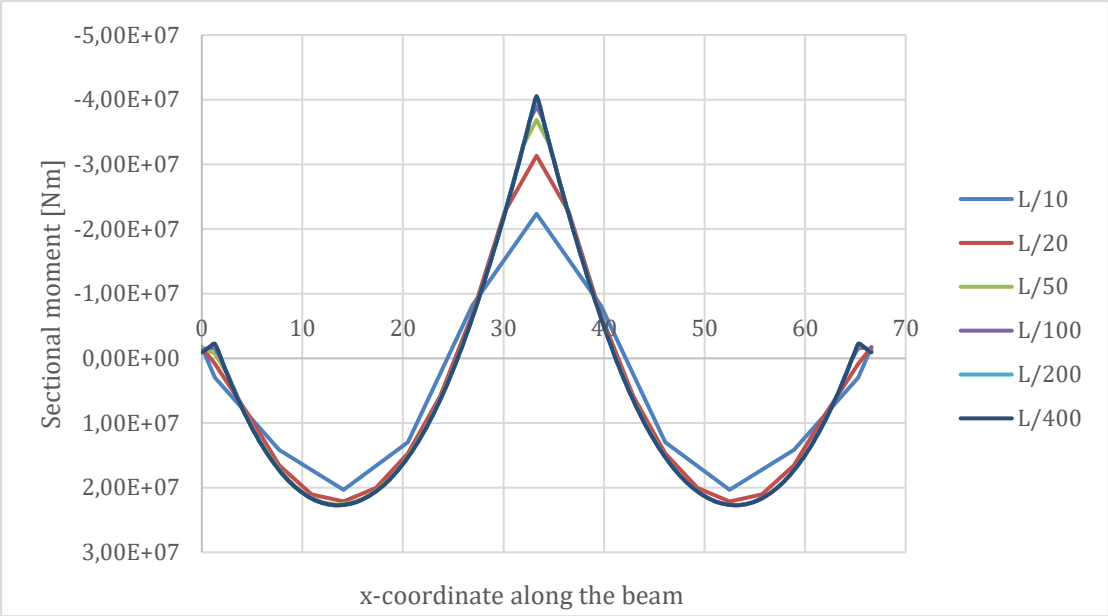

Figure 4.11 - Moment diagram for different element sizes.

Figure 4.12 demonstrates the result of the convergence study. The study is conducted by analysing the error between the current mesh size and the converged solution. The converged solution is set to $\frac{L}{400}$, which for the current model corresponds to a mesh size of 166.5 mm.

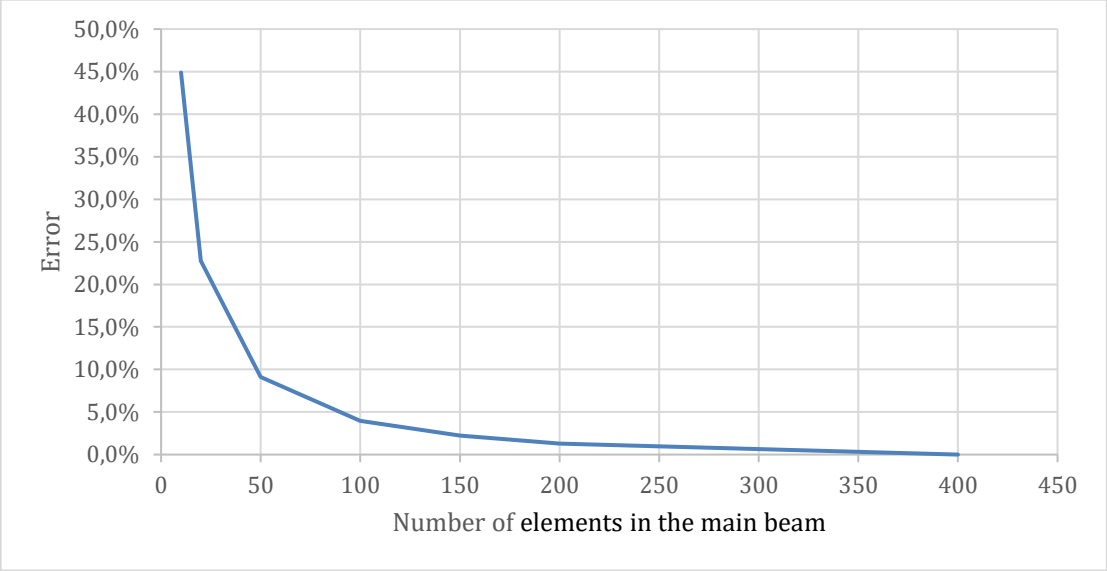

Figure 4.12 - Support moment error for a different number of elements in the main beam

The convergence study shows that an element size of $\frac{L}{100}$ gives a result that has an error of 4.0 % for the support moment and 0.1 % for the field moment. This is considered acceptable for the analysis when also considering computational time, which increases with the number of elements.

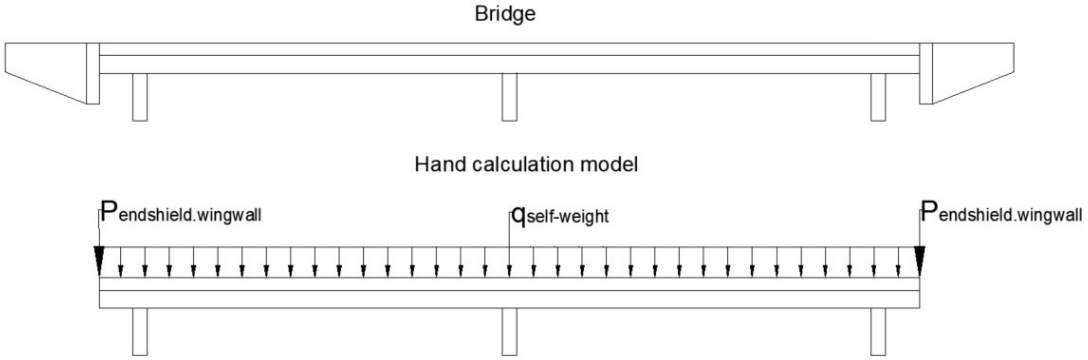

Figure 4.13 - Model used in hand calculations.

4.2.5 FE-model verification

In addition to the convergence verification of the model, a verification that the FE-model works and represents the reality correctly is made. The moment in the midspan and at the mid support are chosen to be compared for verification. Figure 4.11 shows that the chosen mesh size is not of such importance in the mid-span, but differs more over the support. The converged mesh size, L/400, is chosen for the verification of the model to obtain the most accurate comparison at the two sections.

The studied bridge is symmetric, where Figure 4.13 shows the geometry of the bridge and the simplified model used for hand calculations. The cantilevers with corresponding wingwalls and end-shields are included but simplified for the hand calculation by adding a point load on the end of each cantilever, which represents the self-weight of these parts.

The hand calculations are presented in Appendix A and in Table 4.1 the comparison with the FE model results is shown.

Table 4.1 – Verification results of FE-Model.

Maximum moment at	Hand Calculations	FE-Model	Difference
Span	18 980 kNm	19 060 kNm	0.383%
Mid support	34 040 kNm	33 910 kNm	-0.408%

The comparison together with the mesh study in Section 4.2.4 provides enough conviction that the model has good accuracy and reliability.

4.3 FINITE ELEMENT MODEL LOADS

This section describes how the loads are implemented in the FE model and which simplifications are made. The horizontal loads will not be included in the model since the analysis focus on the superstructure the horizontal loads mainly influence the substructure.

4.3.1 Permanent loads

In this section, the permanent loads included in the FE model is described.

4.3.1.1 Self-weight

The self-weight is applied as a gravity load to the whole model according to the density of the material that has been specified. The gravity constant is set to 10 m/s^2 to correspond to the material values in Eurocode 1 (SIS, 2002b). Since the bridge deck is already included in the cross-section of the beam, a surface load representing the self-weight of the 100 mm thick paving is added onto the bridge deck. The density of the paving is set to 2400 kg/m^3 according to Eurocode 1 (SIS, 2002b) and the same gravity constant of 10 m/s^2 is used.

4.3.1.2 Earth pressure

Earth pressure is applied as a hydrostatic surface load on the end-shields and the zero-pressure height is set to be at the top of the end-shield. The earth pressure at rest is calculated according to Equation (4.2). The density of the earth and the coefficient for earth pressure at rest is regulated by the Swedish Transport Administration (Trafikverket, 2019a).

$$q_{earth.rest}(z) = K_0 * \gamma \tag{4.2}$$

$q_{earth.rest}$	Earth pressure at rest depending on depth (z)
z	Depth from zero-pressure level
K_0	Coefficient for earth pressure at rest
γ	Density of the earth

4.3.1.3 Support displacement

The vertical support displacement should be based on the case specific condition (Trafikverket, 2019b). For this study the value is set to 20 mm on each of the three supports and is placed in three different load cases to allow for the least favourable combination. No horizontal support displacement is considered since the effect on the superstructure is neglectable and no analysis of the substructure is made.

4.3.1.4 Shrinkage

The shrinkage is applied as a decreased temperature for the entire bridge which corresponds to the calculated shortening of the bridge due to shrinkage. This corresponding temperature, $T_{shrinkage}$, is calculated with Equation (4.3). The shrinkage strain, ε_{cs} , is calculated according to Eurocode 2 (SIS, 2005a).

$$T_{shrinkage} = \frac{\varepsilon_{cs}}{\alpha_c} \quad (4.3)$$

ε_{cs}	Shrinkage strain
α_c	Thermal expansion coefficient for concrete

4.3.2 Variable loads

In the following section, the variable loads and how they are applied to the model is presented. The braking force has been excluded from the analysis since the load effect on the superstructure is assumed to be neglectable.

4.3.2.1 Temperature

Elongation of the bridge due to a uniformly increased temperature gives an increased earth pressure on the end-shields. This increased earth pressure, $q_{earth.increased}$, is calculated with Equation (4.4) and placed as a hydrostatic surface load on the end-shields, similar to the permanent earth pressure.

$$q_{earth.increase} = \delta * 200 * \left(K_p - K_0\right) * \gamma \quad (4.4)$$

$q_{earth.increased}$	Increased earth pressure due to movement against earth
δ	horizontal movement of the bridge on each side. Maximum $H_1/200$ [m]
H_1	Height of end-shield
K_p	Coefficient for passive earth pressure
K_0	Coefficient for earth pressure at rest
γ	Density of the earth

For the load case with uneven temperature distribution, the recommended values in Eurocode 1 (SIS, 2003b) is a temperature difference of 15 degrees when the upper side is warmer than the lower side and a difference of 8 degrees when the lower side is warmer. These values can be reduced depending on the paving on the bridge. For the studied case with 100mm paving, the reduction factor is 0.7 for the case with warmer temperature on the top and 1.0 for the other case. This results in that the temperature is set to +5.25 degrees on the top and -5.25 degrees on the bottom for one load case and -4 degrees on the top and +4 degrees on the bottom for the other case.

4.3.2.2 Surcharge load

When a vehicle is placed outside of the bridge deck, an extra earth pressure is obtained onto the end-shields, this load is called surcharge load. When the superstructure of the bridge is designed, only double-sided surcharge load needs to be considered (Trafikverket, 2019a). Since the substructure is not analysed, the case with one-sided surcharge load is excluded from the analysis.

According to the Swedish regulations (Trafikverket, 2019a), a 6 m wide strip is set to have a higher load compared to the remaining width of the bridge. The 6-meter-wide area of the higher load will be summarized together with the remaining area with the

lower load to give an average, evenly distributed, surface load ($q_{surcharge}$) on the end-shields. This load is calculated according to Equation (4.5).

$$q_{surcharge} = K_0 * \frac{6m*20\,\frac{kN}{m^2} + (B_e - 6m)*10\,\frac{kN}{m^2}}{B_{es}} \quad (4.5)$$

K_0 Coefficient for earth pressure at rest
B_{es} Width of the end-shield

4.3.2.3 Traffic loads

To reduce the computational time, the amount of vehicle models in the analysis is reduced. To decide which vehicles to include, the load effect on a bridge is analysed for all vehicle models to see which has the largest impact. The studied bridge has the dimensions of 32 m long spans and a carriageway width of 11 m, which is a good representation for the type of bridge studied in this thesis. A plot of the summarized results is presented in Figure 4.14 and the results can be studied in detail in Appendix B. The load effect studied is the sectional moment since the optimization only considers bending in the longitudinal direction. In the figure, the traffic load models chosen to be included in the analysis is presented with different colours while the rest of the vehicle models is presented in black.

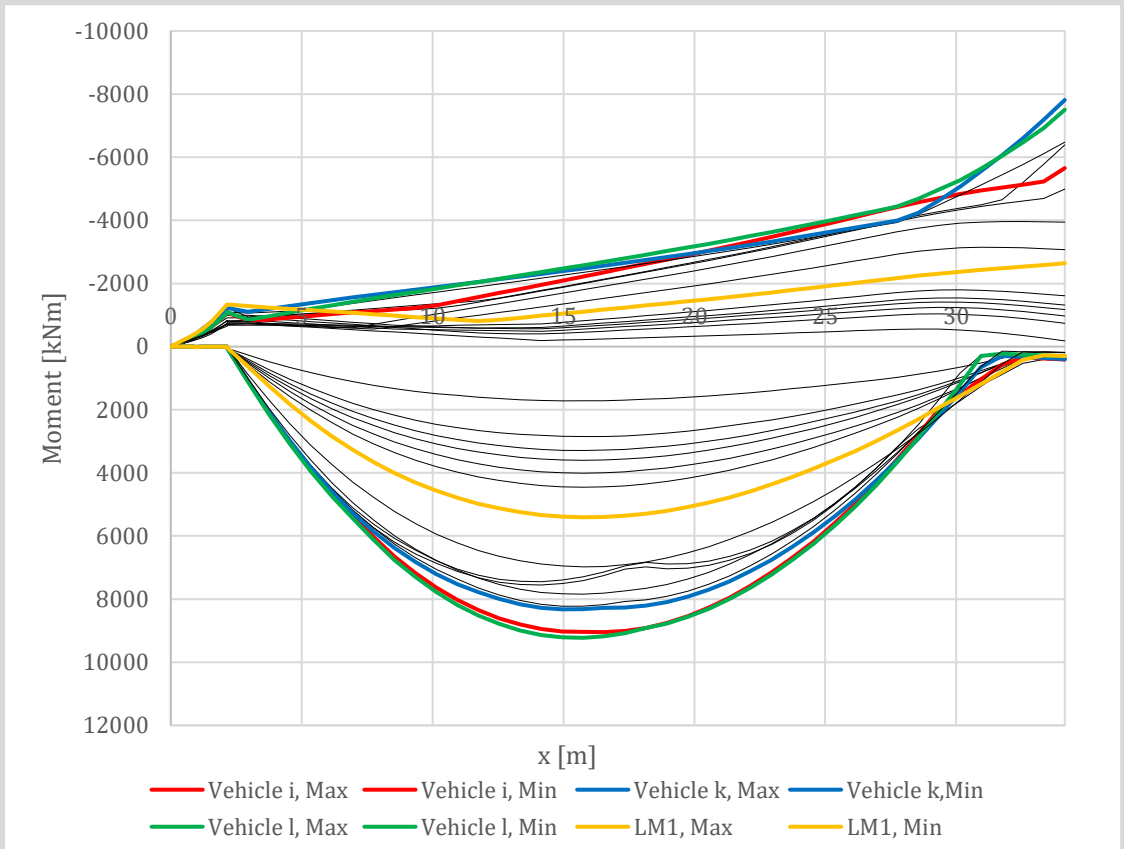

Figure 4.14 - Bending moment in the main beam for different load models, including LM1 (SIS, 2003a) and national vehicle models (Trafikverket, 2019a). Due to symmetry only half of the bridge is displayed.

From this study, it can be seen that the highest support moment appears for Classification vehicle k and slightly lower for Classification vehicle l. For the span moments, it is Classification model i and l that has the largest load effects. Load model 1 (LM1) is also chosen to be included, which results in that the following four vehicle models are used for the analysis:

- Classification vehicle i
- Classification vehicle k
- Classification vehicle l
- Load Model 1

The number of load fields and the width of each field for the traffic loads are depending on the total carriageway width according to the description in Section 2.2.1. The placement in the transverse direction is not varied since it only affects the torsion and rotation, while the bending in the longitudinal direction is not affected by this placement. The crosswise placement of the load fields is set according to Section 2.2.1, Figure 2.6.

The placement of the traffic loads along the bridge is to set to give the least favourable effect. To achieve the most accurate results, the number of placements needs to be large, but many placements require more computational time. To achieve a result that is accurate enough with the least computational time needed, a convergence study is made for the model.

In BRIGADE/Plus (Scanscot Technology, 2021) the size of each step along the bridge where the traffic load can be placed is set to 0.1 m for this model. The number of actual placements that are studied is then controlled by the increment size. It describes how many placements are skipped when the traffic moves forward over the bridge. For example, when the increment is set to 10, the load placement will be at every 1 m with the current step size of 0.1 m.

To reduce the computational time as much as possible, a study has been made to find the largest possible number for the increment that still gives a result that is accurate enough. In Figure 4.14 it can be seen that the setting for the increment has almost no effect on the moment in the longitudinal direction, which is the sectional force that is analysed in this thesis. The increment is therefore set to 80. A larger value on the first increment has a neglectable effect on the computational time and is therefore not taken into consideration.

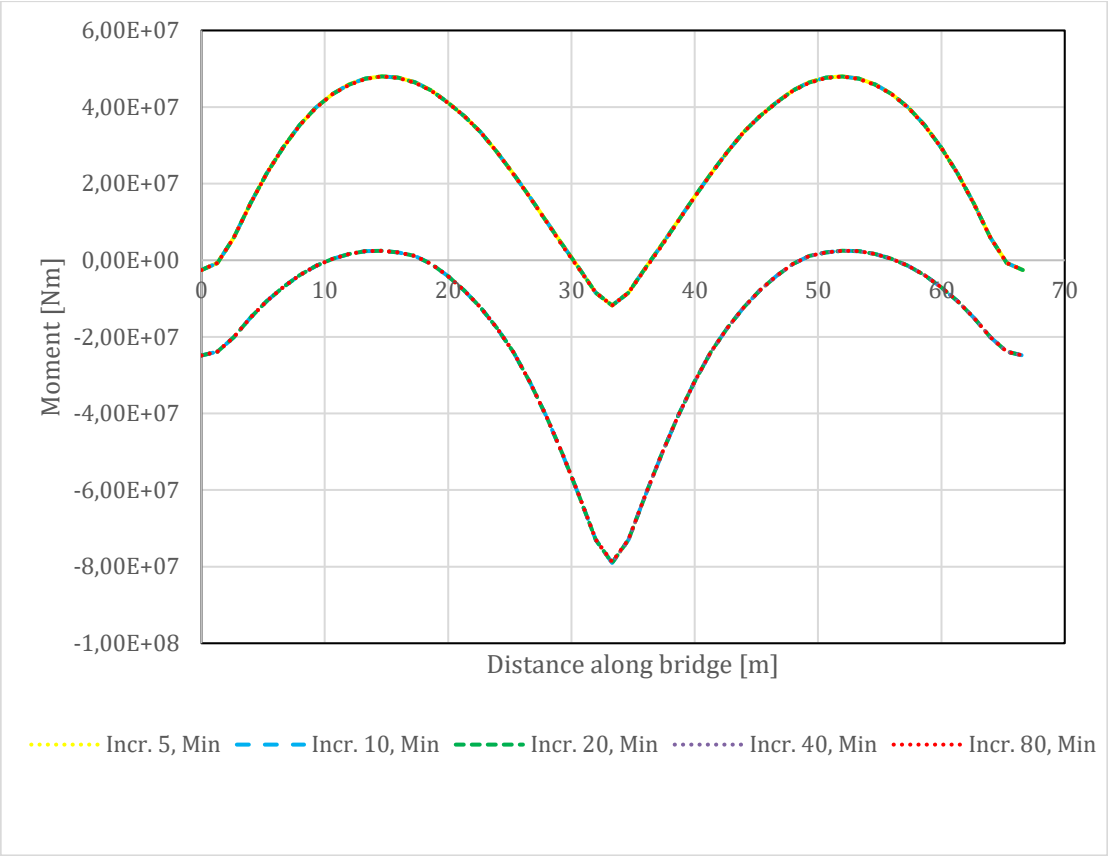

Figure 4.15 - Maximum and minimum moment for different settings on the increment.

4.3.3 Load groups and combinations

For the load combinations described in Section 2.2.2 the module *load combinations* in BRIGADE/Plus has been used. The module creates load groups that place the loads into categories and load cases that later are used in the different load combinations. The needed load combinations for both ULS and SLS described in Section 2.3.2 and 2.3.3 is used.

Envelopes are created by the module for both the load groups and combinations. An envelope contains the maximum and minimum value for the selected output. E.g., the envelope for a specific load combination evaluates the favourable and unfavourable effect of each load and then the maximum and minimum section force can be obtained for post-processing.

5 Optimization with set-based parametric design

The optimization is performed with the Set-based parametric design (SBPD). The parameters to be included in the optimization are chosen to the beam height, h, the number of tendons, n_{tendon} and the two parameters regarding the tendon layout, e_{span} and L_0. The SPBD is performed in the python script where an FE model is constructed for each combination of the parameters and a linear FE analysis of each model is done in BRIGADE/Plus (Scanscot Technology, 2021). The results are checked in both ULS and SLS to evaluate if the combination of parameters gives a bridge design that fulfils the requirements.

As described in Section 3.2, the parameters need initial sets, respectively. The set for h will be decided by the user, in the form of choosing a maximum, minimum and number of heights to be tested inside the interval. The maximum number of tendons, $n_{tendon.max}$, is decided due to the chosen beam width and how many tendons can be fitted into the beam in one single layer throughout the beam. At the ends, the sizes of anchorage and hydraulic jacks have not been considered and therefore a solution with two tendon groups that are separating into two layers at anchorage might be needed, this is not taken into consideration in this thesis. The set for the number of tendons is set from 0 to $n_{tendon.max}$. The sets for the tendon layout parameters, e_{span} and L_0, are also decided by the user. The computational time is the main factor determining the number of values in each set. Section 4.1 described the ranges for these two parameters used in this thesis.

5.1 Optimization of beam height

The evaluation of the solutions is conducted of cost or GWP and the optimal relation between concrete and prestressing steel in terms of these evaluations is unknown. Therefore, all the beam heights in the set are tested since the number of tendons needed can differ between the heights. The evaluation method is described more in Section 5.3.

5.2 Optimization of the tendon layout

The tendon layout optimization is focusing on the effect of the secondary moment and if it is favourable or not. Since both parameters have an impact on the size of this moment the entire sets for e_{span} and L_0 are combined to find the best solution for the bridge, although the sets can be modified before the optimization.

5.3 Optimization for number of tendons

For each beam height, the number of tendons is optimized such that the minimum number that still fulfils the design checks in ULS and SLS is found. An FE analysis is done for all combinations of beam height and number of tendons, which is computationally heavy and time-consuming. To reduce the number of combinations for the FE analysis, the number of tendons needed to be analysed is chosen with an approach based on evaluating the result of the previous number of tendons.

The approach used is including limits on n_{tendon} referred to as lower and upper limit, where the specific number of tendons that is to be analysed is set to the mean value of the two limits. As Chapter 5 described, the set for n_{tendon} is ranging between 0 and $n_{tendon.max}$. The upper limit $n_{tendon.max}$ is set when choosing the centre-to-centre distance, cc_{duct}, between the ducts. This distance together with the concrete cover will determine how many tendons is possible to fit in one layer over the web width.

Every height is first analysed and evaluated with the maximum number of tendons possible, $n_{tendon.max}$. If the evaluation of the results says that more tendons are needed to fulfil all the requirements, no more analyses are performed for the current beam height. If the evaluation results in that the design fulfils the requirements or that the failure is due to too many tendons are used, the number of tendons checked is then set to be the upper limit. If a solution is not fulfilling the criteria due to lack of prestressing force, the current number of tendons will set to be the lower limit. With this approach, the number of analyses needed to reach the minimum value of n_{tendon} is decreased and a lot of computational time is saved.

Figure 5.1 illustrates the main idea and function of this optimization approach, the design checks and how the evaluation works for each check is described in more detail under Section 5.3 and under Section 5.4 a more detailed flow chart of the entire SBPD optimization is presented.

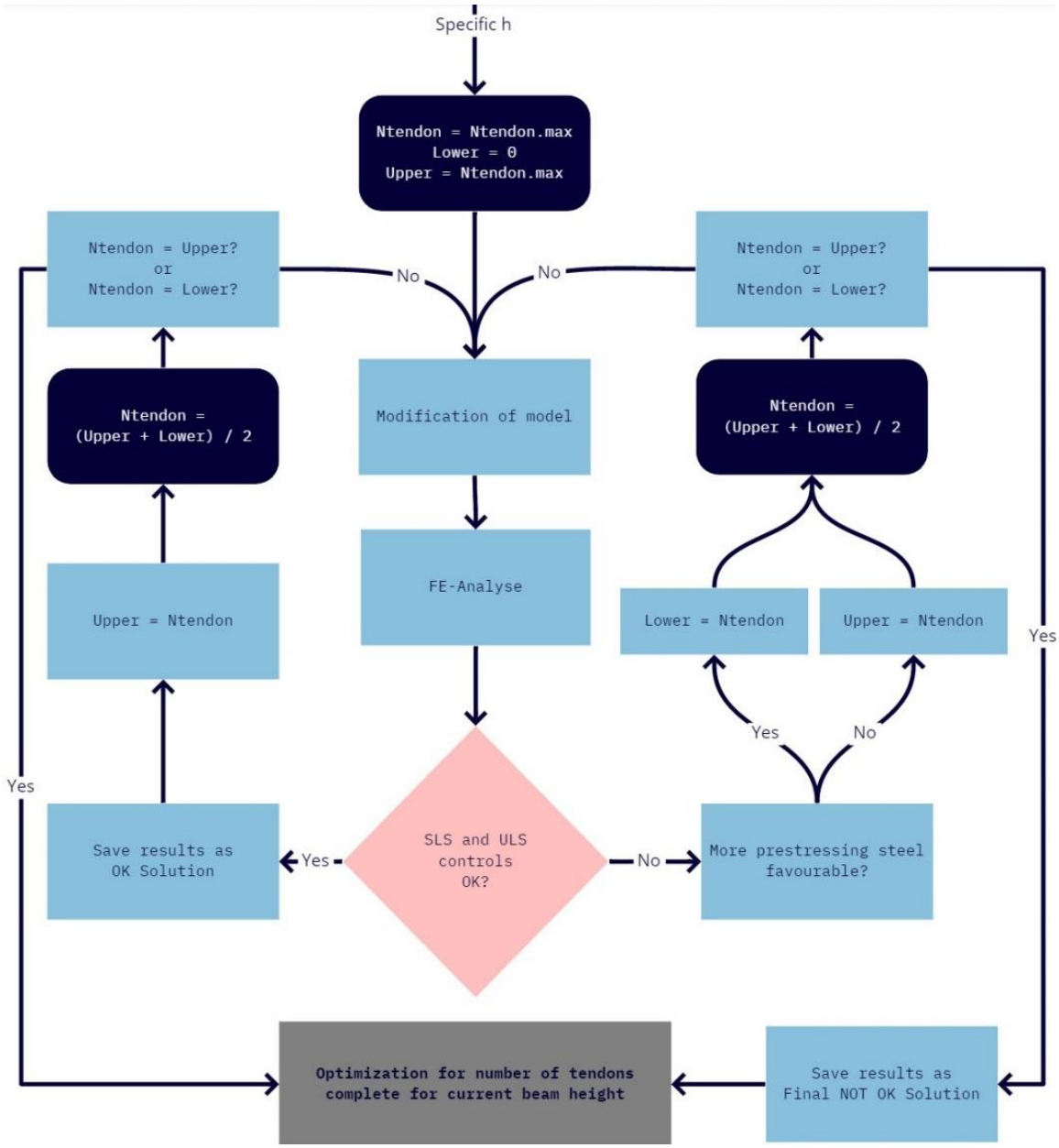

Figure 5.1 – Illustration of the optimization approach to obtain a minimum number of tendons

5.4 Evaluation method and design checks

As explained in Section 5.2, the optimization method is evaluating the previous results to choose the next number of tendons to analyse. The design checks that are done with the results from the FE analysis, also explained in more detail under Section 2.3.2 and 2.3.3, are as follows:

- SLS – Characteristic: $|\sigma_{cc}| \leq 0.6 * f_{ck}$
- SLS – Frequent: $\sigma_{cp.\pm 150mm} \leq 0$
- SLS – Frequent only traffic load: $\delta_{max} \leq \frac{L}{400}$

- SLS – Quasi-permanent: $\sigma_{cc} \leq 0$
- ULS: $M_{Ed} \leq M_R$

To assume linear creep, the concrete stress under quasi-permanent loading needs to be limited to $|\sigma_{cc}| \leq 0.45 * f_{ck}$. Together with experienced structural engineers, the decision has been made not to include this check in the evaluation. This check is generally fulfilled when the bridge has fulfilled the check $|\sigma_{cc}| \leq 0.6 * f_{ck}$ under characteristic loading.

If one check is not fulfilled, the evaluation of the results is to determine if it is due to too many or too few tendons. An increased number of tendons is resulting in an increased tendon force, together with the layout this is favouring all the design checks except in two special cases:

SLS – Quasi-permanent
Over the mid support, the tendons are creating tensile stresses at the bottom due to an increased secondary moment, which may cause problems fulfilling the SLS – Quasi-permanent check. This check is only to determine if crack width calculation is required or not. Since the normal reinforcement is not included or designed in this thesis the crack width control cannot be performed. The SLS-Quasi check is therefore chosen to not affect the approval or disapproval of a solution. The stresses under quasi-permanent loading are extracted together with the other design checks for post-processing.

ULS
The tendons create, as described in Section 2.1.3, a secondary moment that increases the positive sectional moment over the entire beam. At the mid support, the prestressing steel is located at the top of the cross-section and therefore the positive moment capacity is based mainly on the capacity for the concrete, i.e., the capacity is low. To reduce the sectional moment for this design check, a reduced number of tendons is decreasing the secondary moments and then also the total sectional moment. Therefore, the number of tendons causing a too large positive moment over the mid support is set to the new upper limit in the optimization approach and a lower number of tendons is tested.

If one of the remaining checks, including the sections outside the mid support for SLS – Quasi-permanent or ULS, is not fulfilled the number of tendons is set to be the new lower limit.

If one combination of beam height and number of tendons is fulfilling all the stated design checks, the cost and GWP calculations are performed. Based on the values stated in Section 2.5 the total cost and CO_2–equivalents are calculated for the approved solutions. The number of tendons is then set to be the upper limit and a new analysis is made for a lower number of cables until the lowest number of cables that fulfils the requirements is found.

The choice of the design solution is then determined by the structural engineer that is using the optimization tool. When the number of tendons has been optimized for all the chosen heights, a list with the solutions that are fulfilling the checks together with their cost and GWP respectively is obtained. It is then up to the designer to determine which factor to be the decisive one for the specific project.

5.5 Entire optimization

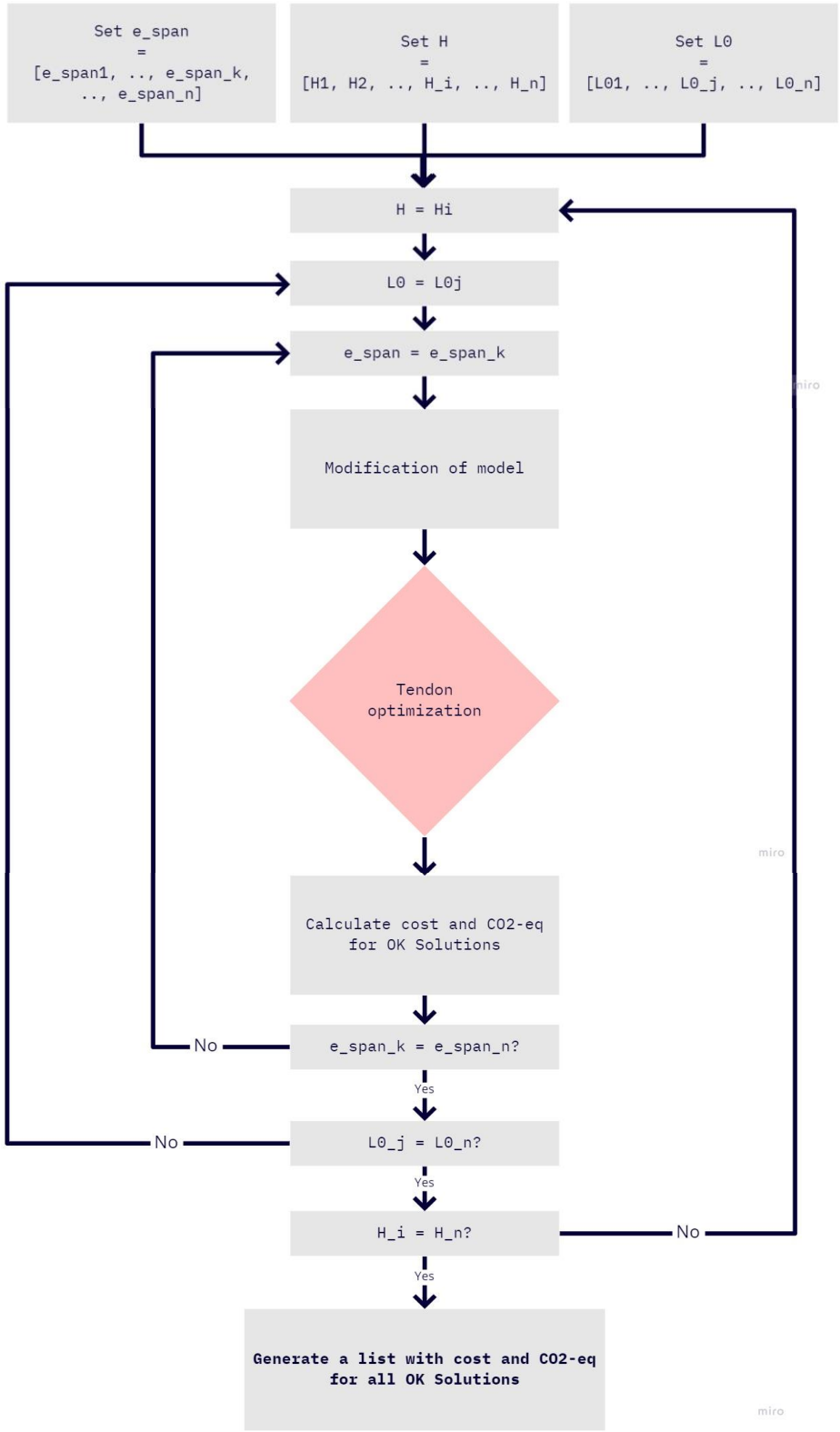

Figure 5.2 – Flow chart of the SBPD-method design for the optimization process.

6 Results

The results are evaluated and presented with two different approaches. The first part shows patterns and relations between different geometries and resulting dimensions such as span lengths, beam height and number of tendons. The second part is a comparison with two existing bridges.

The first part is treated in Sections 6.1 – 6.3. For these results, the mesh size is set to $L/50$ to keep the computational time down. It is not possible within the time frame for this thesis, to run all the different bridges with a mesh size of $L/100$ with the computational power available. The chosen mesh size gave an error of approximate 9% over the mid support, while the span error is 0.5 %. This error is considered acceptable for this part since the focus is to study patterns and behaviours when varying different beam heights, number of tendons and tendon layouts.

For the comparison with existing bridges, only two different bridges are evaluated. Therefore, the mesh size is set to $L/100$, which is the desirable mesh size concerning the errors described in Section 4.2.4.

Some input for the optimization is chosen to be the same for every bridge that is studied, and these parameters are presented in Table 6.1. For each result presentation, an additional table is presented with the case-specific input data chosen for each case.

Table 6.1 - Fixed input in entire Chapter 6.

Bridge	
Span lengths [m]	**
Width [m]	**
Cross Section	
Thickness top flange, t_f [m]	0,3
Web width, b_w [m]	Width/2 *
$_{CCduct}$ [m]	0,25
Wing walls and end-shields	
Length of wing walls, L_{ww} [m]	5,8
H_2 [m]	1,1
Edge Beam	
Width [m]	0,5
Height [m]	0,5
Materials	
Concrete class	C35/45
Prestressing steel, f_{pk} [MPa]	1860
, Strand area [mm^2]	150
, Number of strands per tendon [-]	15
Earth pressure	
K_p [-]	5,83
K_0 [-]	0,29
γ-earth [kN/m3]	22
Temperature diff over cross section	
ΔT - Warm top surface [^oC]	10,5
ΔT - Cold top surface [^oC]	8
Uniform temperature increase	
High T [C]	65
Support yield	
Deflection [m]	-0,02
Surcharge	
q_{6m} [kPa]	20
$q_{remaining.area}$ [kPa]	10

** Chosen for each case.

* Except in Section 6.3.

As Figure 5.2 shows, the optimization contains three different sets to be combined to find an optimized solution with respect to cost or GWP. For the first part (Section 6.1-6.3) both e_{span} and L_0 have sets of three and two values respectively. L_0 is chosen to 75 % and 85 % of the span length and e_{span} is set to the values presented in Section 4.1. The two extreme values have been chosen for L_0 to see the effect this parameter has on the bridge and to keep the computational time down. The set of e_{span} is chosen to include

three parameters, the two extreme values and the middle of the range, i.e., the factor α_{span} is set to 0 %, 10 % and 20 %.

For the second part of the results, Section 6.4, the set L_0 is increased with an additional value of 80 % and the set of e_{span} is increased with additional two values corresponding to the value on α_{span} at 5 % and 15 %.

The final set of *h* is chosen by the user for each bridge optimization. Due to computational time, the number of variables in the set of the beam height is limited and therefore the most optimized result might be in between two different beam heights. Although the behaviour and effect of different geometries can be seen, and the choice of the set *h* used for each result is presented under the sections respectively. The beam heights in the set which have no solution that fulfils the requirements are not presented in the results.

6.1 Relation between beam height and number of tendons

To show the relationship between the minimum number of tendons needed with different beam heights, two specified bridges with chosen geometries are evaluated. The geometries for the bridges evaluated are presented in Table 6.2. The main purpose of the two bridge designs is to include one wider with longer spans and one smaller regarding both the width and the span length, to study if there are similarities or differences in the results for the bridges.

Table 6.2 – Bridge used for relation between beam height and the number of tendons.

	Bridge 1	**Bridge 2**
Span lengths [m]	30	34
Width [m]	8	11
Web width [m]	4	5.5
Max number of tendons	15	21

Figure 6.1 displays the combinations of beam height and the minimum number of tendons that fulfil the design check for each beam height in the set *h*. In this Section, Section 6.1, the set *h* will contain beam heights with an interval of 100 mm ranging from 1.3 m to 2.2 m.

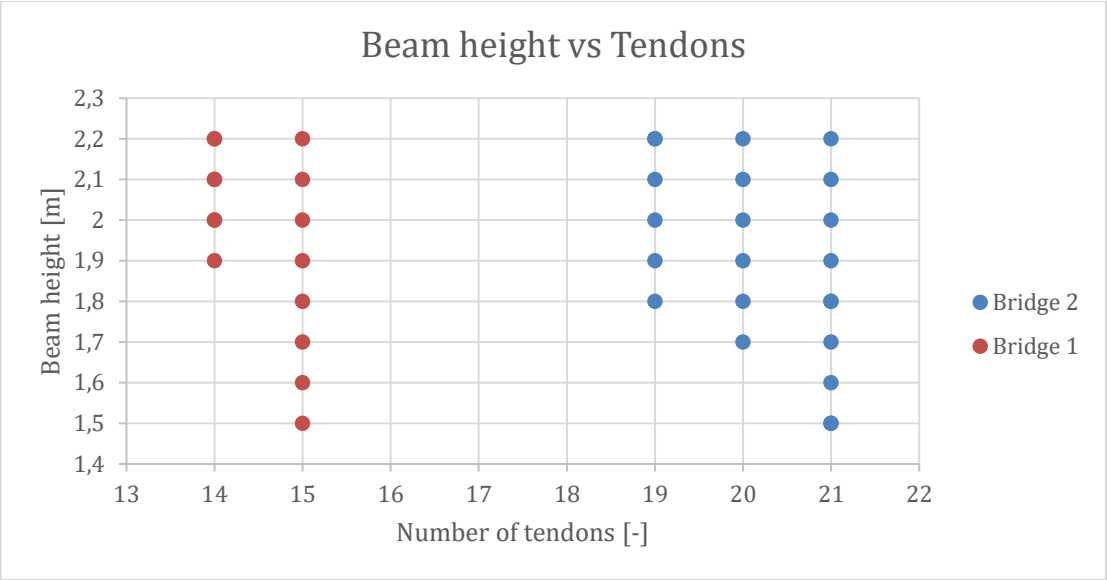

Figure 6.1 - Approved combinations of beam height and number of tendons for the two bridges

For the combinations in Figure 6.1, the total cost and total GWP are presented in Figure 6.2 and 6.3 respectively.

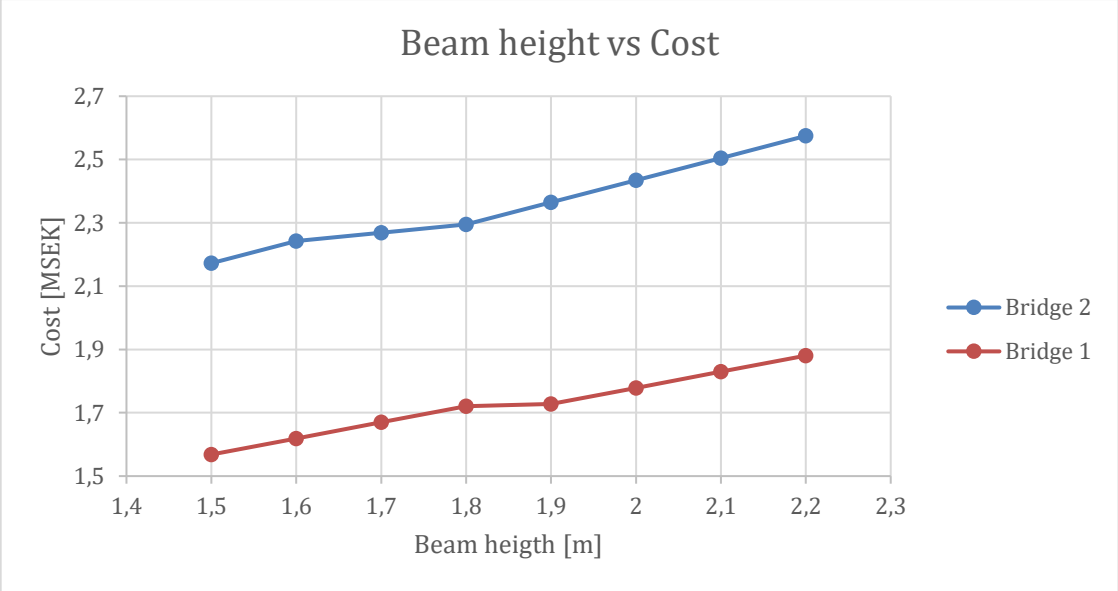

Figure 6.2 - Cost for different beam heights with the corresponding number of tendons.

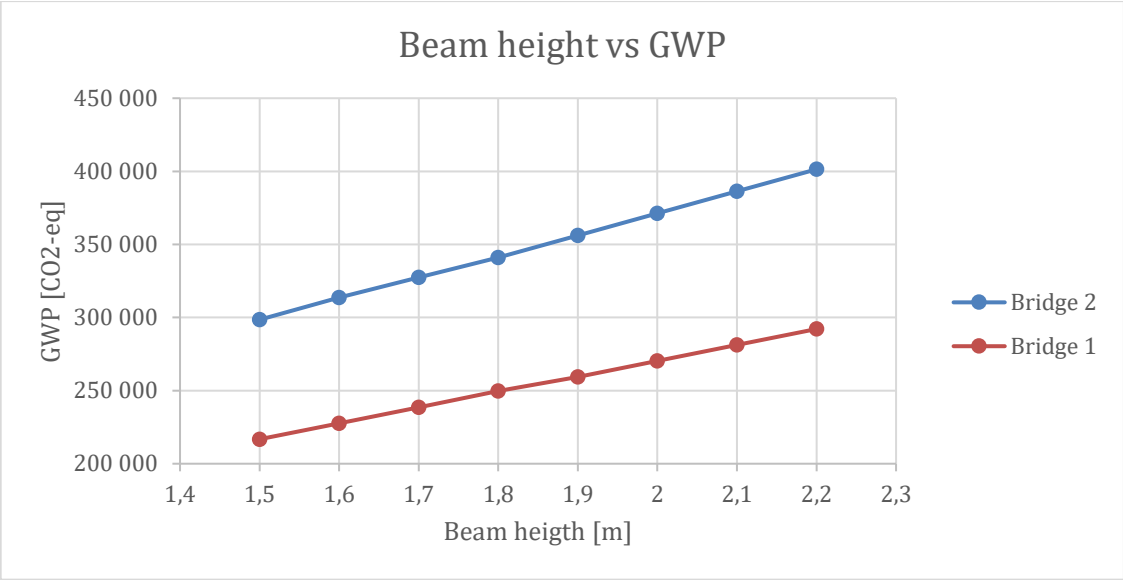

Figure 6.3 - GWP for different beam heights with the corresponding number of tendons.

6.2 Minimum beam height for different span lengths

To see the development of minimum beam height needed over different span lengths, and the effect of the tendon layout parameters, the two bridges presented in Table 6.2 are evaluated by varying their span lengths in the range of 28 m – 38 m. The lowest beam height for each span length that fulfils the design checks are presented in Figure 6.4. In Table 6.3 the same solutions are stated for both bridges with the corresponding number of tendons together with the resulting combination of the two parameters L_0 and e_{span}.

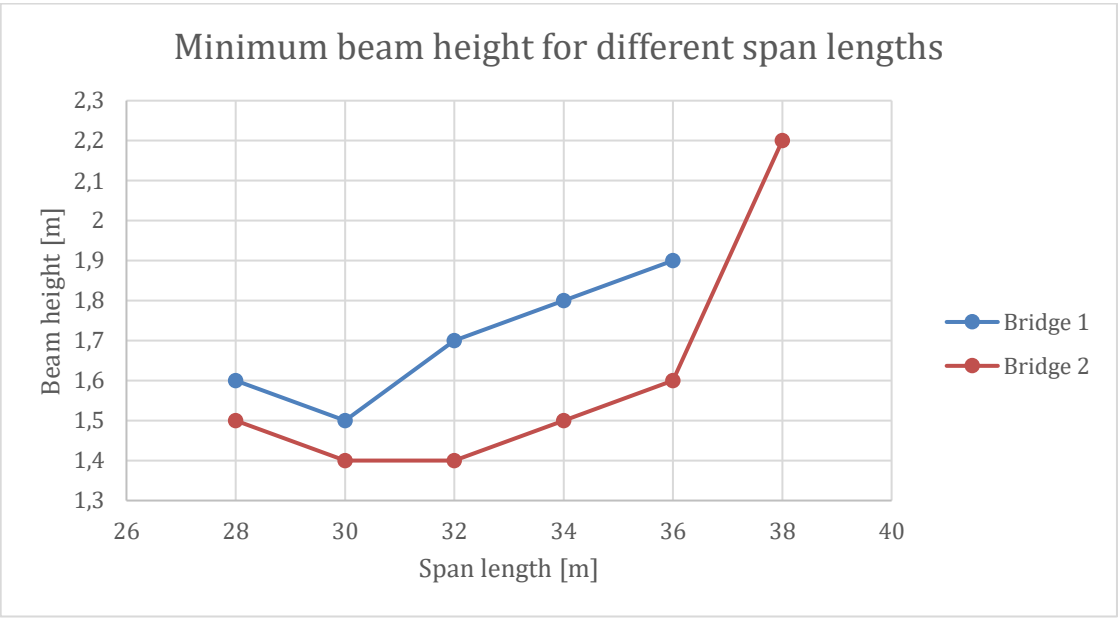

Figure 6.4 - Minimum beam height for different span lengths for the two bridges.

Table 6.3 - Minimum beam height for different span lengths with the corresponding number of tendons, L_0 and e_{span} parameters.

	Span length	Beam height	Number of tendons	L_0	α_{span}*
Width 8m	28m	1.6m	13	0.75 * L_{span}	20 %
	30m	1.5m	15	0.75 * L_{span}	20 %
	32m	1.7m	14	0.85 * L_{span}	20 %
	34m	1.8m	15	0.85 * L_{span}	10 %
	36m	1.8m	15	0.85 * L_{span}	0 %
	38m	>2.3m	-	-	-
Width 11m	28m	1.5m	18	0.75 * L_{span}	20 %
	30m	1.4m	21	0.75 * L_{span}	20 %
	32m	1.4m	20	0.85 * L_{span}	20 %
	34m	1.5m	21	0.85 * L_{span}	10 % / 20 %
	36m	1.6m	21	0.85 * L_{span}	0 %
	38m	2.2m	21	0.85 * L_{span}	0 %

* $e_{span} = L_{CG} – (200mm + \alpha_{span} * L_{CG})$

6.3 Effect of chosen beam width and maximum number of tendons

The width of the beam is chosen as input data and is set to half the width of the bridge as a standard value. The web width sets the limit for the maximum number of tendons and the results in Section 6.1 show that an increased number of tendons and a reduced concrete cross-section is preferable. Therefore, a comparison of three different combinations of web width and the maximum number of tendons is performed with the standardized 8 m wide bridge from Section 6.1. The two new bridges will have the same input except one will have a reduced cc_{duct} distance to allow more tendons while the last bridge will have the same number of tendons, i.e., 15, but the web width is decreased by 0.5 m. The minimum concrete distance between the tendons is the diameter of the duct (SIS, 2005a), so the minimum centre to centre distance is twice the diameter which for this comparison is 190 mm. The input that differs between the bridges are presented in Table 6.4 and the remaining input is the same as presented in Table 6.1.

Table 6.4 – Differences of the input for the bridges compared in Section 6.3.

	Bridge 1	Bridge 2	Bridge 3
Width [m]	8	8	8
Web width [m]	4	4	3.5
Max cc_{duct} [m]	0.25	0.19	0.22
Max number of tendons	15	19	15

The bridges are evaluated for different spans ranging from 28 m to 38 m where only the lowest beam height that fulfils the criteria is presented. This is most likely the most cost and environmentally efficient as described above. The set *h* is set to have an interval of 100 mm ranging from 1.3 m to 2.3 m. Figure 6.5 shows the lowest beam height needed and its corresponding number of tendons for different span lengths for each of the bridges in Table 6.4.

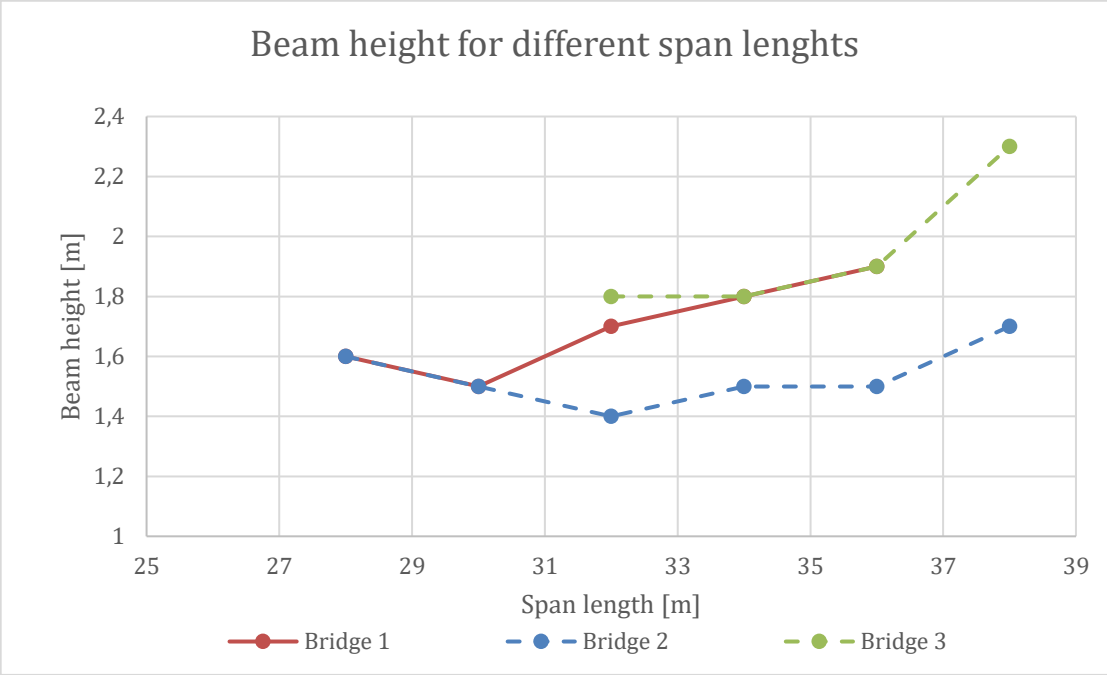

Figure 6.5 - Minimum beam height for different span lengths for the different input data for the bridge design.

In Figure 6.6 and Figure 6.7 the cost and GWP are presented for the bridges respectively.

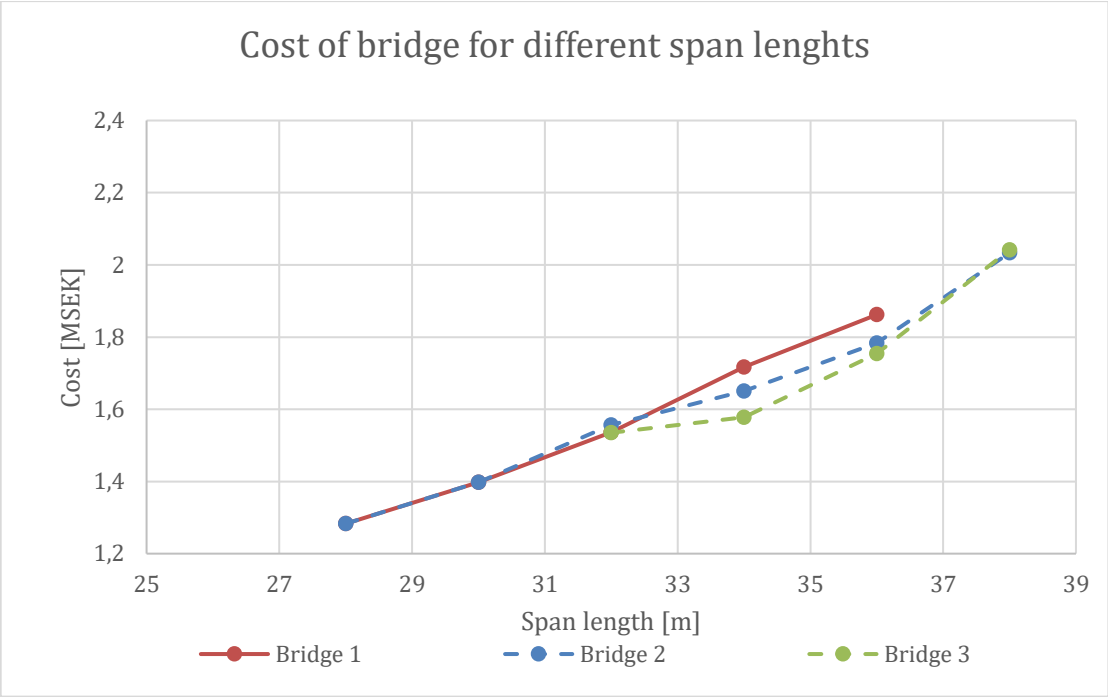

Figure 6.6 - Cost comparison of different input data for the bridge design.

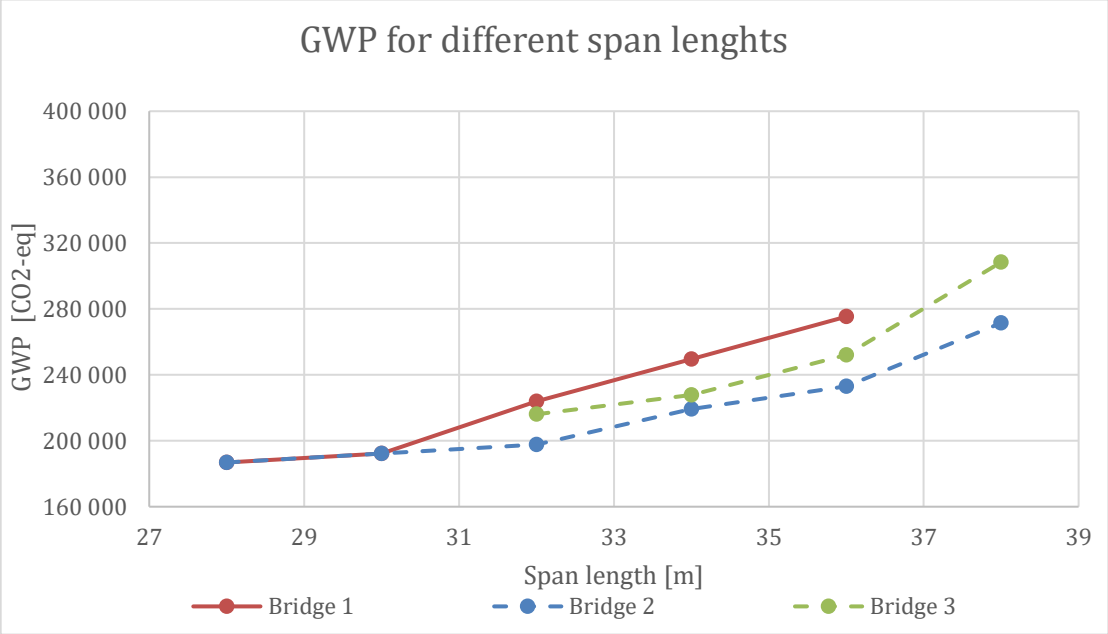

Figure 6.7 - Comparison of GWP for different input data for the bridge design.

6.4 Comparison to existing bridges

To evaluate the potential of the optimization method implemented in the created python tool, comparisons of the optimized solutions with two existing bridges designed by Inhouse Tech Göteborg AB is performed.

6.4.1 Bridge 100-411-1

The first bridge to be compared has two equal spans of 32m each and a width of 11m. Table 6.5 contains detailed information about both the existing bridge and the optimized bridge.

Table 6.5 – Information about the two compared bridges.

Bridge	**Optimized Bridge**	**100-411-1**
Span lengths [m]	32	32
Width [m]	11	11
Cross Section		
Thickness top flange, t_f [m]	0,30	0.29
Height, H [m]	(1.3 - 2.0)	1.67
Web width, b_w [m]	5.5	5.6
cc_{duct} [m]	0.19	0.25
Wing walls and end-shields		
Length of wing walls [m]	5.8	5.8
H_2 [m]	1.1	1.1
Edge Beam		
Width [m]	0.50	0.50
Height [m]	0.50	0.455
Materials		
Concrete class	C35/45	C35/45
Prestressing steel, f_{pk} [MPa]	1860	1860
, Strand area [mm^2]	150	150
, Number of strands per tendon [-]	15	15
Tendon layout		
e_{span} [mm]	(e_1, e_2, e_3 e_4, e_5)*	710
L_0 [m]	(24.0, 25.6, 27.2)	27.0
Number of tendons	(0-27)	19

*Dependent on beam height.

Figure 6.8 displays the combinations of beam height and the minimum number of tendons that fulfil the checks for each beam height in the set *h*. The set *h* contains beam heights with an interval of 100 mm ranging from 1.3 m to 2.0 m for the optimized bridge. The existing bridge is also displayed for comparison.

The lowest beam height that did work was 1.4 m with 22 tendons. Designs with 23-27 tendons were generated, but the beam height was not decreased for any of them. These results are excluded from Figure 6.8-6.10 since more tendons for the same beam height only uses more material and therefore will not be a better solution.

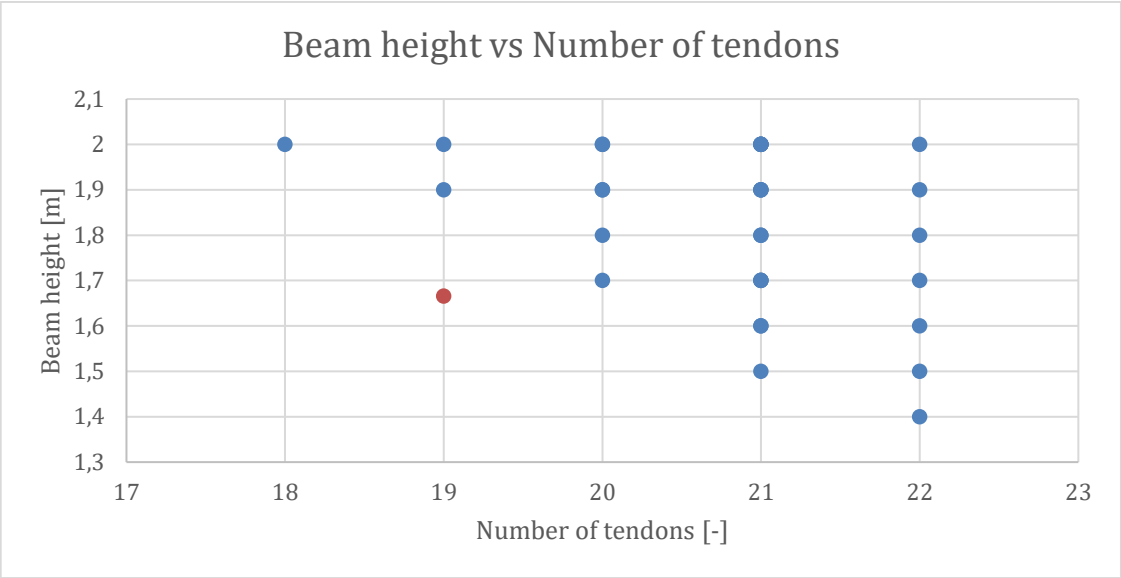

Figure 6.8 - Number of tendons needed for different beam heights compared with existing bridge.

For the combinations in Figure 6.8, the total cost and total GWP are presented in Figure 6.9 and 6.10 respectively for both bridges.

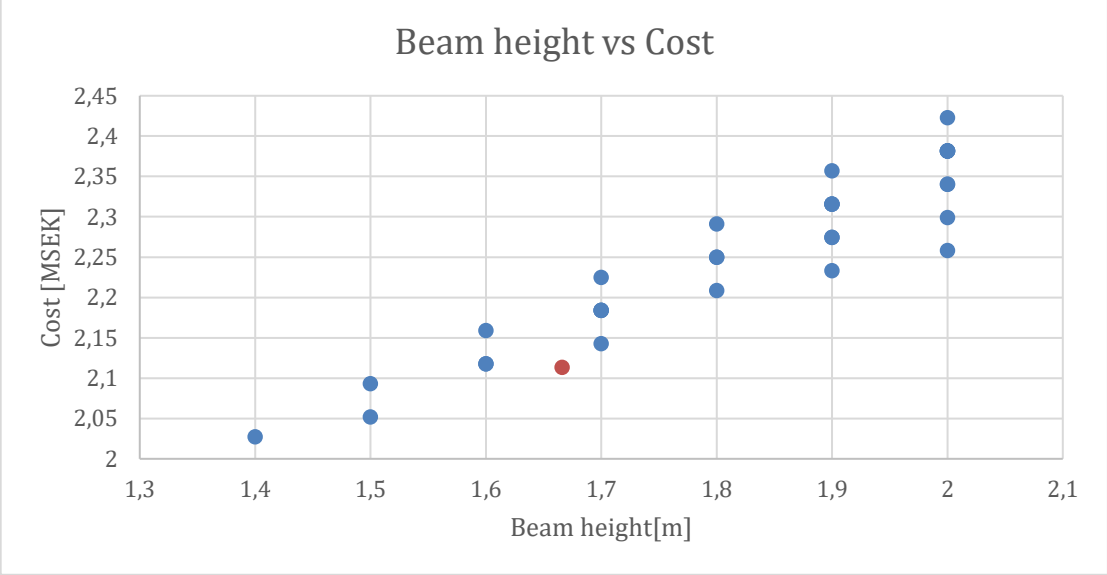

Figure 6.9 - Cost for different beam heights with the corresponding number of tendons compared with the existing bridge.

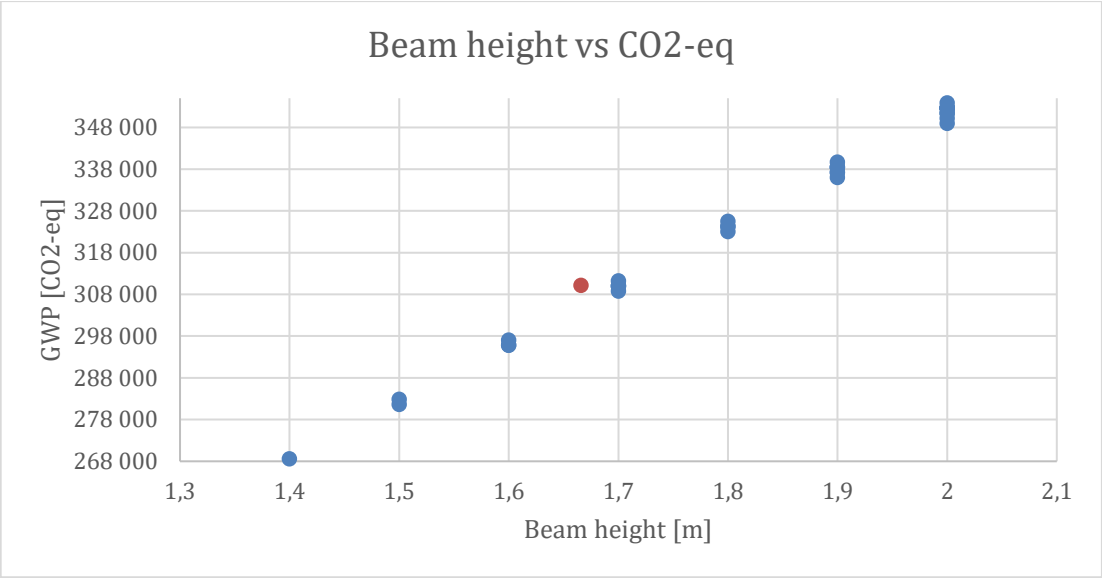

Figure 6.10 - GWP for different beam heights with the corresponding number of tendons compared with the existing bridge.

In Table 6.6 the values of the design checks are presented. Both for the existing bridge and the most optimized bridge from both an economic and environmental perspective.

Table 6.6 - Result comparison of ULS and SLS checks between the optimized and the existing bridge.

Checks	**Optimized bridge** (h=1.4m, 22 tendons)	**100-411-1**
SLS Cha. Max compression [MPa]	-18,5	-14.4
SLS Freq. ±100mm from tendon [MPa]	-0.25	-0.12
SLS Quasi [MPa]	-0.37	2.76
Utilization ratio MRd+*	112 % / 89 %	189 % / 85 %
Utilization ratio MRd-	85 %	74 %

*Including two utilization ratios, one without normal reinforcement and one with the minimum normal reinforcement included in the capacity.

6.4.2 Bridge 100-412-1

The second bridge to be compared has two equal spans of 36.8 m each and a width of 8 m. Table 6.7 contains detailed information about both the existing bridge and the optimized bridge.

Table 6.7 – Information about the two compared bridges.

Bridge	**Optimized Bridge 1**	**Optimized Bridge 2**	**100-412-1**
Span lengths [m]	36.8	36.8	36.8
Width [m]	8	8	8
Cross Section			
Thickness top flange, t_f [m]	0.30	0.30	0.275
Height, H [m]	(1.3 - 2.3)	(1.3 - 2.3)	1.9
Web width, b_w [m]	4	3.44	3.4
cc_{duct} [m]	0.2	0.19	0.18
Wing walls and end-shields			
Length of wing walls [m]	5.8	5.8	5.8
H_2 [m]	1.1	1.1	1.1
Edge Beam			
Width [m]	0.50	0.50	0.50
Height [m]	0.50	0.50	0.455
Materials			
Concrete class	C35/45	C35/45	C35/45
Prestressing steel, f_{pk} [MPa]			
, Strand area [mm^2]	1860	1860	1860
, Number of strands per	150	150	150
tendon [-]	15	15	15
Tendon layout			
e_{span} [mm]	(e_1, e_2, e_3 e_4, e_5)*	(e_1, e_2, e_3 e_4, e_5)*	876
L_0 [m]	(27.6, 29.4, 31.3)	(27.6, 29.4, 31.3)	31.2
Number of tendons	(0-19)	(0-17)	17

*Dependent on beam height.

Figure 6.11 displays the combinations of beam height and the minimum number of tendons that fulfil the design checks for each beam height in the set *h*. The set *h* will contain beam heights with an interval of 100mm ranging from 1.3m to 2.3m for the optimized bridge. The existing bridge is also displayed for a comparison.

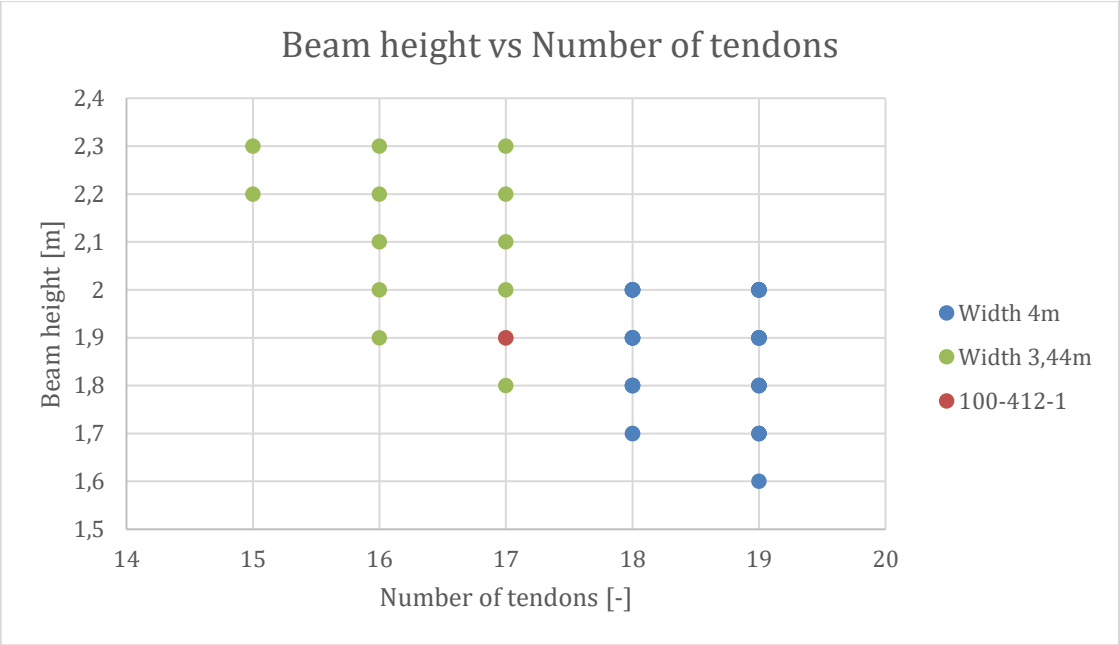

Figure 6.11 - Number of tendons needed for different beam heights compared with existing bridge.

For the combinations in Figure 6.11, the total cost and total GWP are presented in Figure 6.12 and 6.13 respectively for both bridges.

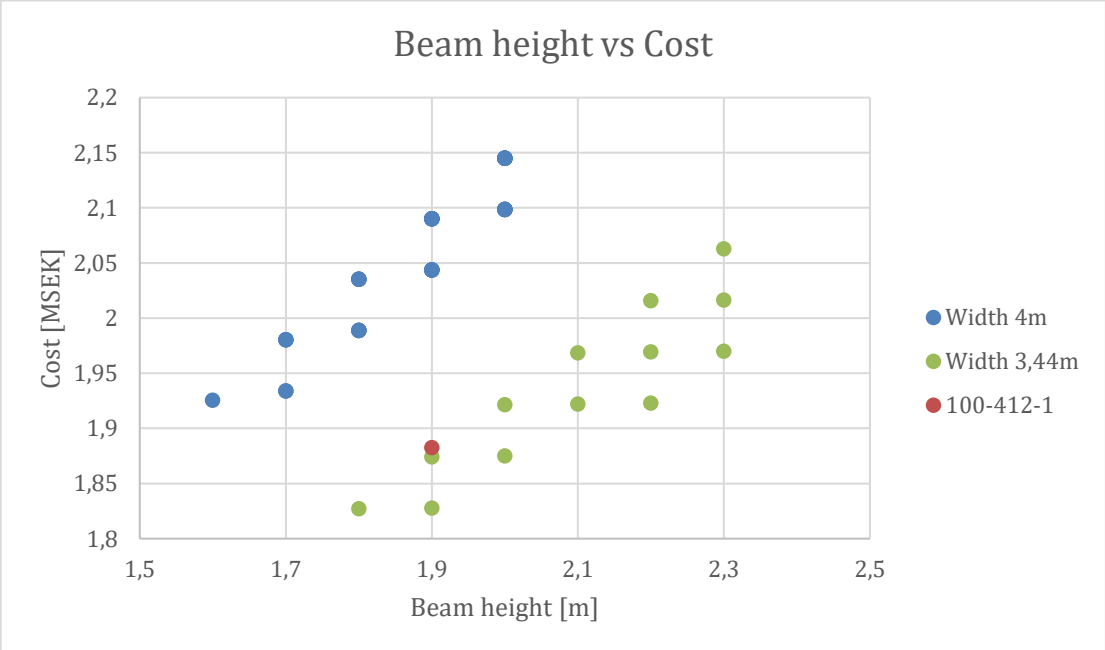

Figure 6.12 - Cost for different beam heights with the corresponding number of tendons compared with the existing bridge.

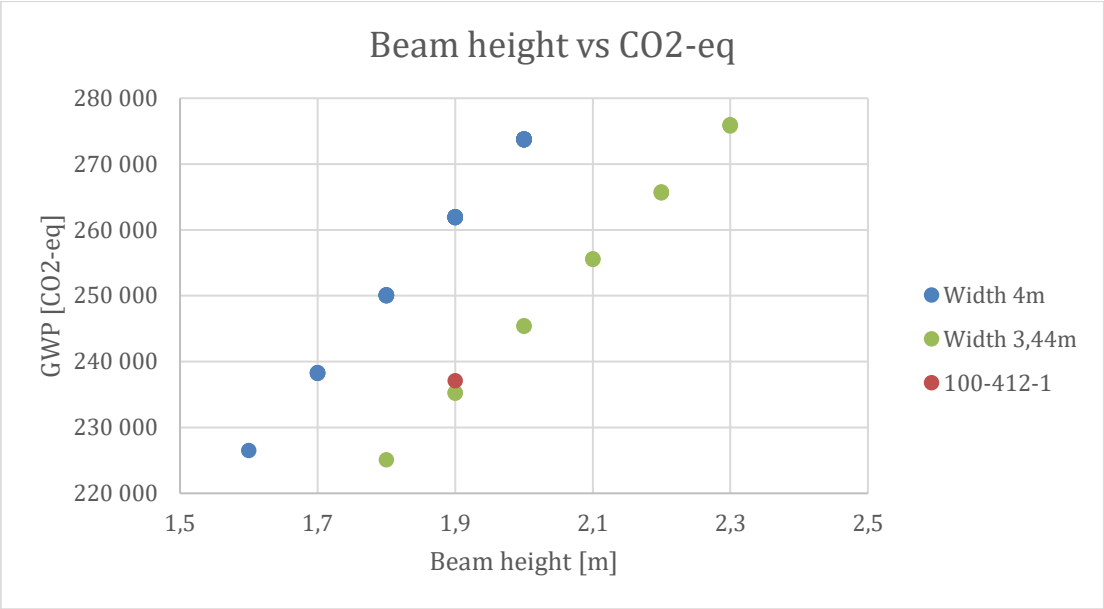

Figure 6.13 - GWP for different beam heights with the corresponding number of tendons compared with the existing bridge.

In Table 6.8 the values of the design checks are presented. Both for the existing bridge and the most optimized bridge from an economical perspective.

Table 6.8 - Result comparison of ULS and SLS checks between the optimized and the existing bridge.

Checks	**Optimized bridge** (h=1.8m, 17 tendons)	**100-412-1**
SLS Cha. Max compression [MPa]	-14.9	-15.65
SLS Freq. ±100mm from tendon [MPa]	-0.48	-0.03
SLS Quasi [MPa]	1.44	2.89
Utilization ratio MRd+*	147 % / 97 %	79%
Utilization ratio MRd-	81 %	77 %

*Including two utilization ratios, one without normal reinforcement and one with the minimum normal reinforcement included in the capacity.

Table 6.9 shows a summarize of the reduction concerning both cost and GWP for the optimized solutions compared to the existing bridges 100-411-1 and 100-412-1.

Table 6.9 – Summarization of the reduction for the cost and GWP compared to the existing bridge designs.

	100-411-1	**100-412-1**
Reduction of cost	4.1 %	3.0 %
Reduction of CO_2 - equivalent	13.4%	5.1%

7 Discussion

The part of the results which aims to simulate and show different patterns regarding the relation between the design solutions and their cost and global warming potential is discussed in Section 7.1. The comparison between the optimised design and the previous design of two existing bridges is treated in the following Section 7.2. Some simplifications have been made in the study and how these can affect the result is explained in Section 7.3.

7.1 General Results

The result in Section 6.1 shows that the smallest beam heights with a large number of tendons are the best solutions from both economic and environmental point of view. However, figure 6.2 shows that there can be cases where this is not true, and that this is the case for the narrower bridge geometry, denoted Bridge 1. Here, one tendon could be taken away when increasing the beam height from 1.8 m to 1.9 m and these two designs has an equal cost. The larger concrete cross-section could lead to that the amount of normal reinforcement can be decreased. A larger cross-section generally also requires less shear reinforcement and a decrease in construction hours on site. On the other hand, the higher beam had larger GWP and was thus worse from an environmental point of view. Consequently, the smaller beam height may be considered as a better solution anyway.

A general pattern that was noticed is the importance of the tendon layout to balance the positive and the negative effects from the prestressing in the design of the cross-section. This is of special importance for the shorter spans, where the secondary moment creates a positive moment over the mid support as described in Section 2.1.3, and the positive moment capacity is rather small due to that the tendons are placed at the top of the beam. This positive moment needs then to be counteracted with the negative moment from the self-weight, but the load effect from the self-weight is rather small due to the short spans. For the same reason, this is of less importance for spans of 34 m and longer, where the negative moment from the self-weight is larger than the secondary moment. For the longer spans, the maximum compression stress in the concrete at the top of the cross-section can be decisive and limit how many tendons can be used.

To get the most optimal solution, especially for the short spans, the set of the parameters L_0 and e_{span}, described in Section 4.1, that influences the tendon layout should be modified. The sets should include more values with smaller intervals to find this balance between the positive and negative effect of the prestressing. This takes a lot of computational power and time, which is why a larger set was not used in this study. The sets could also be modified depending on span lengths. From Table 6.3 it can be seen that there is a correlation between span lengths and the variables for the tendon layout. For the shorter spans, 28 m and 30 m, the most optimal solutions had L_0 equal to 75 % of the span length and a high position of the cable in the span (i.e., when α_{span} is 20 %). For the medium-length spans, the value on L_0 changes to 85 % but the cable remains high in the span, and for the longer spans the position of the cable is changed so that it has the lowest placements possible in the span. With this knowledge, the set for L_0 could be changed so that it, for example, contains more values closer to 75 % and

skip 85 % if the spans that are studied is around 28-30 m. Since only these two values on L_0 have been used for the general results, the increase of L_0 between 75 % and 85 % might not be the most optimal values for the intermediate span lengths. For bridge 100-411-1 with a span of 32 m, the most optimized solution has L_0 at 80 % which makes it reasonable to assume that the most optimal value for L_0 has a linear pattern for the spans between 28 and 38 m.

In Section 6.3 it can be seen that even more optimized bridges can be obtained by increasing the number of tendons and by reducing the beam width. When the span lengths are above 32 m both the increased maximum number of tendons and the decreased width of the beam gives more optimal bridges than the original input. If the economical aspect is of priority, the decreased beam width (Bridge 3) gives the most optimal bridge. Figure 6.5 shows that the beam height is almost the same for Bridge 1 and 3, and since the number of tendons is the same for the two bridges, the only thing that differs is the amount of concrete due to the different beam widths. For span lengths above 32 m, it is rather clear that the concrete which adds self-weight to the structure is not needed and can be taken away to reduce both the cost and GWP. However, for Bridge 3 with spans of 28-30 m, the self-weight is needed to counteract the secondary moment, and therefore the reduced web width only has negative effects and there are no solutions found that fulfils the design requirements.

The increased number of tendons with the standard beam width (Bridge 2) gives the best results concerning the GWP for the span lengths of 32 m and longer, which can be seen in Figure 6.7. This is due to that the increased number of tendons allows for a lower beam height. The decreased beam height results in that the amount of concrete could be decreased even more than when the beam width is reduced (Bridge 3). The increased number of tendons makes the solution more expensive than reducing the beam width, but since the GWP is very much connected to the amount of concrete used, this solution is to prefer.

As can be seen in Figure 6.4 and in Section 6.3, the optimal beam height increases for 28 m span length compared to 30 m span length. This is due to that the load effect from the self-weight is rather small compared to the secondary moment from the prestressing steel. This leads to that the number of tendons needs to be reduced to lower the effect of the secondary moment and, consequently, the height of the beam then needs to be increased to have enough capacity. This is a case where the tendon layout is of high importance if a lower beam height is wanted. To obtain a lower beam height, the tendon layout would need to be modified such that the secondary moment is reduced even more than allowed with the sets chosen in this study. However, this would probably lead to that more tendons are needed and therefore may not be the most optimal solution anyway.

7.2 Comparison to two existing bridges

Bridge 100-411-1

For bridge 100-411-1, with two spans of 32 m, the comparison shows that there are design solutions where the height of the beam could be decreased if more tendons are added. The optimization shows three cheaper design solution and six design solutions with lower GWP. The optimized bridge, presented in Table 6.6, has a decreased cost of

4.1% compared to the existing bridge. The largest improvement is on the GWP, where the optimized bridge has a 13.4% smaller GWP. This is achieved through decreased beam height and smaller amount of concrete needed, which has a strong influence on the GWP.

For the most optimal design solution, with a beam height of 1.4 m and 22 tendons, the maximum compression stress under Quasi-permanent loading is 0.37 MPa. The existing bridge has large tensile stress under Quasi-permanent loading (2.76 MPa) which requires a crack width check to be performed. For the optimized bridge, no extra crack width check needs to be performed since the entire beam cross-section is under compression, which is desirable in the design. The design solution which has almost the same beam height as the existing solution, but one more cable, has smaller tensile stress than the existing bridge for the same load case (0.76 MPa). The maximum tension stresses are in the bottom of the beam over the support, which is caused by the secondary moment. So, the difference between the existing bridge and the optimized designs is that the optimized solution has a tendon layout which decreases the secondary moment more compared to the existing bridge.

It can also be seen in Figure 6.8 that, for the same number of tendons as in the existing bridge, the optimal design solution has 230 mm higher cross-section. Furthermore, for about the same cross-section height, the optimal design solution has one more cable. This shows that the positive moment capacity above the mid support is not enough for the existing bridge without non-prestressed reinforcement for crack control. However, for the existing bridge, this reinforcement was designed to handle the torsional moment. Consequently, it could be used also for crack control in SLS. This crediting could be used for the design of the bridge in a later design phase where the information about the torsional reinforcement was available. For the early estimation, which the script is supposed to be used for, this information is not available; the capacity is only crediting the minimum reinforcement, which is the only amount of reinforcement that is known to be provided in the beam at this stage. This leads to that the script does not accept the design which is similar to the existing bridge, since the positive moment capacity is not enough, and is instead searching for a design that fulfils all criteria. For this case, an experienced engineer could study the results for the designs which fulfil all criteria except the positive moment capacity at the mid support and do an estimation if the design check is likely to be fulfilled in a later stage when more information is available.

Bridge 100-412-1

For bridge 100-412-2, with two spans of 36.8 m, the optimized bridge with a beam width of 3.4 m. Here, there are both a design solution which has the same beam height as the existing bridge but fewer tendons, and a solution with the same number of tendons but lower beam height. These two designs are cheaper solutions than the existing bridge. There are also two design solutions that have less GWP, where one of them is a bridge with a 4 m wide beam, 19 tendons and 1.6 m beam height. This gives the smallest cross-section of all designs for this comparison, which then gives the lowest GWP. The most optimal solution is reducing the cost by 2.3 % and the GWP with 4.5 %, which is considered good, but it could be stated that the existing design is close to optimal regarding both cost and GWP. This result was expected based on two important patterns discussed under Section 7.1. These are (1) that the number of tendons should be maximized (set cc_{duct} to 190 mm) and (2) for span lengths around 34 m and above the web width can be decreased from the initial 50 % of the total width

assumption. In the design of the existing bridge, both these conditions are implemented and therefore it is relatively close to the optimized solution.

The optimized design shows good values for the SLS-checks compared to the existing solution, which can be seen in Table 6.8. The stress under Quasi-permanent loading is lower than for the existing bridge, which favours the crack width check that remains to be made. It also has more margin in the stress check for Frequent loading, where the existing bridge is very close to the limit. For the ULS-checks, the utilization ratio for the optimized design is higher and the positive sectional moment is close to the capacity. It is still a design that works and is less demanding with respect to the crack width check. Consequently, it can be seen as a better design solution than the existing bridge since probably less non-prestressed reinforcement is needed to avoid too large crack widths.

7.3 Simplifications

The optimization process for this study is only taking the prestressing steel and the dimensions of the cross-section into account with respect to its capacity in bending. This results in that the design which is determined to be cheapest or to have the smallest GWP is also only considering these two parameters. A very slim solution may then become the best solution according to this study, but it may also lead to the need for more shear and non-prestressed reinforcement in the beam, something that will lead to an increase of the cost and GWP.

Since no crack width control is included in the analysis, this is something that needs to be designed for later in the design process. To avoid the need to perform this later, a check to analyse if the whole beam is in compression under quasi-permanent loading could have been added to the optimization loop. When this was included, several design solutions did not fulfil this criterion and were therefore not considered to be acceptable solutions. This resulted in that the final design solutions gave considerably higher cost and GWP than the ones that did not include the crack check. Therefore, the decision was taken not to include the crack width check in the optimization algorithm to allow more slim solutions and accept that a crack width check must be done later in the design process. This may then lead to increased amounts of non-prestressed reinforcement. The stresses in the beam under quasi-permanent loading is although included in the output from the optimization tool, together with the results from the analysis for post-processing.

This could potentially result in that a solution that is accepted by the optimisation tool is not possible to use, if the crack width criteria cannot be fulfilled. However, this is not expected to be a common case since other checks are usually not fulfilled if the beam shows this behaviour with large tensile stresses under quasi-permanent loading. This include, for example, the check in SLS that the concrete is in compression 100 mm over and under the cable, and the check of the positive moment capacity over the support in ULS. Furthermore, the structural engineer that is using this optimization method could easily implement an upper limit on the allowed tensile stress under quasi-permanent loading. This upper limit could then be determined from experience to a value that give good solutions with respect to the crack width check.

8 Conclusion

In this master's thesis, a tool was developed for optimization of two-span continuous prestressed concrete beam bridges, suitable for early design stages. When comparing to two newly designed existing bridges, the optimization tool designed more material-efficient solutions, especially for one of the bridges where the GWP was reduced by 13 %. It was shown that a slim bridge design with a high number of tendons is preferable compared to an increased beam height with fewer tendons when considering both economy and GWP.

To obtain the most optimized design solutions using the tool, the distance between the ducts should be minimized to allow the maximum number of tendons possible and iterate different design solutions. The iterative process should be continued until the lowest beam height with a corresponding number of tendons is reached. The web width should be chosen to approximate 50 % of the bridge width for spans equal to or lower than 32 m, while for longer spans it can be reduced. In this thesis, it has been reduced to 43% of the total width which resulted in a good design from both an economic and environmental point of view. However, a more slim cross-section leads to an increased amount of shear and non-prestressed reinforcement, something that is not studied in this thesis.

It is important to find a good balance between the positive effect of the longitudinal compression from the tendons and the negative effect of the secondary moment they are causing. This is of most importance for spans of 32 m or shorter, and therefore the tendon layout is an important factor to handle for the optimization to work successfully. For these shorter span lengths, it is important that the tendon layout leads to a small secondary moment. Since the moment from the self-weight is smaller for shorter spans the secondary moment has a larger effect on the bridge design. In the tool developed, this was done by modifying the two sets for the parameters that affect the tendon layout, L_0 and e_{span}, such that the lowest point of the tendon in the span has a higher position and that the tendon intersects with the beam's centre of gravity further away from the mid support. With a good layout of the tendons, the number of tendons could be increased, and the concrete cross-section decreased.

More optimal design solutions were found using the optimization tool, compared to the experience-based design solutions used for the existing bridges studied. Consequently, it can be concluded to be beneficial and relevant to use such a tool in the preliminary design phase. The results show that the set-based parametric design (SBPD) method can be used to find an optimized combination between a tendon layout, number of tendons and beam height for each specific bridge design. More conclusions can be drawn for each bridge geometry by using the optimization tool, but it is hard to generalise these into simple design recommendations for early design stages. Instead, the most optimal solution is changing from case to case. However, the optimization tool with the implemented SBPD-method is generating a low-cost design that is environmentally friendly with a slim cross-section together with a high number of tendons.

8.1 Further investigations

In this thesis, the model and analysis have been limited to only include the basic layout of the structure, which is often enough for estimations in the early design phase. The tool could be extended in several ways to include more parts of the bridge design.

The design of non-prestressed reinforcement could be included, which would give an even more accurate optimization concerning economy and GWP due to that a slim design often results in more non-prestressed reinforcement to reach enough shear and torsion capacity. An increased amount of reinforcement would also lead to an additional increase in cost due to more labour work on site.

When analysing different bridge designs, the effect of a changed tendon layout has been found to have a large impact on the optimization results. Therefore, it could be of interest to further investigate this to develop and implement a larger and more advanced optimization of the tendon layout in the tool. This could be performed in two different ways: If a new optimization study regarding the tendon layout results in a general conclusions regarding optimal tendon design, these could easily be implemented in the tool. However, as discussed in Chapter 7, the most optimal values of the two parameters e_{span} and L_0 depends on the bridge geometry, and the most optimal values on the two parameters can change. Therefore, a further investigation in the choice of these two sets could lead to that more accurate values can be chosen for the sets, which would likely result in an even more optimized bridge design.

As mentioned in the discussion, the SBPD method used in this optimisation tool shows good results and could most likely be implemented in more design phases for other bridge types, or other geometries with good results. A fairly large amount of re-coding of the developed python-script would be necessary, however the structure and layout of the tool could be used in the future for other optimization tools.

9 References

Boverket. (2021). *Utsläpp av växthusgaser från bygg- och fastighetssektorn*. Https://Www.Boverket.Se/Sv/Byggande/Hallbart-Byggande-Och-Forvaltning/Miljoindikatorer---Aktuell-Status/Vaxthusgaser/.

Dolan, C. W., & Hamilton, H. R. (2019). *Prestressed Concrete : Building, Design, and Construction*. Springer Nature Switzerland. https://doi.org/10.1007/978-3-319-97882-6

Engström, B. (2011a). *Design and analysis of deep beams, plates and other discontinuity regions.* 55.

Engström, B. (2011b). *Design and analysis of prestressed concrete structures*.

Fu, F. (2018). *Design and Analysis of Tall and Complex Structures* (Issue 2018). Elsevier Science and Techonology. ProQuest Ebook Central, https://ebookcentral.proquest.com/lib/chalmers/detail.action?docID=5257306.

Gosavi, A. (2015). *Simulation-Based Optimization - Parametric Optimization Techniques and Reinforcement Learning* (2nd ed.). Springer Scince+Business Media. https://doi.org/10.1002/9781119019770.ch13

Naturvårdsverket. (n.d.). *Koldioxidekvivalenter*. Retrieved March 12, 2021, from https://www.naturvardsverket.se/Sa-mar-miljon/Statistik-A-O/Vaxthusgaser-konsumtionsbaserade-utslapp-fran-exporterande-foretag/Koldioxidekvivalenter/

Naturvårdsverket. (2020). *Bygg- och fastighetssektorns klimatpåverkan*. Https://Www.Naturvardsverket.Se/Sa-Mar-Miljon/Klimat-Och-Luft/Klimat/Tre-Satt-Att-Berakna-Klimatpaverkande-Utslapp/Bygg--Och-Fastighetssektorns-Klimatpaverkan/.

Pacoste, C., Plos, M., & Johansson, M. (2012). *Recommendations for finite element analysis for the design of reinforced concrete slabs*. KTH.

Rempling, R., Mathern, A., Tarazona Ramos, D., & Luis Fernández, S. (2019). Automatic structural design by a set-based parametric design method. *Automation in Construction*, *108*, 102936. https://doi.org/10.1016/j.autcon.2019.102936

Rombach, G. A. (2004). *Finite element design of concrete structures*.

Scanscot Technology. (2015). *Brigade Plus -User's manual*. *6.2*.

Scanscot Technology. (2021). *BRIGADE/Plus 6.2-20*.

SIS. (2002a). *Eurokod - Grundläggande dimensioneringsregler för bärverk*.

SIS. (2002b). *Eurokod 1: Laster på bärverk - Del 1-1: Allmänna laster - Tunghet, egentyngd, nyttig last för byggnader*. *08*(121687).

SIS. (2003a). *Eurokod 1 : Laster på bärverk – Del 2 : Trafiklast på broar*. Svenska institutet för standarder. Stockholm.

SIS. (2003b). *Eurokod 1 – Laster på bärverk – Del 1-5 : Allmänna laster – Temperaturpåverkan*.

SIS. (2005a). Eurokod 2: Dimensionering av betongkonstruktioner - Del 1-1: Allmänna regler och regler för byggnader. In *Euro code SS-EN-1191-2* (Issue 138227).

SIS. (2005b). Eurokod 2: Dimensionering av betongkonstruktioner - Del 2: Broar. In *Euro code SS-EN-1191-2*.

Ström, M., Raudberget, D., & Gustafsson, G. (2016). Instant Set-based Design, an Easy Path to Set-based Design. *Procedia CIRP*, *50*, 234–239. https://doi.org/10.1016/j.procir.2016.04.194

Svensk Betong. (2017). *Environmental product declaration - Betong för vägbro*.

Trafikverket. (2019a). *Bärighetsberäkning av broar - TDOK 2013:0267*.

Trafikverket. (2019b). Krav Brobyggande. *Trafikverket*, 0–351. http://trvdokument.trafikverket.se/Versioner.aspx?spid=289&dokumentId=TDOK 2016%3A0204

Trafikverket. (2020). *Klimatkalkyl* (7.0).

Yavari, M. S., Pacoste, C., & Karoumi, R. (2016). Structural Optimization of Concrete Slab Frame Bridges Considering Investment Cost. *Journal of Civil Engineering and Architecture*, *10*(9), 982–994. https://doi.org/10.17265/1934-7359/2016.09.002

Appendix A

Hand calculations

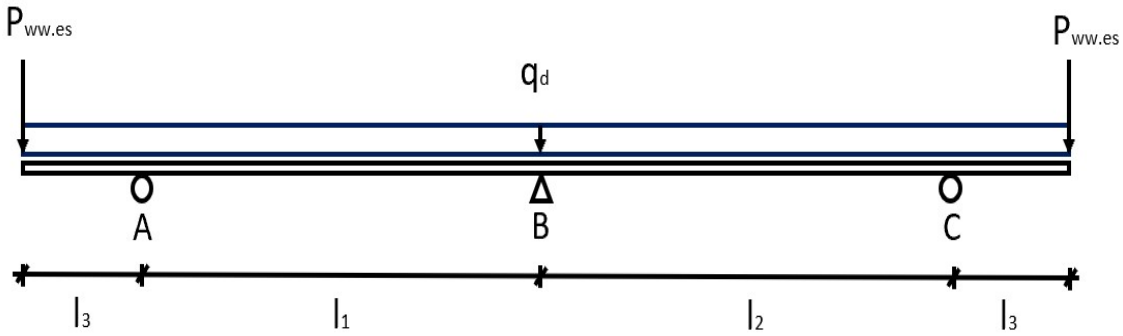

$EI := N \cdot m^2$

Geometry

$l_1 := 32m$

$l_2 := 32m$

$l_3 := 1.3m$

$h := 2m$ Height if beam

$b := 7.8m$ Width of top flange in T-section

$b_w := 4m$ Width of web

$t_f := 0.55m$ Thickness of top flange

$h_w := h - t_f = 1.45\,m$ Height of web

$A_c := t_f \cdot b + h_w \cdot b_w = 10.09\,m^2$ Cross section area

$$x_{TP} := \frac{b_w \cdot \frac{h_w^2}{2} + b \cdot t_f \cdot \left(h_w + \frac{t_f}{2}\right)}{A_c} = 1.15\,m$$ Distance from bottom to centre of gravity

$$I := \frac{b_w \cdot h_w^3}{12} + b_w \cdot h_w \cdot \frac{h_w^2}{2} + \frac{b \cdot t_f^3}{12} + b \cdot t_f \cdot \left(h_w + \frac{t_f}{2}\right)^2 = 19.987\,m^4$$ Moment of intertia

$E_c := 34GPa$ Modulus of elasticity for concrete

$EI := E_c \cdot I = 6.796 \times 10^{11} \frac{m^3 \cdot kg}{s^2}$

$t_{paving} := 100mm$ Thickness of paving

$t_{ww} := 0.5m$ Thickness of wingwall

$t_{endscreen} := 0.6m$ Thickness of endshield

$h_{endscreen} := 4m$ Height of end-shield

$V_{endscreen} := t_{endscreen} \cdot b \cdot h_{endscreen} = 18.72 \cdot m^3$

$V_{ww} := \left[h_{endscreen} \cdot 1.1m + \frac{(4.7m)^2}{2} \right] \cdot t_{ww} = 7.723 \cdot m^3$

Loads

$\rho_c := 25 \frac{kN}{m^{(3)}}$ Density of concrete

$\rho_{paving} := 23 \frac{kN}{m^3}$ Density of paving

$q_d := A_c \cdot \rho_c + t_{paving} \cdot b \cdot \rho_{paving} = 270.19 \cdot \frac{kN}{m}$ Evenly distributed self weight

$P_{ww.es} := \left(V_{endscreen} + V_{ww}\right) \cdot \rho_c = 661.063 \cdot kN$ Point load at the end of the bridge due to self weight of wingwall and end-shield

Condition: θ.B1 + θ.B2=0

Load : $\theta_{B1.q} := \frac{q_d \cdot l_1^3}{24 \cdot EI}$

$\theta_{B2.q} := \frac{q_d \cdot l_2^3}{24 \cdot EI}$

Support moment $\theta_{B1.M} := \frac{-M_B \cdot l_1}{3 \cdot EI}$

$\theta_{B2.M} := \frac{-M_B \cdot l_2}{3 \cdot EI} + \frac{-M_C \cdot l_2}{6 \cdot EI}$

$M_C := \frac{q_d \cdot l_3^{\,2}}{2} + P_{ww.es} \cdot l_3 = 1.088 \times 10^3 \cdot kN \cdot m$

$M_B := 1000 kN \cdot m$

$M_B := \text{root}\left[\frac{q_d \cdot l_1^{\,3}}{24 \cdot EI} + \frac{q_d \cdot l_2^{\,3}}{24 \cdot EI} + \frac{-M_B \cdot l_1}{3 \cdot EI} + \left(\frac{-M_B \cdot l_2}{3 \cdot EI} + \frac{-M_C \cdot l_2}{6 \cdot EI} \cdot 2\right), M_B\right] = 3.404 \times 10^4 \cdot kN \cdot m$

$M_B = 3.404 \times 10^4 \cdot kN \cdot m$

$R_{B2} := \frac{q_d \cdot l_2}{2} + \frac{M_B}{l_2} - \frac{M_C}{l_2} = 5.353 \times 10^3 \cdot kN$

$x_{0.2} := \frac{R_{B2}}{q_d} = 19.811 m$

$M_{2.max} := \frac{q_d \cdot x_{0.2}^{\,2}}{2} - M_B = 1.898 \times 10^4 \cdot kN \cdot m$

$\frac{M_B}{M_{2.max}} = 1.793$

Support moment comparison with BRIGADE

$M_{B.BRIGADE} := 3.391 \cdot 10^4 \cdot kN \cdot m$

$\frac{M_B - M_{B.BRIGADE}}{M_B} = 0.383 \cdot \%$

Field moment comparison with BRIDGADE

$M_{1.max.BRIGADE} := 1.906 \cdot 10^4 kN \cdot m$

$\frac{M_{2.max} - M_{1.max.BRIGADE}}{M_{2.max}} = -0.408 \cdot \%$

Appendix B

Project: 100-411-1
Designer: JNt
Systemberäkning, styv grundläggning

BRIGADE/Standard version 4.3.23
Project File Name: 100-411-1
Model ID: 58327530
Last save at: 2021-02-02 07:29:55
Calculated with version: 4.3.23
Last calc. started at: 2021-02-02 07:30:00
Time: 2021-02-02 09:41:55

Result Set Name: Trafiklaster_Moment

Case 1: Classification vehicle a (no surface load), Max, Bending Moment Mh (kNm)
Case 2: Classification vehicle a (no surface load), Min, Bending Moment Mh (kNm)
Case 3: Classification vehicle b (no surface load), Max, Bending Moment Mh (kNm)
Case 4: Classification vehicle b (no surface load), Min, Bending Moment Mh (kNm)
Case 5: Classification vehicle c (no surface load), Max, Bending Moment Mh (kNm)
Case 6: Classification vehicle c (no surface load), Min, Bending Moment Mh (kNm)
Case 7: Classification vehicle d (no surface load), Max, Bending Moment Mh (kNm)
Case 8: Classification vehicle d (no surface load), Min, Bending Moment Mh (kNm)
Case 9: Classification vehicle e (no surface load), Max, Bending Moment Mh (kNm)
Case 10: Classification vehicle e (no surface load), Min, Bending Moment Mh (kNm)
Case 11: Classification vehicle f (no surface load), Max, Bending Moment Mh (kNm)
Case 12: Classification vehicle f (no surface load), Min, Bending Moment Mh (kNm)
Case 13: Classification vehicle g (no surface load), Max, Bending Moment Mh (kNm)
Case 14: Classification vehicle g (no surface load), Min, Bending Moment Mh (kNm)
Case 15: Classification vehicle h (no surface load), Max, Bending Moment Mh (kNm)
Case 16: Classification vehicle h (no surface load), Min, Bending Moment Mh (kNm)
Case 17: Classification vehicle i (no surface load), Max, Bending Moment Mh (kNm)
Case 18: Classification vehicle i (no surface load), Min, Bending Moment Mh (kNm)
Case 19: Classification vehicle j (no surface load), Max, Bending Moment Mh (kNm)
Case 20: Classification vehicle j (no surface load), Min, Bending Moment Mh (kNm)
Case 21: Classification vehicle k (no surface load), Max, Bending Moment Mh (kNm)
Case 22: Classification vehicle k (no surface load), Min, Bending Moment Mh (kNm)
Case 23: Classification vehicle l (no surface load), Max, Bending Moment Mh (kNm)
Case 24: Classification vehicle l (no surface load), Min, Bending Moment Mh (kNm)
Case 25: Classification vehicle m (no surface load), Max, Bending Moment Mh (kNm)
Case 26: Classification vehicle m (no surface load), Min, Bending Moment Mh (kNm)
Case 27: Classification vehicle n (no surface load), Max, Bending Moment Mh (kNm)
Case 28: Classification vehicle n (no surface load), Min, Bending Moment Mh (kNm)
Case 29: Traffic Load Model 1, TS, Max, Bending Moment Mh (kNm)
Case 30: Traffic Load Model 1, TS, Min, Bending Moment Mh (kNm)

Title	Node	Pos_ln	Pos_tn	Thickness	Case1	Case2	Case3	Case4
	2551	0			-0,07913	-1,244	-0,06938	-1,521
	2552	0,23			0,7507	-77,47	0,6953	-54,68
	2553	0,45			1,606	-151,7	1,31	-104,7
	2554	0,68			0,02804	-224,5	0,02417	-169,5
	2555	0,9			0,4304	-297,2	0,3287	-253,7
	2556	0,9			16,73	-297,1	12,35	-266,1
	2557	1,21			0,1288	-397,3	0,152	-423,9
	2558	1,53			0,04969	-497,5	0,0459	-582,5
	2559	1,84			0,4918	-599,2	0,7209	-744,4
	2560	2,15			1,252	-702,5	1,835	-909,7
	2561	2,15			48,55	-700,6	50,5	-908
	2562	2,95			266,7	-716,4	397,7	-914,5
	2563	3,75			474,6	-684,5	733,4	-875,2
	2564	4,55			658,3	-650,5	1035	-835,2
	2565	5,35			825,3	-614,3	1312	-792,7
	2566	6,15			976,9	-576,7	1565	-748,7
	2567	6,95			1110	-538,3	1793	-703,5
	2568	7,75			1228	-499,2	1995	-657,6
	2569	8,55			1334	-459,9	2176	-611,4
	2570	9,35			1420	-420,8	2330	-565,4
	2571	10,15			1491	-382,1	2462	-519,8
	2572	10,95			1548	-343,9	2568	-474,9
	2573	11,75			1601	-306,2	2658	-430,8
	2574	12,55			1648	-269	2728	-416,3
	2575	13,35			1681	-232,3	2780	-407,6
	2576	14,15			1705	-195,8	2815	-399,2
	2577	14,95			1719	-206,3	2839	-425
	2578	15,75			1718	-225,1	2849	-457,3
	2579	16,55			1711	-243,9	2849	-489,7
	2580	17,35			1694	-262,8	2831	-522,4
	2581	18,15			1669	-283	2795	-556,4
	2582	18,95			1645	-303,4	2745	-590,6
	2583	19,75			1608	-323,8	2679	-625
	2584	20,55			1565	-344,5	2601	-660
	2585	21,35			1517	-365,5	2509	-695,4
	2586	22,15			1460	-386,9	2416	-731,7
	2587	22,95			1400	-408,8	2321	-768,8
	2588	23,75			1334	-431,1	2208	-806,8
	2589	24,55			1268	-453,9	2088	-845,6
	2590	25,35			1203	-477	1963	-884,9
	2591	26,15			1126	-500,2	1818	-924,4
	2592	26,95			1053	-523,3	1676	-963,7
	2593	27,75			976,3	-545,8	1531	-1002
	2594	28,55			875,5	-558,5	1372	-1030
	2595	29,35			772,1	-551,9	1186	-1038
	2596	30,15			654,3	-526,7	981,9	-1026
	2597	30,95			521,2	-484,3	759,6	-995,1
	2598	31,75			365,5	-426,6	540,6	-948,2
	2599	32,55			211,8	-355,8	311,7	-887,7
	2600	33,35			167,5	-274,4	243,5	-817,1
	2601	34,15			183,3	-184	266,4	-738,8
	2602	34,15			183,1	-183,7	266,3	-738,6
	2603	34,95			177,3	-279,1	243,9	-821,5
	2604	35,75			211,2	-364,6	311,1	-896,2

2605	36,55	364,2	-439,2	539,5	-960,6
2606	37,35	517,8	-500,2	756	-1011
2607	38,15	648,9	-545,5	975,5	-1044
2608	38,95	763,6	-572,6	1178	-1058
2609	39,75	862,5	-579,6	1359	-1051
2610	40,55	950,7	-564,5	1510	-1021
2611	41,35	1030	-544,7	1651	-984,9
2612	42,15	1101	-524,1	1793	-948,1
2613	42,95	1176	-503,4	1936	-911
2614	43,75	1239	-482,7	2061	-874,2
2615	44,55	1299	-462,3	2175	-837,8
2616	45,35	1365	-442,4	2288	-802,3
2617	46,15	1427	-422,9	2386	-767,5
2618	46,95	1479	-404	2473	-733,7
2619	47,75	1527	-385,4	2559	-700,7
2620	48,55	1566	-367,3	2636	-668,3
2621	49,35	1597	-349,4	2697	-636,4
2622	50,15	1622	-331,6	2748	-604,8
2623	50,95	1644	-313,9	2779	-573,4
2624	51,75	1660	-296,4	2800	-542,1
2625	52,55	1668	-278,9	2802	-511
2626	53,35	1662	-261,5	2785	-480,1
2627	54,15	1651	-244,3	2760	-449,4
2628	54,95	1624	-267,6	2723	-448,9
2629	55,75	1588	-304,6	2668	-458,2
2630	56,55	1545	-342,1	2601	-473,6
2631	57,35	1487	-380,1	2510	-518,6
2632	58,15	1425	-418,8	2397	-564,3
2633	58,95	1349	-458,1	2260	-610,9
2634	59,75	1260	-497,9	2104	-657,9
2635	60,55	1158	-537,9	1925	-705,2
2636	61,35	1035	-577,7	1718	-752,3
2637	62,15	899,8	-617,1	1489	-798,7
2638	62,95	748,7	-655,8	1235	-844,3
2639	63,75	580,3	-693,8	956,3	-888,9
2640	64,55	399	-730,7	657,3	-932,1
2641	65,35	201,3	-770,5	331,9	-979,5
2642	66,15	48,56	-808,3	47,98	-1027
2643	66,15	0,6337	-808	1,221	-1026
2644	66,46	0,2256	-681,1	0,4495	-837
2645	66,78	0,04824	-556,3	0,07505	-652
2646	67,09	0,05484	-433,3	0,07944	-470,2
2647	67,4	18,44	-309,8	13,47	-288,6
2648	67,4	0,2776	-310,6	0,2123	-275,3
2649	67,63	0,00643	-222,1	0,006781	-177,2
2650	67,85	0,4126	-132,4	0,3047	-97,15
2651	68,08	0,1979	-55,11	0,2777	-41,57
2652	68,3	9,053	-0,1056	8,344	-0,079

Case5	Case6	Case7	Case8	Case9	Case10	Case11	Case12	Case13
-0,1981	-1,04	-0,1375	-1,145	-0,1514	-1,351	-0,2692	-0,9182	0,6497
0,6299	-62,93	0,6908	-70,14	0,6197	-47,38	0,5558	-54,12	0,6972
1,343	-122,4	1,473	-137	1,165	-89,93	1,183	-104,7	1,312
0,02746	-180	0,03021	-202,3	0,02459	-145,4	0,02773	-153,3	0,04237
0,3708	-237,8	0,4079	-267,4	0,3007	-218,1	0,3365	-202	0,3629
14,04	-237,6	15,44	-267,4	10,96	-229,1	12,36	-201,9	12,36
0,1726	-331,3	0,1896	-357,1	0,1872	-377,3	0,2101	-281,2	0,4117
0,05216	-461,9	0,05737	-446,6	0,04554	-555	0,05136	-393	0,07721
0,818	-635,6	0,8984	-543,3	0,9576	-768,5	1,077	-544,4	2,397
2,083	-828,2	2,286	-646,7	2,439	-998,9	2,742	-714,1	5,963
41,34	-823,4	45,47	-677,3	45,48	-994,6	37,14	-736,2	34,81
448,7	-833	489,1	-682,6	529,5	-996,8	582,9	-740,1	1092
833,4	-796,5	912,1	-672,8	998,4	-954,2	1103	-730,2	2106
1181	-759,1	1294	-669,1	1426	-911,8	1579	-718,8	3010
1500	-719,2	1646	-663,2	1819	-866,8	2014	-705	3823
1791	-677,9	1966	-655,7	2175	-820	2410	-689,7	4555
2050	-635,5	2250	-647,1	2493	-772,1	2766	-673,2	5193
2281	-592,5	2501	-637,6	2774	-723,4	3082	-655,9	5739
2488	-553,5	2728	-627,4	3022	-677,8	3359	-640,6	6198
2665	-543,2	2920	-617,1	3234	-654,5	3599	-651,4	6574
2818	-533	3085	-606,8	3420	-631,5	3806	-662	6870
2946	-523,2	3223	-596,9	3579	-609	3980	-672,8	7123
3055	-513,8	3343	-587,6	3714	-587,2	4126	-684	7325
3140	-504,8	3434	-578,6	3823	-591,4	4245	-695,6	7462
3207	-496,3	3508	-570,2	3905	-601,1	4335	-707,7	7537
3255	-488,2	3559	-562,3	3965	-611,2	4401	-720,2	7553
3283	-517,7	3588	-593,5	4002	-651,1	4440	-764,1	7510
3291	-555,8	3602	-636,2	4010	-697,4	4455	-817,4	7412
3282	-594	3596	-679,1	4000	-743,9	4444	-870,9	7258
3254	-632,4	3566	-722,4	3965	-790,6	4411	-924,8	7054
3209	-672,2	3523	-767	3911	-838,9	4352	-980,2	6983
3152	-712,3	3457	-811,8	3846	-887,4	4269	-1036	7038
3080	-752,7	3374	-857,1	3759	-936,4	4168	-1092	7015
2997	-793,6	3278	-903	3657	-986	4050	-1149	6926
2899	-835,3	3168	-949,6	3537	-1036	3914	-1207	6768
2787	-877,8	3041	-997,3	3399	-1088	3758	-1266	6549
2663	-921,4	2899	-1046	3249	-1141	3588	-1327	6265
2528	-966	2752	-1096	3081	-1195	3402	-1389	5912
2380	-1012	2595	-1147	2900	-1250	3197	-1453	5495
2227	-1058	2421	-1199	2719	-1306	2973	-1517	5010
2071	-1104	2240	-1251	2521	-1363	2736	-1582	4455
1902	-1150	2044	-1303	2315	-1419	2495	-1647	3849
1723	-1195	1837	-1354	2093	-1474	2239	-1709	3179
1526	-1230	1613	-1393	1844	-1517	1958	-1761	2611
1301	-1244	1373	-1412	1576	-1540	1651	-1791	2172
1071	-1237	1111	-1410	1302	-1541	1320	-1799	1717
824,6	-1212	830,3	-1389	1005	-1523	984,4	-1787	1262
563,9	-1169	536,4	-1350	693,7	-1487	635,1	-1757	807
319,7	-1113	354	-1297	388,4	-1437	384,2	-1712	346,3
278,5	-1047	307,7	-1235	296,8	-1378	299	-1659	338,8
304,3	-976,7	335,9	-1175	319,1	-1313	317,7	-1606	361,4
304,2	-976,5	335,8	-1175	319	-1313	317,6	-1605	361,3
278,9	-1052	308,2	-1240	297,1	-1382	299,6	-1663	328,5
327,5	-1122	362,7	-1306	394,3	-1446	387,9	-1721	358,3

562,9	-1182	535,8	-1362	693,3	-1500	634,6	-1769	813,1
821,7	-1227	827,7	-1404	1003	-1539	982	-1803	1281
1066	-1256	1106	-1429	1297	-1560	1315	-1818	1752
1291	-1264	1364	-1432	1569	-1560	1644	-1811	2223
1511	-1251	1602	-1414	1831	-1538	1949	-1782	2672
1703	-1214	1818	-1372	2069	-1492	2220	-1728	3204
1880	-1172	2022	-1324	2290	-1440	2473	-1667	3863
2046	-1128	2215	-1275	2496	-1387	2711	-1606	4453
2201	-1084	2396	-1225	2693	-1333	2948	-1543	4975
2353	-1040	2566	-1176	2872	-1279	3168	-1481	5440
2495	-997,1	2720	-1127	3046	-1226	3370	-1420	5847
2630	-954,9	2869	-1080	3215	-1174	3557	-1360	6196
2752	-913,7	3007	-1033	3367	-1124	3724	-1302	6477
2861	-873,6	3132	-987,8	3499	-1075	3876	-1245	6695
2960	-834,4	3244	-943,6	3620	-1027	4013	-1190	6845
3041	-796	3339	-900,3	3719	-979,6	4127	-1135	6929
3105	-758,2	3414	-857,6	3798	-933,2	4225	-1082	6943
3163	-720,7	3475	-815,3	3865	-887,3	4304	-1028	6891
3203	-683,4	3519	-773,2	3915	-841,6	4362	-975,6	7087
3234	-646,3	3542	-731,4	3951	-796,2	4394	-923,1	7293
3238	-609,5	3548	-689,8	3959	-751	4402	-870,9	7444
3227	-572,8	3535	-648,5	3945	-706,1	4387	-819,1	7536
3201	-536,4	3499	-607,5	3913	-661,5	4346	-767,6	7578
3150	-535,3	3451	-607,3	3849	-644,3	4276	-748,9	7555
3080	-544,4	3374	-616,1	3763	-635,3	4183	-737,4	7471
2994	-553,8	3278	-625,4	3657	-632,1	4063	-726,5	7328
2884	-563,9	3158	-635,3	3520	-654,8	3916	-716,1	7120
2751	-574,4	3017	-645,8	3356	-678,3	3739	-706,1	6844
2595	-585,4	2849	-656,8	3164	-702,4	3530	-696,5	6517
2414	-596,6	2653	-667,9	2949	-726,8	3286	-686,8	6124
2209	-636,6	2430	-678,8	2703	-773,7	3007	-703,3	5646
1975	-680,7	2174	-689,2	2418	-823,7	2690	-721,8	5088
1712	-724,2	1887	-698,9	2097	-873,1	2332	-739,6	4452
1422	-767	1567	-707,6	1740	-921,5	1935	-756,4	3722
1101	-808,8	1214	-715,4	1346	-968,7	1499	-772,3	2902
757	-849,4	835,5	-722,2	921,9	-1015	1026	-787,1	2004
382,5	-893,6	422,8	-739,6	463,1	-1065	516,2	-804,7	1020
41,11	-938,3	45,36	-783,4	43,05	-1117	36,77	-851,9	11,51
1,471	-937,2	1,677	-755,6	1,829	-1116	2,137	-828,4	5,566
0,5448	-723,6	0,6232	-628,3	0,6808	-863,8	0,7981	-636,8	2,169
0,08821	-528,4	0,09905	-509,2	0,1039	-628,4	0,1194	-463,8	0,2472
0,09666	-373,6	0,111	-396,7	0,1139	-426,6	0,1339	-328	0,3529
15,32	-257,6	16,88	-283,8	11,91	-255,5	13,45	-226,4	13,45
0,242	-258,4	0,2671	-284,5	0,1966	-243,7	0,2222	-227	0,2497
0,008342	-184,8	0,009646	-203,5	0,008516	-156,9	0,01016	-162,4	0,02746
0,3438	-110,4	0,3784	-121,3	0,2701	-86	0,302	-97,06	0,303
0,1677	-46,02	0,1815	-50,49	0,2483	-36,92	0,1472	-40,44	0,2777
7,571	-0,08959	8,293	-0,09904	7,386	-0,07137	6,654	-0,08039	8,358

Case14	Case15	Case16	Case17	Case18	Case19	Case20	Case21	Case22
-1,54	0,7842	-1,734	0,5802	-1,158	0,6678	-1,54	0,7842	-1,734
-63,16	0,7896	-79,14	0,6925	-78,59	0,6978	-63,29	0,7896	-79,14
-126,4	1,579	-158,8	1,478	-157,5	1,312	-126,4	1,581	-158,8
-203,5	0,04355	-238,9	0,04294	-236,7	0,05122	-204,2	0,05578	-238,9
-301,5	0,439	-344,8	0,4384	-315,7	0,3641	-302,6	0,4401	-344,8
-313,9	15,38	-358,9	15,45	-315,6	12,36	-314,9	15,42	-358,9
-490,8	0,3866	-561,1	0,4173	-439,1	0,4648	-492,3	0,4742	-561,1
-668,9	0,07417	-764,7	0,07387	-604,8	0,08181	-670,7	0,08314	-764,7
-857,3	2,214	-975,9	2,499	-821,2	2,402	-857,9	2,226	-975,9
-1056	5,597	-1194	6,301	-1061	5,966	-1056	5,633	-1194
-1092	47,76	-1230	35,6	-1071	31,6	-1090	47,76	-1230
-899	1054	-944,8	1089	-825,1	1086	-1065	1073	-1103
-933,6	2037	-978,4	2097	-864,7	2082	-1092	2072	-1194
-991,4	2928	-1012	3019	-921,4	2969	-1122	2980	-1288
-1048	3756	-1043	3856	-975,8	3765	-1181	3823	-1381
-1103	4506	-1071	4629	-1028	4482	-1277	4587	-1471
-1156	5171	-1098	5338	-1079	5104	-1370	5264	-1559
-1207	5753	-1124	6032	-1128	5633	-1461	5860	-1644
-1257	6259	-1148	6656	-1175	6074	-1550	6378	-1727
-1305	6692	-1176	7187	-1221	6453	-1637	6827	-1808
-1353	7061	-1213	7637	-1311	6786	-1724	7208	-1889
-1402	7362	-1296	8026	-1439	7046	-1810	7522	-1970
-1451	7644	-1411	8351	-1568	7242	-1897	7777	-2051
-1542	7874	-1527	8613	-1697	7370	-1985	7997	-2134
-1660	8046	-1644	8804	-1827	7439	-2075	8161	-2218
-1779	8164	-1761	8942	-1957	7449	-2165	8273	-2303
-1898	8222	-1879	9023	-2089	7400	-2256	8325	-2389
-2018	8224	-1998	9042	-2221	7296	-2348	8321	-2477
-2140	8174	-2118	9047	-2355	7142	-2443	8274	-2566
-2263	8078	-2239	9012	-2490	6951	-2538	8267	-2656
-2386	8024	-2360	8915	-2625	6834	-2634	8206	-2747
-2510	7915	-2482	8756	-2761	6893	-2730	8090	-2839
-2635	7746	-2606	8538	-2899	6880	-2828	7920	-2932
-2762	7528	-2731	8270	-3038	6798	-2928	7701	-3027
-2891	7261	-2859	7948	-3181	6648	-3030	7431	-3124
-3024	6941	-2990	7576	-3327	6438	-3136	7114	-3225
-3160	6578	-3124	7155	-3476	6164	-3245	6753	-3329
-3300	6159	-3262	6685	-3630	5828	-3357	6341	-3436
-3442	5699	-3403	6173	-3787	5434	-3471	5887	-3547
-3587	5194	-3546	5602	-3946	4972	-3588	5384	-3658
-3732	4637	-3689	4978	-4105	4444	-3705	4835	-3771
-3877	4041	-3832	4299	-4264	3853	-3821	4241	-3882
-4019	3395	-3971	3576	-4420	3194	-3938	3599	-3992
-4154	2705	-4105	2801	-4569	2474	-4184	2918	-4235
-4279	1984	-4228	1981	-4707	1680	-4490	2195	-4629
-4392	1572	-4340	1514	-4832	831,6	-4804	1435	-5071
-4493	1231	-4439	1040	-4943	272,4	-5121	654,6	-5554
-4652	883,9	-4527	568,5	-5041	298,3	-5439	292	-6063
-5198	531,8	-4609	341,8	-5134	322,9	-5769	327,2	-6603
-5779	411,8	-4695	380,5	-5231	347	-6115	361,8	-7189
-6391	444,1	-4990	411,3	-5655	379,7	-6478	395,8	-7814
-6388	443,9	-4988	411,1	-5653	379,5	-6476	395,7	-7811
-5774	403,6	-4703	374,8	-5240	356,3	-6100	369,2	-7188
-5193	492,1	-4619	330,1	-5145	332,6	-5757	342	-6605

-4648	842,4	-4538	680,1	-5054	308,2	-5432	314,3	-6069
-4502	1193	-4451	1092	-4957	282,5	-5114	597,4	-5564
-4403	1607	-4353	1506	-4847	921,8	-4797	1370	-5087
-4291	2006	-4243	1923	-4723	1779	-4483	2112	-4652
-4167	2652	-4120	2739	-4586	2567	-4177	2831	-4268
-4033	3340	-3987	3515	-4438	3274	-3931	3513	-4018
-3892	3981	-3848	4246	-4284	3914	-3820	4153	-3901
-3749	4573	-3707	4925	-4126	4488	-3712	4747	-3783
-3605	5125	-3564	5549	-3968	5006	-3603	5296	-3665
-3461	5635	-3422	6125	-3810	5464	-3494	5799	-3547
-3320	6094	-3283	6644	-3654	5853	-3387	6251	-3430
-3182	6511	-3146	7111	-3502	6182	-3282	6662	-3317
-3047	6881	-3012	7525	-3353	6450	-3181	7026	-3207
-2915	7204	-2883	7887	-3209	6656	-3083	7343	-3100
-2787	7479	-2756	8197	-3068	6795	-2989	7612	-2997
-2662	7706	-2631	8455	-2929	6869	-2897	7832	-2896
-2538	7881	-2509	8660	-2793	6875	-2807	8002	-2797
-2415	8007	-2388	8826	-2658	6810	-2718	8121	-2699
-2293	8073	-2267	8968	-2524	6981	-2629	8181	-2602
-2172	8127	-2147	9060	-2391	7181	-2542	8230	-2506
-2052	8189	-2028	9089	-2258	7324	-2456	8287	-2410
-1932	8197	-1910	9055	-2126	7415	-2370	8289	-2316
-1813	8154	-1793	8963	-1996	7456	-2286	8238	-2223
-1695	8051	-1676	8808	-1866	7431	-2202	8127	-2131
-1617	7890	-1560	8599	-1736	7348	-2120	7961	-2040
-1573	7674	-1444	8340	-1608	7208	-2039	7741	-1949
-1531	7396	-1378	8036	-1490	7002	-1959	7465	-1860
-1489	7087	-1362	7659	-1453	6745	-1881	7145	-1772
-1447	6711	-1346	7203	-1415	6431	-1802	6763	-1684
-1406	6266	-1331	6663	-1378	6041	-1722	6313	-1595
-1363	5756	-1315	6036	-1339	5587	-1641	5798	-1504
-1318	5165	-1297	5332	-1299	5045	-1558	5200	-1411
-1272	4492	-1278	4608	-1257	4415	-1473	4527	-1316
-1224	3734	-1257	3827	-1213	3694	-1384	3781	-1218
-1173	2897	-1234	2981	-1167	2882	-1294	2949	-1119
-1122	1999	-1209	2052	-1120	1988	-1202	2037	-1018
-1073	1013	-1189	1038	-1076	1011	-1113	1031	-918,9
-1051	57,19	-1216	35,63	-1089	12,22	-1061	49,09	-1216
-1043	5,238	-1186	5,866	-1057	5,42	-1045	5,357	-1186
-842,7	2,007	-958,9	2,252	-804,4	2,112	-842,8	2,01	-959
-652	0,2425	-742,2	0,2534	-582,2	0,2461	-652	0,2489	-742,1
-470,3	0,3243	-535,3	0,3553	-411,7	0,3956	-470,4	0,409	-535,4
-289	16,88	-328,8	16,88	-284	13,54	-289,2	16,89	-329
-275,3	0,3006	-313,3	0,2981	-284,6	0,2487	-275,3	0,3012	-313,3
-177,2	0,02543	-203,5	0,02665	-203,5	0,03417	-177,2	0,03624	-203,5
-97,16	0,3779	-121,3	0,3796	-121,6	0,3037	-97,16	0,3795	-121,3
-41,57	0,3167	-50,49	0,1854	-50,66	0,278	-41,57	0,3139	-50,49
-0,09183	9,508	-0,1093	8,335	-0,1073	8,368	-0,09835	9,52	-0,1184

Case23	Case24	Case25	Case26	Case27	Case28	Case29	Case30
0,5802	-1,196	-0,1959	-1,049	-0,1363	-1,15	1,124	-1,488
0,6934	-78,59	0,6285	-62,88	0,6911	-70,21	0,865	-97,94
1,478	-157,5	1,341	-122,3	1,475	-137,1	1,805	-196,8
0,05575	-236,7	0,03629	-180	0,03751	-202,3	0,03615	-296,9
0,4384	-315,7	0,3883	-237,7	0,4284	-267,5	0,5026	-397,6
15,38	-315,6	13,94	-237,7	15,34	-267,4	18,53	-397,2
0,5182	-439,1	0,3639	-326,3	0,3177	-366,6	0,2382	-556,9
0,08087	-604,8	0,05684	-439,4	0,04596	-490,3	0,04545	-767
2,573	-821,2	2,084	-581,1	1,697	-643,3	1,111	-1038
6,491	-1064	5,28	-735,6	4,314	-809,6	2,815	-1338
43,34	-1089	20,97	-761,3	14,95	-799,4	32,1	-1334
1121	-848,7	1017	-745,5	881,3	-784,6	633,5	-1282
2148	-963,1	1957	-712,2	1698	-736,2	1254	-1236
3087	-1079	2809	-677,4	2443	-700,7	1826	-1197
3946	-1194	3597	-640,3	3122	-662,8	2354	-1157
4740	-1307	4310	-601,8	3737	-623,6	2837	-1114
5439	-1418	4943	-593	4287	-583,4	3271	-1071
6131	-1526	5500	-706,2	4778	-551,6	3661	-1026
6764	-1631	5998	-817,6	5224	-641,8	4007	-980,9
7305	-1735	6422	-927,5	5610	-730,8	4307	-935,8
7784	-1838	6779	-1036	5940	-818,9	4569	-891,2
8187	-1941	7078	-1144	6221	-906,5	4791	-847,7
8520	-2045	7332	-1252	6457	-993,9	4977	-805,1
8789	-2149	7539	-1361	6643	-1081	5127	-850,7
8995	-2255	7688	-1469	6789	-1169	5246	-913,9
9140	-2361	7786	-1579	6891	-1258	5333	-977,5
9215	-2469	7835	-1688	6952	-1347	5389	-1042
9227	-2578	7844	-1799	6978	-1436	5407	-1106
9180	-2689	7806	-1910	6967	-1526	5399	-1171
9075	-2800	7736	-2022	6913	-1616	5360	-1236
8920	-2913	7657	-2135	6825	-1708	5293	-1302
8773	-3027	7535	-2250	6696	-1801	5200	-1368
8564	-3141	7364	-2365	6533	-1894	5080	-1434
8308	-3258	7147	-2482	6337	-1989	4940	-1502
7997	-3378	6885	-2601	6112	-2086	4776	-1571
7634	-3502	6585	-2723	5855	-2185	4581	-1642
7222	-3629	6248	-2849	5566	-2286	4367	-1715
6761	-3760	5866	-2977	5251	-2390	4129	-1789
6250	-3893	5444	-3108	4907	-2496	3870	-1865
5681	-4029	4983	-3241	4533	-2604	3596	-1942
5062	-4166	4481	-3375	4124	-2712	3304	-2020
4389	-4301	3939	-3508	3693	-2819	2996	-2097
3660	-4436	3360	-3638	3244	-2924	2659	-2173
2885	-4680	2734	-3754	2762	-3017	2303	-2245
2058	-4977	2064	-3844	2239	-3085	1928	-2313
1195	-5269	1360	-3908	1687	-3128	1560	-2376
296,3	-5636	626,8	-3946	1127	-3148	1186	-2433
224,2	-6040	140,9	-3961	550,6	-3146	803,8	-2484
250,9	-6466	161,3	-3960	165,3	-3129	419,1	-2533
277	-6924	175	-3952	179,1	-3104	279,4	-2584
302,5	-7505	189,1	-3942	194,2	-3075	294,1	-2641
302,4	-7502	189	-3939	194	-3073	293,9	-2639
281,6	-6924	183	-3956	188	-3108	287,8	-2584
260	-6448	168,5	-3968	173,4	-3137	420,6	-2532

237,8	-6037	146,9	-3974	551,2	-3158	805,9	-2483
319,8	-5670	625,9	-3962	1126	-3163	1188	-2432
1218	-5306	1357	-3927	1684	-3147	1562	-2376
2072	-4996	2058	-3864	2235	-3105	1930	-2313
2886	-4710	2726	-3774	2752	-3037	2305	-2245
3657	-4463	3341	-3656	3227	-2943	2660	-2172
4383	-4324	3921	-3529	3675	-2840	2998	-2097
5058	-4184	4460	-3398	4100	-2735	3304	-2020
5676	-4043	4957	-3267	4508	-2629	3598	-1942
6247	-3903	5417	-3136	4880	-2524	3873	-1865
6762	-3765	5835	-3008	5221	-2421	4129	-1789
7230	-3630	6213	-2882	5537	-2319	4370	-1714
7648	-3499	6553	-2759	5821	-2220	4583	-1641
8012	-3371	6850	-2639	6076	-2124	4775	-1571
8325	-3248	7107	-2523	6302	-2030	4941	-1502
8580	-3127	7322	-2408	6495	-1937	5082	-1434
8778	-3008	7489	-2295	6655	-1846	5197	-1367
8921	-2890	7612	-2184	6779	-1756	5292	-1301
9049	-2774	7690	-2072	6866	-1667	5356	-1236
9137	-2658	7753	-1962	6913	-1578	5403	-1170
9162	-2543	7791	-1852	6925	-1489	5407	-1106
9123	-2429	7778	-1743	6898	-1401	5384	-1041
9027	-2316	7732	-1635	6833	-1314	5337	-977,2
8868	-2204	7629	-1527	6731	-1227	5246	-913,6
8655	-2094	7476	-1420	6582	-1141	5126	-850,3
8381	-1984	7271	-1314	6392	-1055	4978	-788,2
8074	-1875	7012	-1207	6155	-969,4	4791	-824,7
7694	-1767	6710	-1101	5872	-883,8	4566	-867,2
7234	-1659	6353	-994,4	5537	-797,7	4305	-910,5
6691	-1549	5922	-886,6	5149	-710,9	4004	-954,5
6082	-1438	5426	-777,4	4703	-622,8	3659	-998,4
5399	-1325	4865	-666,4	4210	-625,6	3270	-1042
4687	-1209	4230	-648,2	3657	-666,9	2835	-1084
3916	-1091	3517	-688,1	3042	-707,5	2352	-1125
3048	-970,5	2727	-727,1	2360	-747,2	1822	-1165
2101	-849,4	1878	-765,2	1619	-785,8	1251	-1203
1070	-798,9	948,6	-806,3	813,5	-841,6	631	-1246
40,42	-1089	18,62	-875,1	11,93	-908,7	32,4	-1294
5,968	-1057	4,691	-845,6	3,72	-915,4	2,836	-1286
2,256	-804,5	1,781	-669,7	1,403	-728	1,084	-997,4
0,2615	-582,2	0,2258	-505,8	0,1942	-553	0,1492	-730,1
0,4467	-411,7	0,2765	-369	0,2305	-405,6	0,1977	-518,9
16,81	-284,1	15,27	-257,8	16,88	-283,9	20,72	-360,3
0,2997	-284,6	0,2618	-258,4	0,2883	-284,5	0,3395	-360,9
0,03789	-203,5	0,01837	-184,8	0,01647	-203,5	0,01633	-260,9
0,3789	-121,6	0,3432	-110,3	0,3782	-121,5	0,4605	-160,6
0,2085	-50,66	0,1667	-45,96	0,1839	-50,59	0,2491	-70,85
8,334	-0,1158	7,556	-0,09375	8,316	-0,1017	10,19	-0,1179

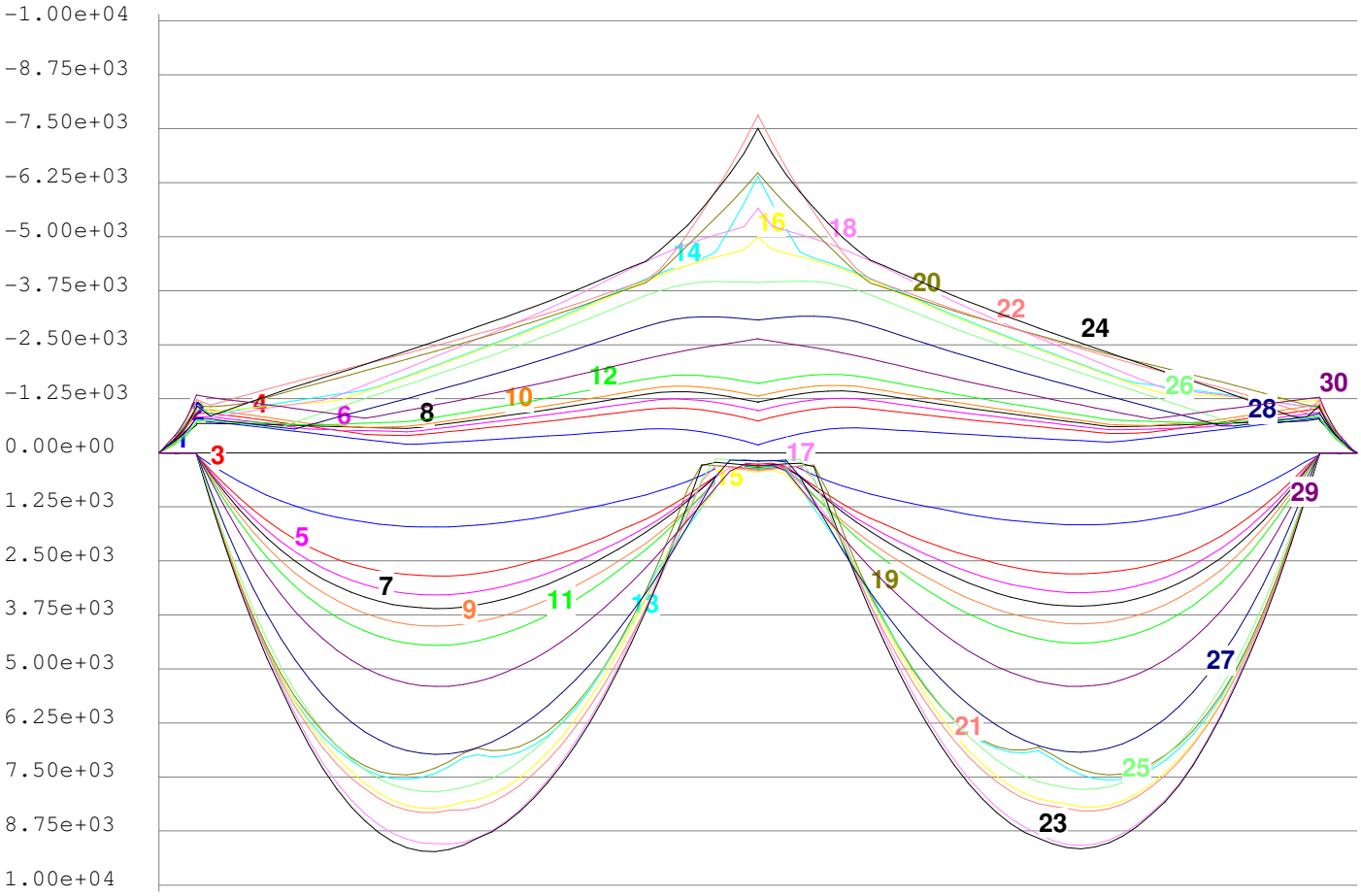
-1.00e+04
-8.75e+03
-7.50e+03
-6.25e+03
-5.00e+03
-3.75e+03
-2.50e+03
-1.25e+03
0.00e+00
1.25e+03
2.50e+03
3.75e+03
5.00e+03
6.25e+03
7.50e+03
8.75e+03
1.00e+04
1
2
3
4
5
6
7
8
9
10
11
12
13
14
15
16
17
18
19
20
21
22
23
24
25
26
27
28
29
30

ᵀm)

DEPARTMENT OF ARCHITECTURE AND CIVIL ENGINEERING
DIVISION OF STRUCTURAL ENGINEERING
CONCRETE STRUCTURES
CHALMERS UNIVERSITY OF TECHNOLOGY
Gothenburg, Sweden 2021
www.chalmers.se

CHALMERS
UNIVERSITY OF TECHNOLOGY